Wind Turbine Design for a Hybrid System

with the emphasis on generation complementarity

F. A. Qamar

Wind Turbine Design for a Hybrid System

with the emphasis on generation complementarity

by

Fadhil Ahmad Qamar

to obtain the degree of Master of Science
in Sustainable Energy Technology

at the Delft University of Technology,

to be defended publicly on Tuesday August 18, 2020 at 13.00 PM.

Student number:	4741986	
Project duration:	October 17, 2019 – August 18, 2020	
Thesis committee:	Prof. dr. D. A. von Terzi,	TU Delft, chairperson
	Dr. ir. M. L. Zaayer,	TU Delft, First supervisor
	Dr. ir. J. Quist,	TU Delft, Second supervisor

TU Delft

Summary

Reason for this research

The global issue on global warming and climate change are one of the motivations that led nations to reform their means of generating power and meeting the electricity demand. Decarbonisation of the power system is imperative to reduce the carbon emission, and the penetration of renewable energy to the power system is expected to rise in the future. However, as the nature of renewable energy source being weather dependent, high penetration of this technology in the power system will pose additional challenges to the utilities and system operators. The hybrid power plants that include multiple generation technologies can combine the strengths and weaknesses of different technologies and results in a power system with better performance. For instance, combining wind, solar or other generation technologies can results in a more stable generation with a generation profile similar to the base-load generation technology. Thus, the hybrid power system may serve as one of the solutions to compensate the renewable technology integration issues. This research studies and optimises the hybrid power system through designing the wind turbine that operates in such a system. The design approach taken emphasises the complementary generation feature of the hybrid power system to reduce the variations of the generation profile.

Goal and method

This research considers the generation complementarity of the wind and solar in the hybrid power system. Wind and solar energy have different diurnal and seasonal variation. Thus, the generation complementarity can be achieved when one technology is operating at its optimum when the other is not generating. This design decision is then translated to the need for designing the wind turbine that optimally operates when the solar power output is low, which includes designing the wind turbine that operates during the night-time, and during the season with low solar irradiance. The full-year operation mode is also analysed as the baseline design. The wind turbine design process itself is focused on the conceptual design phase with the objective of finding optimum rotor diameter while the generation capacity is capped at 3 MW. The wind turbine rotor diameter is optimally designed for particular periods with the objective of cost of electricity minimisation. The cost function employed to define the cost of electricity is taken from the NREL cost model with some adjustment due to the different design approach of this research. This research aims to identify the implication of the different operational modes to the wind turbine design. The wind turbines are then modelled operating in different hybrid power system topologies and coupled to a solar PV with 3 MW capacity to analyse the performance of the designs. These topologies include zero-curtailment, grid-constrained and demand load-supplying topology. The storage system is later applied to the system to enables the shifts of generation between different time steps and enhance the performance of the hybrid power system. In order to represent the real generation and demand data, a case study is considered.

Diurnal and seasonal wind turbine design

The result first identifies the wind turbine design parameters that are affected by specific operational modes, namely: the wind speed distribution, wind shear profile and turbulence intensity. The wind speed distribution and wind shear profile are employed in the analysis to define the optimum design. The analysis on the site condition of the case study reveals that the wind speed distribution for the night time period is similar to the full-year period, while the low solar irradiance period, which coincides

with the low wind speed season, have lower wind speed distribution. It is also found that for The wind turbine design results identify the wind turbine with optimum rotor diameter designs for different operational modes and topologies. In zero-curtailment topology, higher wind speed distribution leads to smaller optimum rotor diameter and vice versa. In the grid-constrained and demand load supplying topology, larger rotor diameter suffers from curtailment due to the limited grid capacity and low demand load level. This condition leads to the shifts of optimum rotor diameter to the smaller rotor. The level of curtailment is higher in the demand load-supplying topology due to the overall lower evacuation capacity. When the night-time design and low-wind speed period design is fully operated in a year, the wind turbines are not operating at its optimum, and higher cost of electricity is expected. This result implies the higher cost for designs that correspond to the diurnal and seasonal variation. The storage system is applied to save the curtailment of wind energy. The result of this analysis suggests that the relationship between the amount of saved curtailment and the capacity of the storage is linear for higher storage capacity (<10%) and non-linear at lower storage capacity. It is found that the first few additions of storage yield the most cost-efficient of curtailment saving. The cost and benefit analysis of the storage system also indicates that the current cost of the storage technology is not compensated by the benefit of evacuating the curtailment.

Reccomendation for further reserach

It is suggested that further research should incorporate the turbulence intensity into the analysis of the diurnal and seasonal effect to get a better insight into the effect of these operational modes on the wind turbine design. The different methodology of optimisation, such as profit maximisation may also provide insights from a different perspective. The results presented in this research are based on the chosen case study. Thus, future research should consider exercising similar research at a different location and with different components of the hybrid power system. This kind of research will give broader insights on the implication of the specific operation modes on the wind turbine design.

Preface

Alhamdulillahi rabbil alamiin. This report is the final milestone of my Master in Sustainable Energy Technology at the Delft University of Technology. It really has been a great subject to dedicate my life to for the last 10 months as a student. All praise belongs to God, for Whom I owe everything; for the strength to finish this thesis, and for the opportunity to meet the remarkable people who helped me reach the position where I am today.

I would like to express my sincere gratitude to my supervisor, Dr.ir. Michiel Zaayer, who has guided me throughout the project, through ups and downs, until the final day of my thesis. I am truly thankful for the insights through a lot of constructive discussions and detailed feedback he gave to help me steer this thesis to the correct direction. I would also say many thanks to Prof.dr.ir. Dominic von Terzi. His critical input is beyond helpful in shaping this project. My sincere gratitude to Dr.ir. Jaco Quist for the on-point comments and feedback.

I would also like to thank the academic counsellor, Leonie and Michel, who have provided me with support and encouragement during my student life in Delft, which also would be incomplete without the presence of my friends and my Indonesian housemates of ”Alstublieft”. Thank you for the endless laughter and joy that brighten up the cloudy days.

Furthermore, if not due to the prayers and support from my families, this journey may not be possible. Thank you for your kindness Ayah, Ibu, Bapak, Ibu, my brother and sisters. Last but not least, to my wife, Azizah, who always see the best in me and have faith even in the darkest hour. *Jazakumullah ahsanal jaza. May God rewards you with the best*.

Fadhil Ahmad Qamar
Delft, August 12, 2020

Contents

List of Figures

List of Tables

Nomenclature

List of abbreviation

ABL	Atmospheric Boundary Layer
AEP	Annual Energy Production
CAPEX	Capital Expenditure
CF	Capacity Factor
COE	Cost of Electricity
CSP	Concentrated Solar Power
DLC	Design Load Cases
FCR	Fixed Charge Rate
GHI	Global Horizontal Irradiance
GW	Gigawatt
GWh	Gigawatt hour
HAWC2Aero	Horizontal Axis Wind turbine simulation Code 2^{ns} generation
IEC	International Electrotechnical Commission
kW	Kilowatt
kWh	Kilowatt hour
LCOE	Levelized Cost of Electricity
LCOS	Levelized Cost of Storage
LFC	Levelized Fixed Cost
LVC	Levelized Variable Cost
MAE	Mean Absolute Error
maxSOC	Maximum State of Charge
ML	Mixed Layer
MNRE	Ministry of New and Renewable Energy
MW	Megawatt
NREL	National Renewable Energy Laboratory
NTM	Normal Turbulence Model
NWP	Normal Wind
O&M	Operation and Maintenance

OPEX	Operational Expenditure
PPA	Power Purchase Agreement
PV	Photovoltaics
RL	Residual layer
RMSE	Root Mean Square Error
SBL	Stable Boundary Layer
SOC	State of Charge
TERI	The Energy and Resources Institute
TI	Turbulence Intensity
TIC	Total Installed Cost
WindPACT	Wind Partnership for Advanced Component

List of greek symbols

α	Shear exponent [-]
β	Weibull shape parameter [-]
ΔAEP	Annual energy production difference [kWh]
ΔC_{cap}	Reduction of capacity cost [$/kWh]
ΔC_{curt}	Reduction of curtailment cost [$/kWh]
ΔC_{op}	Reduction of operational cost [$/kWh]
ΔC_{trans}	Reduction of transmission cost [$/kWh]
ΔCOE	Cost of electricity difference [$]
$\Delta cost$	Total investment cost difference [$/kWh]
ΔD	Diameter difference [m]
$\Delta N/N$	Fatigue damage [cycles]
η	Weibull scale parameter [m/s]

List of roman symbols

A	Rotor swept area [m^2]
C_{cap}	Capacity cost [$/kWh]
C_{charge}	Charging cost [$/kWh]
C_{curt}	Curtailment cost [$/kWh]
C_{eol}	End of life cost [$/kWh]
$C_{nacelle}$	Nacelle cost [$]
C_{op}	Operational cost [$/kWh]
C_{pol}	Pollution reduction benefits [$/kWh]
C_p	Coefficient of performance [-]

C_{trans}	Transmission cost [$/kWh]
$m_{bearing}$	Bearing mass [kg]
m_{blade}	Blade mass [kg]
m_{hub}	Hub mass [kg]
$m_{mainframe}$	Mainframe mass [kg]
m_{tower}	Tower mass [kg]
P	Power [kW]
P_{rated}	Rated power [kW]
Q	Total energy output [kWh]
$Q_{discharge}$	Total energy discharged [kWh]
R	Rotor radius [m]
r	Discount rate [%]
T	Project duration [years]
U	Wind speed [m/s]
U_{avg}	Average wind speed [m/s]
U_{cut-in}	Cut-in wind speed [m/s]
$U_{cut-out}$	Cut-out wind speed [m/s]
U_{hub}	Wind speed at hub height [m/s]
z	Measurement height [m]
z_{hub}	Hub height [m]

1 Introduction

Global issues such as climate change and energy crisis have led nations to shift their energy generation from conventional fossil-fueled energy generation to the carbon-free energy generation with renewable energy sources. Yet the integration of renewable energy to the power system comes with additional cost, due to the nature of the renewable energy being weather dependent. Multiple solutions are studied to overcome this shortcoming, and one of the proposed solutions is the hybrid power system-a power plant that employs multiple generation technologies.

This chapter presents the background on the need for a hybrid power system followed by the discussion on the use of the wind turbine in the hybrid power system. The current state of the wind-powered hybrid power system is analysed from the relevant literature. Then the need for wind turbine design tailored to the hybrid power is articulated, followed by the discussion on the diurnal and seasonal variation effect on wind turbine design parameters. This chapter is finalised with the definition of the research goals, scope, research question and report outline.

1.1. Renewable energy integration: drivers and challenges

The world is in a transition towards sustainability. In the power generation sector, conventional fossil-fueled power plants are being phased out and replaced with renewable sourced technology such as wind turbines and solar PV. This transition in the power generation sector is motivated by the reduction of carbon emission that fuels global warming. Local and global policies are rolled out to limit the effect of global warming and climate change, such as the Paris Agreement. By the time this report is written, 189 of 197 countries have ratified the agreement to keep global warming level by 1.5 to 2 degrees [51]. The implementation of such policy boosts the growth of renewable energy source generation plants into the power system. Driven by the electricity demand growth and economic and policy drivers, the worldwide renewable energy consumption is predicted to increased by 3% per year between 2018 and 2050, which is faster than nuclear and fossil fuels. This growth leads the renewable energy to become the leading source of primary energy consumption in 2050 [11].

Renewable energy such as wind and solar power are dependent on the weather condition. Higher penetration of variable energy in the power system can pose additional challenges to utilities and system operators. Thus, the integration of renewable energy is less straightforward [15]. System operators are responsible for maintaining the balance of the grid. Consequently, uncertain disruption from renewable energy requires extra measures. Greater overall power system flexibility is required to accommodate the generation fluctuation while meeting the demand. In the case in which renewable generation increases when the demand is low or vice versa, balancing actions are needed. System operators need to ensure that there is enough reserve capacity to maintain system balance and mitigate the up or

down ramps in wind generation. Gas and coal plants serve as back-up power sources in most cases to curb the mismatch during the underproduction of renewable energy in a grid-connected topology. The required capacity of back-up power increases proportionally to the increase of installed renewable energy sourced power generations [8] [54].

The power inflexibility challenge aggravates with other issues, such as: the economically infeasible conventional plants to reduce and increase output power, demand that cannot absorb excess supply, the excess of renewable energy, and the insufficient transmission capacity to balance supply and demand across broader geographic areas. In 2016, South Australia, which relies on wind for around 40% of its electricity, has suffered several large-scale blackouts that have been caused or exacerbated by the lack of available wind or dispatchable back-up sources [9].

On the other hand, the current partial integration of renewable energy in the energy profile can multiply several times during sunny and windy days. Typically, renewable energies are to be deployed first in the power market due to the lower marginal costs. Utilising renewable energy will require conventional power plants to meet the net load - the remainder load unmet by the renewables. In cases in which renewable generation increases when load level decreases (or vice versa), the net load ramps more quickly than the load level, as shown in figure 1.1. The conventional coal and nuclear power plant may not be able to cope with the volatility constrained by their ramping capacity. Such phenomena will cause oversupply of electricity and lower the electricity prices in the market significantly. Some negative electricity prices have been spotted in European countries with high renewable energy penetration which may indicate a sign of a dysfunctional market [10].

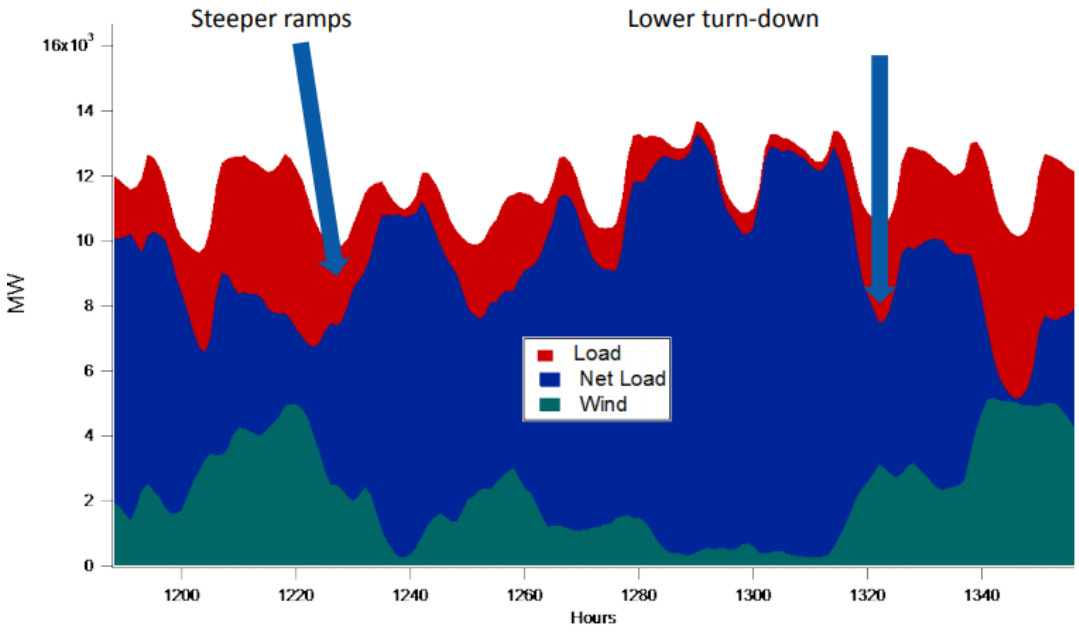

Figure 1.1: Wind energy requires additional flexibility from other generation plant. Data from Minnesota 25% wind energy scenario [15].

The growth of renewable energy penetration in the power system comes with the inevitable necessity of embracing its nature. Straightforwardly, increasing the flexibility of the power system is essential to respond to uncertainty and variability [15]. Along with other solutions, previous studies had suggested that combining different renewable energy sources and storage systems benefit the grid and has become the general trend towards system efficiency and power reliability improvement [23]. This deployment strategy utilizes the complementary nature of the different renewable energy sources to reduce each of their power fluctuations and variability. Combining wind, solar or other renewable generation with storage into ”hybrid power plants” results in a more stable generation from renewable energy sources similar to base load-like generation profile. Aside from being favourable for the grid operation, for renewable generations to have the same degree of capacity value, dispatchability and reliability as the conventional power plant, their profitability is also ensured. With the growing share of renewable

energy above 10-20% or more of overall electricity generation, the future profitability of individual power plants depends on the time-varying energy pricing, capacity and service market [24].

1.2. Hybrid power system roles in renewable energy integration

In their report, [24] NREL defines hybrid power systems as the power plants that contain more than one generation technology. The technology options range between wind turbines, solar PV, Concentrated Solar Power (CSP), storage, geothermal power, hydropower, biomass, natural gas, oil, coal and nuclear power . An additional storage system can shift the generated energy to a different point of time and provide a more predictable and controllable generation, hence increasing the grid system reliability. Different generation technologies have different strengths and weaknesses with the same goal of serving a low cost, secure, stable and reliable operation. This feature of generation complementarity has drawn worldwide research interest in the hybrid power system to articulate the practical advantage.

Merzic et al. [36] compared the hybrid system and single-sourced electricity generation and confirm the reduction of variability feature of the hybrid electricity generation system. Mohammed et al. [37] extensively review substantial issues on the drivers and advantage of the hybrid renewable energy system. The advantage of the hybrid system, in general, includes the increase in reliability of renewable energy exploitation, relieving the integration in the power system, resolution in renewable energy intermittency, boosting the development of power electronics in energy harvesting and the viability for rural electrification. Das et al. [23] analyse the wind-based hybrid power plant added value, which incorporates the increase in availability and capacity factor, reduction in variability and ancillary service capability addition.

Given its complex systems that involve many subsystems, disciplines and stakeholders, research in hybrid power system design employs various optimisation objectives. Historically, designers have used the levelized cost of eletricity (LCOE) as the metric to assess the design feasibility and adequate size of the system [24]. This metric sums the upfront capital expenditure (CAPEX) that is adjusted to a fixed charge rate with the annual operational expenditure (OPEX) and divides them with the expected annual energy production (AEP) of the plant. Lana-Rubio et al. [34] review methodologies on the sizing of renewable hybrid energy systems and report different metrics that incorporate reliability such as loss of power supply probability, level of autonomy and expected energy not supplied. These metrics are often used for optimisation focused on distributed energy systems and off-grid, stand-alone systems.

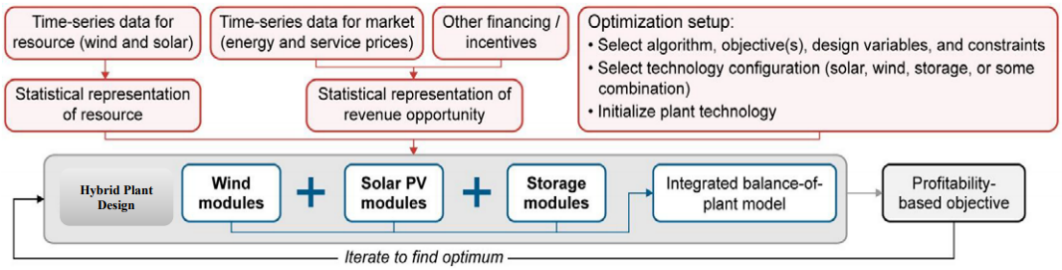

Figure 1.2: General hybrid power system optimisation components for the problem formulation [24].

For solar PV and wind energy-based hybrid power systems, previous research on design optimisation to date focused on technology selection and capacity sizing of the hybrid power system components. General optimisation components of a hybrid power system are shown in figure 1.2. Designing an optimum hybrid power system is similar to individual plant optimisation, which includes the optimisation of technology performance and cost of the generation technology such as wind turbines [24]. Thus wind turbine design optimisation is one way among many to optimise the design of a hybrid power system. Previous studies explore wind turbine design that is more ”system-friendly” with less variability output [28]. This design involves a higher capacity factor wind turbine so that the production profile shifts towards a base load-like profile. The system-friendly design employs a larger rotor diameter for

lower machine rating, thus lower specific rating, to achieve this. Madsen et al. [35] propose a wind turbine design concept with a similar design motivation: to reduce residuals in the power system and the cost of turbine. The design concept maximises power generation at lower wind speed. This wind turbine concept has a cut-out wind speed just above the rated wind speed of normal wind turbines, thus minimising the residuals in the power system and reducing loads on the blades of the wind turbine and, hence, the costs.

In this research, the feature of generation complementarity is further explored. In a solar PV and wind energy-based hybrid power system that supplies a grid system or demand, the wind energy generation should be optimised for times when the solar PV generation is low or even null, and vice versa. The resource availability of wind and solar irradiance are affected by the diurnal and seasonal cycles. The variability of solar PV power output depends on the solar irradiance level that is affected by the short-term weather (cloud coverage), time of the day (peaking at midday) and season (peaking in summer) [12]. On a daily basis, wind energy variability is affected by the atmospheric boundary layer evolution. Wind energy seasonal variation depends not only on the time of the year but also on the geographical condition of the location and how it interacts with adjacent locations.

Thus, the optimisation approach that emphasises on the generation complementarity between wind and solar energy in a hybrid power system will require optimisation of wind turbine design that acknowledges the diurnal and seasonal variations of wind energy.

1.3. Diurnal and seasonal variation-tailored wind turbine design

The need for a new design of wind turbine that corresponds to the diurnal and seasonal variation has been articulated in the previous section. This section will discuss the difference in the wind turbine design; what design parameters will be affected by the different operational condition, diurnally and seasonally. Diurnal variation is driven by the daily cycle of the presence of the sun. In his book, Stull explains the daily evolution of the atmospheric boundary layer (ABL) [49]. The sun heat affects the atmospheric boundary layer, which consists of several sub-layers. During the daytime, there is a statically-unstable mixed layer (ML) and at night, a statically stable boundary layer (SBL) formed. The surface layer is the lowest layer in the ABL, reaching heights of 20 to 200 m from the surface. In this layer, frictional drag, heat conduction and evaporation from the surface affect the wind speed, temperature and humidity.

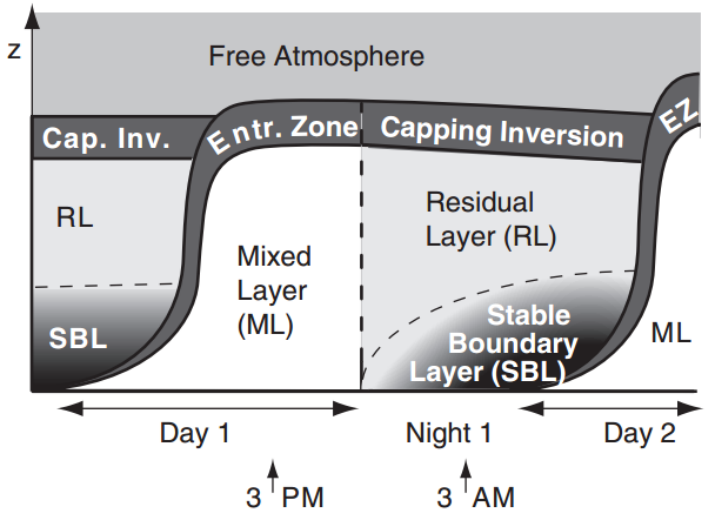

Figure 1.3: Boundary layer evolution during fair weather in summer over land. Darker color indicate stronger static stability reproduced from [49]

The depth of the mixed layer changes over time due to the diurnal cycle and, therefore, the wind profile changes as well. A few hours after the sunrise, the mixed layer is formed with a shallow depth.

As the day progresses, the mixed layer deepens due to turbulence induced by the heating from solar irradiation. During this period, the wind speed is homogenous over a large part of the mixed layer. The wind speed decreases to near zero above the ground surface due to friction. After sunset, the turbulence intensity diminishes. With less mixing, the wind speed close to the ground decreases due to the surface drag, yet the wind speed in the mid-ABL is not affected. As the night progresses, without surface drag affecting the mid-ABL, wind speed increases. After the sunrise, the mixing process starts to occur and mix the high wind speed in the ABL with the lower wind speed close to the ground. This progression can be seen in figure 1.3. From this explanation, it can be concluded that at a certain point of height, the diurnal cycle in the atmospheric boundary layer affects three parameters: wind shear coefficient, turbulence intensity and wind speed.

Wind shear is the gradient of wind speed over a relatively short distance. Vertical wind shear describes the average wind speed gradient as a function of height. The IEC 61400-1 standard employs the power law to describe the normal wind profile (NWP), This atmospheric condition induces higher wind speed at heights above hub height and lower wind speed at heights lower than hub height. As described, a larger difference between these heights will make the wind speed difference greater. In practice, during the operation of the wind turbine, the rotating blade will be exposed to this nonuniform wind profile. Thus, each of the individual blades will experience a different magnitude of loads as a function of height. As the blades rotate, this changing load magnitude becomes cyclic, and in the long run, it affects the fatigue life of the blade. IEC 61400-1 use the NWP model to assess the fatigue of wind turbines during start up and normal shut down in the design load case (DLC) 3.1 and 4.1 respectively [21].

Turbulence intensity (TI) represents the magnitude of the random variations of the wind speed over a particular period of time. IEC 61400-1 defines turbulence intensity as the ratio of the turbulence standard deviation and the average wind speed at hub height. The normal turbulence model (NTM) of the IEC standard defines the value of standard deviation as the 90% quantile of the hub height wind speed. Increasing the turbulence intensity value increases the range of spread of the actual wind speed over a period of time relative to the average wind speed. The fluctuating nonuniform wind speed due to turbulence also induces cyclic loads on the rotating rotor, thus reducing the fatigue life. IEC 61400-1 uses the NTM to assess the fatigue of wind turbine during normal power production, faulty power production and parked or idle conditions in the DLC 1.2, 2.4 and 6.4 respectively [21].

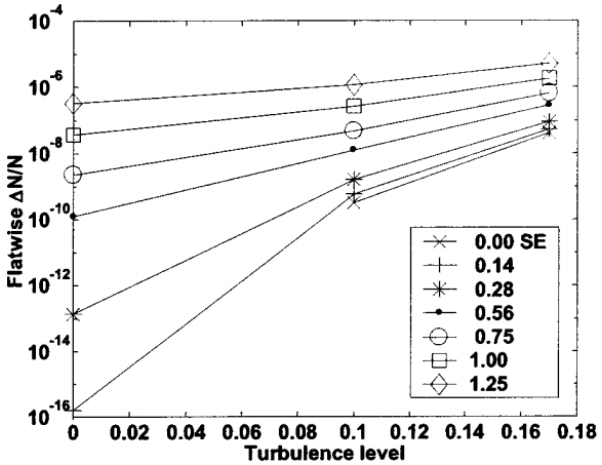

Figure 1.4: Flatwise fatigue damage at average hub height wind speed 12 m/s reproduce from [25]. Horizontal axis refers to the turbulence level. The vertical axis refers to flatwise fatigue damage of the blade and the curves refer the different shear exponent employed

Eggers et al. [25] investigate the effect of various levels of shear and turbulence intensity to the flatwise fatigue life of the blade. The results, see figure 1.4, show that increasing TI or shear exponent leads to a lower blade fatigue life, and so does increasing both parameters. However, the reduction of fatigue life due to increasing shear exponent is lower at higher turbulence intensity level. In practice,

the magnitude of wind shear, expressed in the shear exponent, and turbulence intensity are, to some extent, negatively correlated. Under the stable condition, the mixing in the atmosphere is retained. Thus, turbulence intensity is low and the absence of mixing increases the vertical wind speed gradient [25]. Sathe et al. investigate the influence of atmospheric stability on wind turbine loads and conclude that under stable condition, wind shear is larger than under neutral condition. Thus, fatigue loads due to shear are larger. The turbulent energy during this condition is also found to be small, which induce smaller fatigue loads. The study also suggests that the IEC standard overestimates the shear model when compared to the site-specific wind conditions, hence leaving room for wind turbine cost reduction [42].

The nonuniform wind profile exposure over the rotor swept area also affects the wind turbine power output. In [53] the effect of wind speed shear, wind direction shear and turbulence intensity on generation output is investigated. The result shows that sheared flow according to the power-law decreases the power output compared to uniform inflow. This conclusion is restricted to the aerodynamic model employed in the analysis (HAWC2Aero), and different models may lead to different conclusions.

The seasonal variation is diverse and depends on the geographical condition and location on Earth. The seasons are the effect of uneven heating of the earth by the sun due to the tilted axis of our planet. The seasonal variation corresponds to longer time-scales and larger spatial resolution, and it may affect the control strategy of the wind turbine. Weisser et al. [55] investigate the diurnal and seasonal variation of wind velocity in Grenada to estimate the project viability. The result for the case study is that, as the wind speed varied significantly, taking only an annual average wind speed may underestimate or overestimate the performances of the wind power plant. Hence, this stresses the need for accurate energy output modelling.

1.4. Why designing a wind turbine for hybrid power plants?

There are strong reasons to conduct design exploration research of hybrid power systems. The decarbonisation of the energy sector and climate change are the main drivers for implementing renewable energy. The energy transition comes with a cost: renewable energy being intermittent by nature. Hybrid power systems may serve as one of the options to relieve this shortcoming and lessen the burden of renewable energy integration to the grid, which is made possible due to its assumed feature of complementary generation. In a wind energy and solar PV-based hybrid power system, the wind generation should be optimised when the solar PV is generating less. Wind and solar energy sources vary over the diurnal and seasonal cycle. Thus, wind generation should be optimised to correspond to the diurnal and seasonal cycle. There is currently no research that explores this direction as the current hybrid power system optimisation mostly focuses on technology selection and capacity sizing of the hybrid power system components.

1.5. Research goals

Based on the gaps as mentioned earlier, this thesis aims to

explore a new concept design of a wind turbine for a hybrid power system and analyse its techno-economic feasibility.

The need for a wind turbine designed specifically for a given hybrid power system was discussed in section 1.4. This necessity leads to the first subgoal of this thesis: the proposal for a new design approach that emphasises on the complementary generation of the hybrid power system. The second subgoal is to determine the impact of this emphasis on the design of the wind turbine. The third subgoal is to evaluate the feasibility of the concept design in technical and economic terms. The technical feasibility study evaluates the design alteration in the second subgoal, and the economic feasibility study evaluates the costs in generating power of the design.

1.6. Scope

In this study of the diurnal and seasonal variance effect on the wind turbine design, it is concluded that the three relevant parameters that specify the difference to standard wind turbine design are: wind speed distribution, wind shear and turbulence intensity. To limit the scope of the study, the analysis in this thesis is more focused on the wind speed distribution difference. This decision is taken by considering the aim of this study, which is to investigate the optimum wind turbine design with the minimum electricity generation cost. The wind speed distribution directly governs the wind turbine output, which is then used to analyse the optimum design when coupled with the cost analysis of the system. The wind shear shall be used to estimate wind speed distribution at other hub heights not provided by the dataset. Thus, identifying of optimum hub heights is possible.

In this thesis, the power output analysis is assumed to be using uniform inflow wind profile with the average wind speed at the hub height. Although this may overlook the conclusion of [53], it is more interesting to see the difference between wind turbine power output with different configurations. Van Sark et al. [52] investigate the need for incorporating the shear profile in estimating power output by using the equivalent wind speed. For wind turbines with rotor diameter to hub height ratio lower than 1.8 and in cases where the wind shear coefficient value is uniform over the rotor plane with the value between -0.05 and 0.4, then the equivalent wind speed is within ±1% of the hub height wind speed. It is important to note that the result of the analysis may overestimate the real value of power output due to the wind shear effect. When one compares the results between, for instance, different rotor diameters, the overestimation will be neglected. The fatigue life analysis is beyond the scope of the study; thus, the wind shear analysis is limited to defining the vertical wind speed gradient on energy yield at different hub heights.

1.7. Research question

The dedicated research question is formulated within the borders of the set scope and stated as follows:

What is a technically and economically feasible concept design for a wind turbine for the application in a hybrid power system, and what are the design parameters that critically influence its performances?

The aim is to explore the economic feasibility of a new design concept for a wind turbine. Therefore the drivers that influence the feasibility of the design need to be identified. To simplify the process of answering the research question, subquestions are identified:

1. What is the optimum design of a wind turbine that takes diurnal and seasonal variation into account?

2. What are the important design parameters that influence the optimum design?

3. How does the design choice to emphasis complementary generation affect the wind turbine design?

4. How does the wind turbine perform within the hybrid power system compared to the standard design?

5. How does the wind-based hybrid power system benefit from a storage system?

The guideline described by the research question and subquestions, and limited by the scope defines the following research. The subquestion answers can be found in the following chapters: subquestion 1, 2 and 3 in chapter 4, subquestion 4 in chapter 5 and subquestion 5 in chapter 6.

1.8. Report outline

This first chapter serves as the introduction to the topic of wind turbine design for the hybrid power system to the reader. This introduction chapter helps in defining the goal of this thesis. The background on the need for a hybrid power system, followed by the discussion on the use of the wind turbine in this hybrid power system, is presented here. The current state of the wind-powered hybrid power system is analysed from the relevant literature. The need for wind turbine design tailored to the hybrid power is articulated, followed by the discussion on the diurnal and seasonal variation effect on wind turbine design parameters. The introduction chapter is concluded with the definition of the research goal that is to design a wind turbine for the hybrid power system usage. The conclusions drawn from the reviewed literature helps in defining the knowledge gap, thus used in tuning the research question and subquestions.

In chapter 2, the methodology of the analysis in the later chapters is presented. Chapter 3 presents the case study selection process and analysis. The site condition parameters required for the design of the wind turbine will be elaborated. The consideration of diurnal and seasonal variation in the site condition analysis is relevant in maximising the complementary generation of the designed wind turbine. The analysis of this variance is also presented in this chapter.

The wind turbine design process is the main focus of chapter 4. The chapter analyses the influence of design parameters on the optimum design. The analysis of the design's economic feasibility is conducted by employing a cost model. The design result is then modelled in several hybrid power system configurations to analyse its performance. This is presented in chapter 5. The influence of different operational modes on the design optimum is analysed in the same chapter.

The use of a storage system may be beneficial in a power system with renewable energy, and this is analysed in chapter 6. Further analysis of the design's economic feasibility is conducted by calculating the additional cost and benefit of the storage system.

Chapter 7 contains the discussion of the results of the design and analysis. This chapter reflects on the relevance of the results to the existing literature and possible future studies. The thesis is then finalised with the conclusions and recommendations in chapter 8.

2

Methodology

This chapter presents the methodology to answer the research questions. The methodology describes the background information and the detailed approach in assessing a hybrid power system. The overview of the methodology is presented in 2.1. Section 2.2 until section 2.6 presents the detailed analyses conducted, which is visualised in figure 2.1, to come to the result of this research.

2.1. Purpose and overview of the methodology

Wind turbines are complex machines that involve multiple fields of study: aerodynamics, electronics, electrical, and structural dynamics. Therefore, designing an all-new wind turbine requires organized and comprehensive steps. The design process is initiated with conceptual design and follows with preliminary and detailed design. The design procedure is then followed by a validation process before being released to the market as a full-fledged product [50] . Wiley defines the full process in chapter 6 in [50], which includes:

1. Investigation and justification of business opportunity
2. Product options identified and cross-functional buy-in secured
3. Conceptual design
4. Preliminary design
5. Detailed design
6. Factory test or validation + pre-series production
7. Validation or redesign + product introduction
8. Customer feedback, field experience and resolution

In the early stage of the design process, designers need to define the general product requirement as for instance, what the product should do? In the aforementioned process steps, this stage refers to step 1 to 3. The decision in this stage is often driven by a number of motivations such as market opportunity, new application, technology advancement, etc. The conceptual design defines the product specification that satisfies the product requirements. This design process translates the goals laid in the business proposition into a physically-achievable design. Typically, the conceptual design defines the physical parameters rotor diameter, hub height, nacelle and tower mass, and operational parameters such as rated power, rated wind speed, operational wind speed range, rotor speed range, design tip speed ratio and rated tip speed, control strategy, and peak power coefficient.

The conceptual design serves as the foundation for the preliminary design. The main activity in this design process is to confirm the previously determined concept with the practical values of each of the components [50]. At this stage, the design process is segmented and detailed for each of the wind turbine components. A generic breakdown of wind turbine design often composed of blade aerodynamic and structural design, drive train design, tower design and control design. The detailed design step is embedded within the preliminary design, and it is responsible for analyzing the elements of the wind turbine components. For example, designers perform a detailed analysis of the chord length and twist distribution in designing the rotor aerodynamic design. This design stage refers to step 4-5 in the aforementioned process steps. The rest of the steps relate to the validation and certification process.

This research aims to explore a new design of a wind turbine that takes the diurnal and seasonal variation into account. The impact of these variations on the wind turbine design parameters is what this research is investigating. Therefore, in line with the research objective, the chosen methodology will follow the first three steps of this wind turbine design approach. The wind turbine design process in this research will focus on the conceptual design step, and the detailed design on different components is beyond the scope of the study. Not only the detailed design involves a broad range of different analyses, but also it is not the main point of interest in this research. In addition to the wind turbine design, it is also required to define the environmental conditions for which the design is made and the operation models to simulate the performance. Thus, the proposed methodology aims to accommodate these analyses. The rest of this chapter further details the analyses taken in this research, which are visualised in figure 2.1.

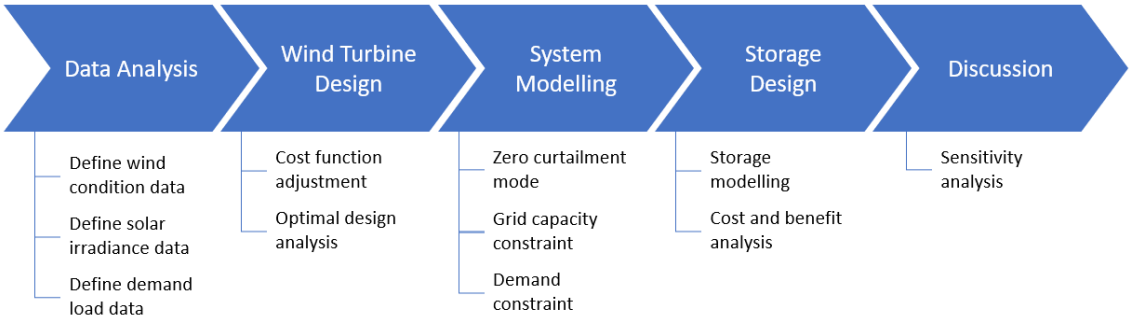

Figure 2.1: Structure of research into the wind turbine design for hybrid power system

2.2. Data procurement and analysis

The research of hybrid power system requires the use of wind speed and solar irradiance data as the input of the model. Such data are location-driven, meaning that different location will most likely have different sets of data. In this research, the location is chosen to be in Muppandal wind farm, located in the state of Tamil Nadu, a state in the southernmost part of India. Several considerations are taken in choosing the location, such as renewable source potential, renewable project development, and data availability and accessibility, being the most important. Chapter 3 further elaborates the reasoning on the choice of location.

Wind speed data are obtained from the India Wind Dataset developed by NREL as part of the India Renewable Integration Study [1]. The dataset contains simulated reanalysis data of wind speed, wind direction, temperature and pressure values at 40m, 80m, 100m and 120m height above the ground. The spatial resolution of the data is 3 km, and the temporal resolution is 5 minutes. The wind dataset is for the year of 2014. For further analysis in this research, the raw data is averaged to get data with 10-minutes temporal resolution. The shear or wind profile can be analysed from wind speed data at four different heights in the data set and represented as shear coefficients. The shear coefficient is useful to extrapolate the wind data to higher heights. We use this wind speed data to calculate the wind power at three different hub heights, i.e., 80m, 120m and 160m, in later chapters on finding the optimum wind turbine design. This analysis also identifies the diurnal and seasonal wind condition.

Given the sunrise and sunset time, the diurnal wind condition is considered from the wind dataset as the wind during the night time. The sunrise and sunset time of the location are extracted from [4]. The seasonal wind condition is considered from the wind dataset as the period with lower average wind speed.

Solar irradiance data are obtained from Solcast, which provide data with a temporal resolution of 10 minutes. The dataset includes values for air temperature, cloud opacity, and global horizontal irradiance (GHI). The solar PV output depends on the amount of tilted GHI absorbed by the surface, thus governed by the GHI value, air mass, and angle of incidence [47]. In this research, the capacity of solar PV is capped at a certain capacity and we only use the GHI value to estimate the power fluctuations at each time steps. Hence, the lack of parameter air mass and angle of incidence is not a problem. The solar datasets are available for multiple years, and 2014 data is used for this research to match with the wind speed data.

Demand profile data used for the system modelling are obtained from the study on demand-side management of The Energy and Resources Institute (TERI) [43]. The report contains typical averaged hourly demand profile for every month in the state of Tamil Nadu. The hourly demand data is translated into data with 10-minutes temporal resolution by interpolation to match with the wind and solar generation data. In this research, the maximum demand value is also capped at a certain capacity, thus, we only use the demand profile to estimate the demand value fluctuations at different time steps. The system modelling requires the demand profile data as the input.

To conclude, this research is working with 52560 data points of 10-minutes averages for the year 2014. The compiled data are then analysed in context with the research theme of complementary generation, i.e., the diurnal and seasonal trend of the dataset are investigated. Chapter 3 presents the full discussion on the data analysis and serves as the basis for analyses in later chapters.

2.3. Wind turbine design

As previously mentioned in the introduction, optimising the wind turbine design is one of the ways to optimise the hybrid power system. While designing a new wind turbine involves several steps and various detailed components design, this research will focus on the conceptual design phase. The conceptual design utilises the scaling trend method to estimate the physical parameter of the wind turbine. [28] propose a system-friendly wind turbine design that employs a larger rotor diameter. This research uses a similar approach in designing the wind turbine by modifying the specific power rating, the ratio of the generator capacity to the rotor size. Thus, the machine rating is kept constant at 3 MW while the rotor size are modified. This design process is then programmed to optimise the design by minimisation of the cost of electricity, based on the wind speed data and the employed cost function.

The cost function used in this research is adapted from the NREL cost and scaling model [26]. NREL estimates the cost of the wind turbine elements by calculating their mass, which are functions of the rotor diameter, hub height, the machine rating or a combination between these. These relationships between parameters, e.g., between rotor diameter and mass and then between mass and cost, are generated from data of commercially available wind turbines as well as conceptual models, especially for wind turbines larger than 1 to 2 MW. Thus, the cost functions are approximated by a fit of the employed wind turbine data. It is important to note that this method overlook the fact that some cost of the components are step functions, e.g., for gear boxes, once a certain torque level is reached, the next size of gear box is needed. The cost function is dissected into 26 components which can be categorised as the capital expenditure (CapEx) and the operational expenditure (OpEx) for the wind turbine.

However, such an approach is only useful for scaling up/down between different wind turbine powers. An increase in diameter includes implicitly an increase in the wind turbine power, which is different from the approach taken in this research. Direct use of the cost model will result in the optimum that is less valid for the optimisation process. The principal difference between the existing model and the intended optimisation process results in the need for a cost model adjustment. The adjustment is made

on the blade mass function; thus, the mass and cost of other parameters that are a function of the rotor size will also be affected. This adjustment is conducted by looking at the commercial wind turbines data with a single machine rating but multiple rotor sizes and learning their mass-to-rotor size trends. Such type of wind turbines has a more similar approach to this research.

With having the wind speed data and cost model identified, **the design for the optimum wind turbine** can be conducted. The optimum design lies where the levelized cost of electricity (LCOE) of the wind turbine is at the lowest. LCOE is calculated by the following equation

$$LCOE_{turbine} = \frac{FCR \times CAPEX + OPEX}{AEP} \tag{2.1}$$

FCR is the fixed charge rate, and AEP is the annual energy produced. The FCR is the percentage of the initial capital cost needed to cover the capital cost, a return on debt and equity, and other fixed charges. Thus, in general, the LCOE is affected by the cost component (CAPEX and OPEX) and the energy Production component (AEP). AEP is a function of the rotor diameter, hub height and wind speed distribution data. Altering these values will change the optimum. The analysis of how this optimum changes is presented in chapter 3. For the modelling purpose in chapter 4, the calculation of LCOE is integral for different operational topologies analysis: zero constraint operation, grid capacity constrained and demand constrained.

2.4. System modelling

Different operation modes are modelled to be able to identify the impact of the hybrid power system's complementary generation on the wind turbine design. The operation modes simulate the power output of the wind turbine and the cost of electricity at different rotor sizes, hub heights and wind datasets. The different datasets that include the full wind dataset, diurnal wind dataset and the seasonal wind dataset define the operational modes analysed in this research. Initially, the optimum wind turbine design for the full-year operation is analysed. The design result of this operation mode is regarded as the baseline design and other operations modes are compared to this mode to identify the modification on the wind turbine design. In this particular analysis, zero-curtailment topology is assumed. This topology is a hypothetical topology that assumes infinite generation evacuation capacity, which has never been the case in the practice.

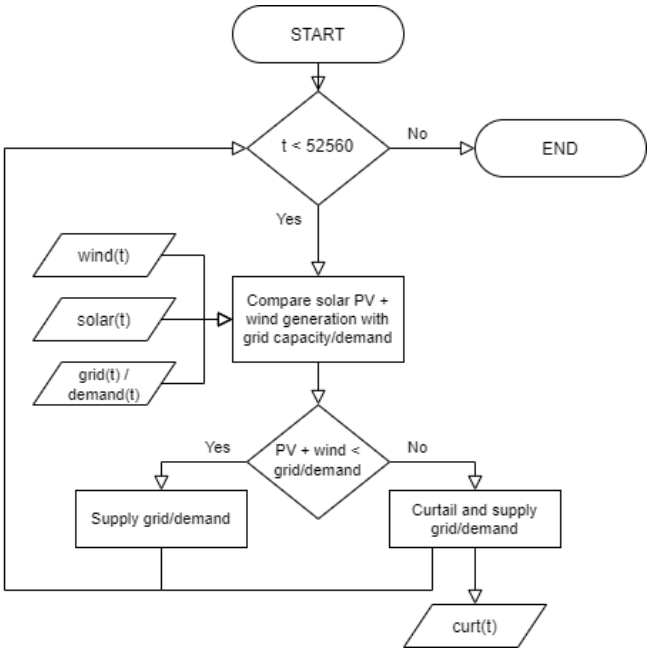

Figure 2.2: Operational model flowchart

In total this research employs three different topologies: zero curtailment, grid constrained and demand load supplying topology. Figure 2.2 presents the general operation procedure for the grid constrained topology and the demand load supplying topology. In the other two topologies, the wind turbine operation is coupled with a solar PV in a hybrid power system. Both of the wind turbine and solar PV capacities are normalised at the same capacity of 3 MW. First, the hybrid power system is modeled supplying a grid with a maximum evacuation capacity normalized at 3 MW. The operation of this hybrid power system is configured such that, in case of a combined wind power and solar PV output larger than the grid capacity, the wind turbine output is curtailed. The curtailment ranges between 0 and 3 MW when the solar PV is not generating and fully generating, respectively. The second hybrid power system model supplies a demand with a maximum load of 3 MW. The same configuration is employed that curtailment is prioritized for wind power generation. In this topology, the solar PV generation may also be curtailed due to the low demand load level. The result of the analysis will identify the AEP reduction due to curtailment and a change of the optimum design due to the AEP change.

2.5. Storage design

The storage system could be beneficial for the hybrid power system as it enables shifts of generation between different time steps. The storage system can reduce curtailment by storing the spilt energy and supplying to the grid/demand when there is a deficit in the generation, thus opening up the power system for an opportunity in a new market; e.g. ancillary services [23]. This analysis aims to identify the maximum storage capacity needed to store the curtailed energy, followed by analysis on cases of partial capacities. **The storage system model** is presented in figure 2.3.

At a certain time step, when the power combined from the wind turbine and solar PV exceeds the grid capacity or load demand, the excess energy will be curtailed. When there is curtailment, which also means that the grid is 100% used or the demand is 100% met, space at that particular time (space(t)) equals to 0. Vice versa, when the power from the wind turbine and solar PV is less than the maximum grid capacity or the load demand, there is no curtailment on the power generated, and the space is equal to the remaining capacity of the grid after being used to evacuate the energy or the unmet demand after being supplied from the wind turbine and solar PV. In short, the negatively correlated values between the curtailment and the available space can be written in equation 2.2.

$$\begin{aligned} curt(t) = 0; space(t) > 0 \\ curt(t) > 0; space(t) = 0 \end{aligned} \tag{2.2}$$

with curt(t) being the curtailment at time t. Initially, to calculate the maximum required storage capacity, the maximum State of Charge (maxSOC) is set to be infinitely large thus all energy curtailed will be either captured in the storage or supplied to the grid/demand. This way we can define the maximum storage capacity in the unit of kWh. When lower capacity storage is applied, a portion of the curtailed energy will be dumped/shed in case of a full storage capacity and at the same time, when a full grid capacity or low load demand. Initially, the SOC is set to be zero in the simulation.

The storage model results in four states of operation: charge, charge and shed energy, partial discharge and supply, and full discharge and supply. At a certain time step, if there is energy curtailment, the battery is programmed to store this energy. If there is enough capacity of battery, then all of the curtailed energy at that time step will be stored. The final state of charge will be the sum of the curtailed energy and the initial state of charge at the particular time step. If there is not enough space to store the curtailed energy, then the battery will be charged until reaching its maximum capacity, and the remainding curtailed energy will be unutilised. In other cases, when there is no curtailment, the battery is programmed to discharge and filling the available space at the particular time step. If the initial battery state of charge is larger than the available space, then the battery will be discharged partially and fills the space. The final state of charge equals to the initial state of charge subtracted by the discharged energy. If the initial state of charge is lower than the available space, then the battery will be fully discharged to its lower bound state of charge.

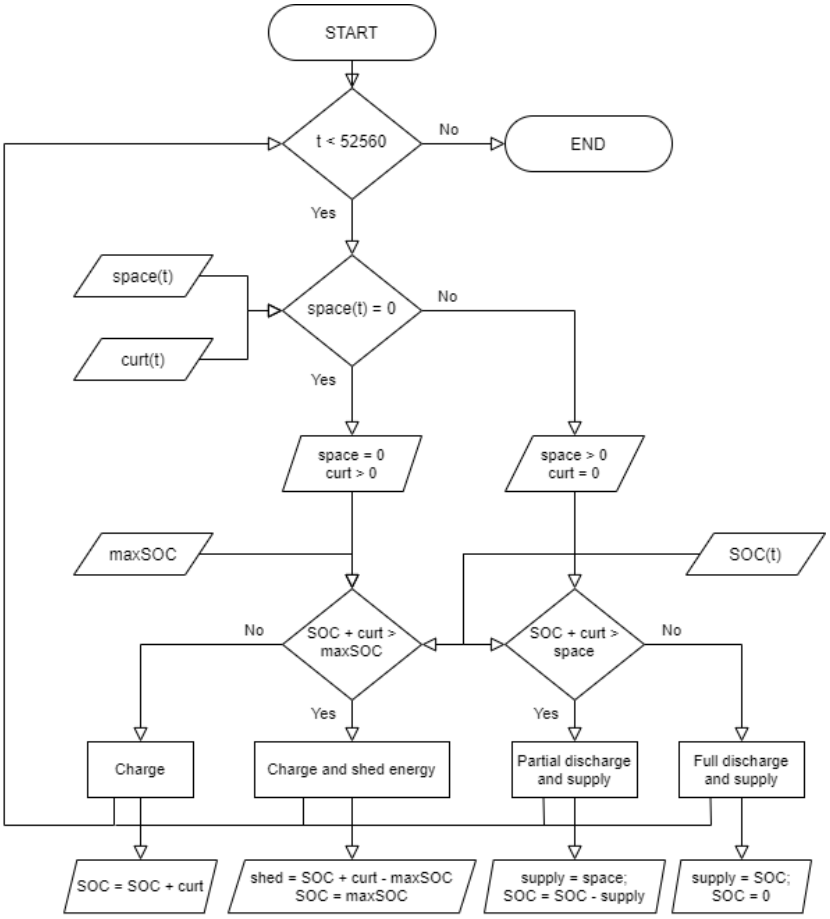

Figure 2.3: Battery model flowchart

The cost and benefit analysis of the storage system is what follows next. This analysis aims to identify the trade-off between the additional cost and benefit of applying a storage system. NREL compiled studies on battery cost projection from over 25 publications [20]. For the year 2020, the cost projections are 299.81$/kWh, 332.94$/kWh, and 366.63$/kWh, for low, mid and high projections. The mid values will be used in this thesis for further analysis. The use of storage enables the hybrid power system to alleviate the integration cost of renewable energy by having an additional dispatchable capacity. Jay et al. [12] identified several unpriced costs and benefits of wind energy . The social costs are the products of wind's variability and partial unpredictability which creates difficulties for system operators in managing the grid, including operational cost, transmission cost, curtailment cost, and capacity cost. Therefore, the benefit of the storage is estimated from the reduction of these social costs. Another substantial benefit of the storage system is the pollution reduction benefits as it enables the use of additional energy generated from renewables.

2.6. Discussion

The results from previous analyses is then discussed to identify the scientific implication and limitation of the research. The analysis is then followed with the sensitivity analysis. In this analysis, alternative scenarios are fed to the model to check the robustness of the results storage model. These scenarios include future projections; e.g., the battery cost reduction. These analyses are presented in chapter 7.

3

Site condition analysis of the case study

This chapter presents the analysis of the input data for this research. This chapter is initialised with the outline of the analysis in section 3.1 which then followed with the arguments on the choice of the site condition, which is presented in section 3.2. Section 3.3 describes the climate and season of the case study. Section 3.4 presents the data of wind conditions, solar irradiance and demand profile that is needed for the input of the hyrbid power system operation modelling. Section 3.5 presents the summary of the data that will be used for further analyses in this research.

3.1. Outline of the analysis

The site condition analysis is a prerequisite to start the wind turbine design process. This analysis indicates the important parameters that influence the design of the wind turbine. This thesis aims to explore the design of the wind turbine operating in a hybrid power system that take the diurnal and seasonal variation into account. The design emphasis on the complementarity of the generations, wind and solar, and the demand load. Hence, it is useful to identify the diurnal and seasonal variation influence on the hyrbid power system components, especially on the design parameters of the wind turbine.

The solar irradiance data and demand load data are required to model the solar PV generation and demand load, respectively, in the hybrid power system. Subsequently, In section 1.3 and scope of research, it is identified that the parameter required to describe the site condition are the wind speed and wind shear, Hence, this chapters results in the definition of the wind speed data for different operational modes, full-year, night-time and low-wind speed season.

3.2. Arguments for Muppandal, India

In order to have a realistic data and realistic correlation between the different parameters, a case study is employed. For the case study, the site Muppandal in India is chosen, as shown in the map in figure 3.1. Before going into the details of the arguments in choosing this location, it is useful to identify the considerations taken in picking the location of the case study. This way, we can narrow down the options and lead to the choice of the case study location. The considerations include :

- **The availability and accessibility of data.** Due to the limited time of the project, there will be no on-site data measurement. A measurement dataset with a year length is the minimum requirement to identify the seasonal variation in this research. Thus, the data availability of the potential

sites is the next priority in searching for the location. The dataset also needs to have a sufficient temporal resolution to identify the diurnal variation. Data with at least an hourly measurement is required, but data with finer details are also applicable. [22][7].

- **The relevance of developing a hybrid power system.** This consideration regards situations where there is an opportunity for the hybrid power system to be applied. These situations include, for instance, the grid capacity congestion due to peaking wind generation and insufficient grid, power blackouts due to the inflexible power system with renewable energy plants, plans for large capacity of renewable integration, and encouraging policy for renewable development.
- **The potential and availability of renewable sources.** As the hybrid power system in this study is based on wind and solar power generation, adequate sources of these renewable sources are essential. To simplify the search, locations with already existing power plants implicitly yield this characteristic. Such analysis is integral for project developers in the planning of renewable-sourced power plants

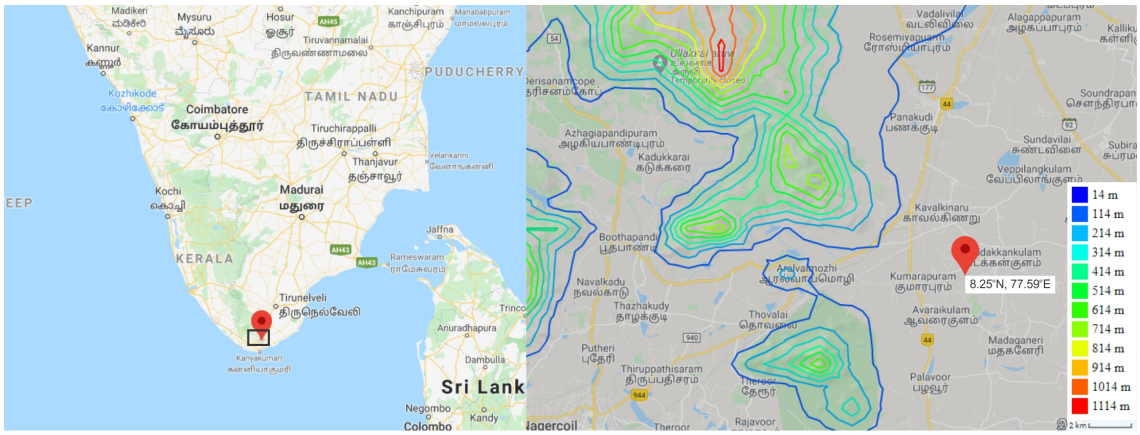

Figure 3.1: Location of Muppandal wind farm and topographical map of its surounding. The map is extracted from Google maps and the topographical map is generated from Contour Map Creator [3]

The availability and accessibility of data

In this research, data acquisition is the highest priority before other considerations. This meteorological data will be based on meteorological institute measurements and simulation. NREL provides extensive met data for the United States, India and Central Asia that includes data for air pressure, air temperature, wind speed and wind direction. As previously mentioned in chapter 2, this research employs the India Wind Dataset. This dataset meets the requirement stated in the consideration, thus, deemed to be sufficient for further analysis in this research. At the same time, India is an ideal place as the starting point in searching for the potential location due to their abundant solar irradiation and the plans on developing the application of wind energy. These reasonings will be elaborated next.

The relevance of developing a hybrid power system

India has been one of the countries who push their implementation on renewable energy into their generation mix, including wind energy. The Government of India has set a target of 175 GW installed of renewable energy capacity by the year 2022, which includes 100 GW from solar, 60 GW from wind, up from 37 GW wind and 32 GW solar in 2019 [39]. The increase in renewable energy penetration, without proper balancing between the mix, may lead up to the loss in flexibility in the power system. This scenario is in line with the study of a hybrid power system and, in fact, acknowledged by the government. In 2018, the Ministry of New and Renewable Energy (MNRE) issued the National Solar-Wind Hybrid policy [39]. The objective of this policy is to provide a framework for developing grid-connected hybrid power systems. With the implementation of this policy, it is projected that 10 GW hybrid power systems will be developed by the end of 2022 [44].

The selection for the location of the case study is further narrowed down by choosing the potential state in India, which leads to Tamil Nadu. Tamil Nadu is a state in southern India, and it is leading the development of wind energy in the country. By the end of 2019, more than 25% of the installed wind power capacity is located in Tamil Nadu with a capacity of 8.9 GW [39]. In the past, this rapid growth of renewable energy plants is not coupled with sufficient evacuation infrastructure [45]. This insufficiency leads to grid congestion, renewable energy curtailment and power outage. During the peak wind seasons, when wind power generation has excess, a curtailment is imperative as the inter-regional grid is unable to deliver power to neighbouring states. Vice versa, power outages occurred during the low generation period due to the grid's inability to draw power from neighbouring states [17]. Central Electricity Authority has proposed to increase the transmission capacity to support the planned growth of renewable energy [14]. This information highlights the importance of increasing the power system flexibility to integrate renewable energy successfully.

The potential and availability of renewable sources

The discussion on two of the considerations leads us to choose an established wind farm in the state of Tamil Nadu as the case study. For this research, it is decided to choose the Muppandal wind farm as the case study location. It is one of the largest wind farms in India with a total capacity of around 1500 MW, which indicate a high wind energy potential [31]. 149.5 MW of the total capacity is comprised of wind turbines commissioned before the year 2002, with capacities of 500kW or below. These wind turbines are subjected to repowering with newer technologies [30]. Hence, replacement with a wind-based hybrid power system can tackle two problems of wind turbines repowering and better integration at the same time. Established wind farms imply the presence of a transmission system, which also motivates choosing the location.

3.3. Climate and season

The Muppandal wind farm is located at Latitude 8.25°N and Longitude 77.59°E. This region is bordered on the east with the coastal area of the bay of Bengal, and on the west with the mountainous area of the Western Ghats and the state of Kerala. The high yield of wind energy in this region is due to its geographical condition where the wind from the Arabian sea gusts through the mountain passes in its west into this region. The wind farm is located in the district of Kanyakumari with arid-interior climate. The southwesterly and northeasterly monsoon drive the four seasons in this location, which includes:

- **Summer (March-May).** This season is also called pre-monsoon. Temperature peaks in this season as the sun moves toward the northern hemisphere. This season is the transition between the relatively dry winter and the wet monsoon season. The rising temperature over the land creates low-pressure areas which attract the flow of the southwesterly monsoon [27].
- **Monsoon (June-September).** The monsoon starts when the humid south-western monsoon flow enters India from the Bay of Bengal and the Arabian Sea. Most parts of India but Tamil Nadu receive their highest rainfall during this season due to the rain shadow effect. The Western Ghast partially blocks the monsoon current from the Arabian Sea. The monsoon lost its humidity in the form of copious rainfalls in the western slope, which leave the eastern slope, where this case study is located, relatively dryer [27].
- **Post-monsoon (October-December).** As the sun moves to the southern hemisphere, temperature over the land begins to fall. From the beginning of October, monsoon begins to recede from this country and brings rainfall to the southern part of the country. Muppandal experiences its highest rainfall during this season. Northeasterly monsoon enters the country while bringing cold, dry air from the Himalayas [27].
- **Winter (January-February).** This season is the aftermath of the cool and dry northeasterly monsoon. As the monsoon retreats to the south, the clouds disappear, and the sky becomes clear. This season is typically dry with the lowest rainfalls. Temperature is also relatively the lowest, and it starts to rise around mid-March.

From the discussion above, it is evident that the monsoon-driven seasons affects the seasonal variation of temperature and precipitation. Thus, the data of average temperature, precipitable water, relative humidity and cloud opacity are obtained from Solcast and analysed to confirm this variation. The precipitable water value is used to estimate the seasonal variation of the rainfall. The precipitable water value tells the amount of liquid water if water vapour from the surface to the top of the atmosphere is condensed [41]. The seasonal variation is confirmed with the data from Solcast, shown in figure 3.2.

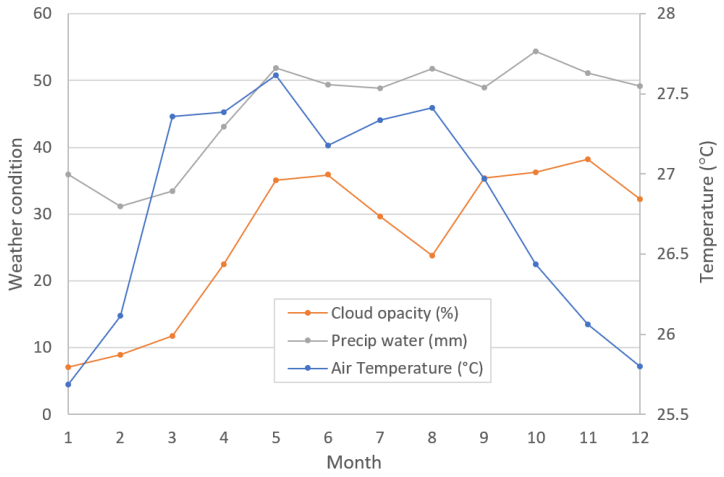

Figure 3.2: Seasonal variation on temperature, precipitable water and cloud opacity of Muppandal for the year 2014

The Muppandal 2014 data shows the peak temperature in May and a dip of temperature between October - February. Low cloud opacity and precipitable water are observed during winter and early summer (January - March) which then rises during summer and early monsoon (March - June). As the passing southwesterly monsoon proceeds to move to the north, cloud opacity lowers, and the temperature rises again in the mid of the year. The Precipitable water value remains high, which indicates the hot and humid air during this period. Ahead of August, monsoon starts to recede and causes heavy rainfall, which can be identified from the rising value of precipitable water and cloud opacity, and dipping temperature. This analysis is indirectly related to the seasonal variation of the wind and solar power output. For instance, cloud opacity will affect the solar generation. The following sections will elaborate more on this subject.

3.4. Diurnal and seasonal variation of wind, solar irradiance and demand

This section presents the input data of wind conditions, solar irradiance and the demand profile. This section also identifies the seasonal variation of these parameters.

3.4.1. Wind condition

As mentioned in the methodology chapter, wind speed data are acquired from the India Wind dataset by NREL. Met data are available at four heights, and the data at 160-meter height is extrapolated from this data. The wind speed seasonal variation shows a significant intra-annual difference, which is shown in figure 3.3. In this figure, wind speed is averaged per month. Wind speed is relatively constant during post-monsoon until summer (October-April). It is observed that the wind speed begins to rise at the end of summer and peaks during the monsoon season (May-September). The peak of the average monthly wind speed is around 2.5 times higher than the low-wind speed period.

Figure 3.4 shows the diurnal variation of the wind speed for different seasons, represented by February for winter, May for summer, July for monsoon and November for post-monsoon. Sunrise and sunset

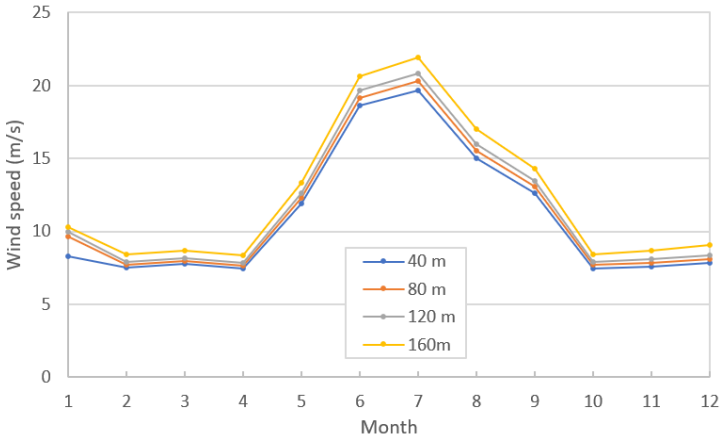

Figure 3.3: Wind speed seasonal variation at hub height of 120m

time is relatively constant, being around 6.20 AM to 6.20 PM with maximum deviations of 20 minutes. It is observed from figure 3.4 that the wind speed diurnal variation is less apparent than the seasonal variation. Wind speed is generally higher during the night time, with an exception for the winter evenings. Between summer and post-monsoon, wind speed dips at the middle of the day, which is negatively correlated to the solar irradiance. Winter has a different wind speed variation profile as it reaches the lowest at around 8 PM. The seasonal variation is also perceivable in this figure.

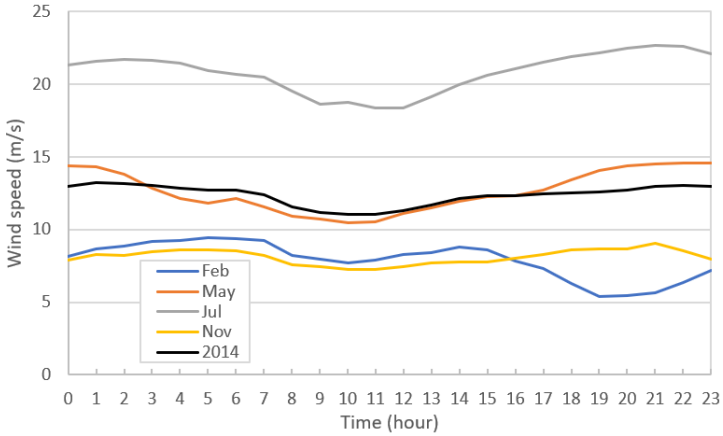

Figure 3.4: Diurnal wind speed variation at hub height=120m

The analysis of the wind data also reveals the diurnal variation of the wind profile. Figure 3.5b shows the diurnal variation of wind speed at four different hub heights. Typically, wind speed gradient over the night is higher than during the day due to the lack of mixing in ABL. The most important factor that drives the mixing is the temperature difference between the ground surface and the air. In general, regardless of the time of the day, warmer surfaces develop a mixed layer, and colder surfaces create stable ABLs [48]. However, ABL mixing is more likely to happen during the day due to the heating from the sun. The diurnal variation is relatively constant throughout the year, as shown by the the similar diurnal pattern in figure 3.4, due to the small average temperature variation throughout the year with only 1.5 °C difference between the highest and the lowest. The wind shear profile can be expressed in the power law, which reads:

$$U(z) = U_{hub}\left(\frac{z}{z_{hub}}\right)^{\alpha} \tag{3.1}$$

with $U(z)$ denotes the average wind speed as a function of height, z. z_{hub} and U_{hub} denotes the hub height and the wind speed at hub height. The exponent α is used to define the wind profile with the power law, described in the equation 3.1. Figure 3.5a presents the histogram for the wind shear

exponent. For the same reason, it is observed that higher shear exponents, α, are more likely to happen during the night than during the day. For standard wind turbine design, IEC standard suggests an exponent of 0.2. For the analysis that considers diurnal variation in this research, the higher shear exponent will be employed.

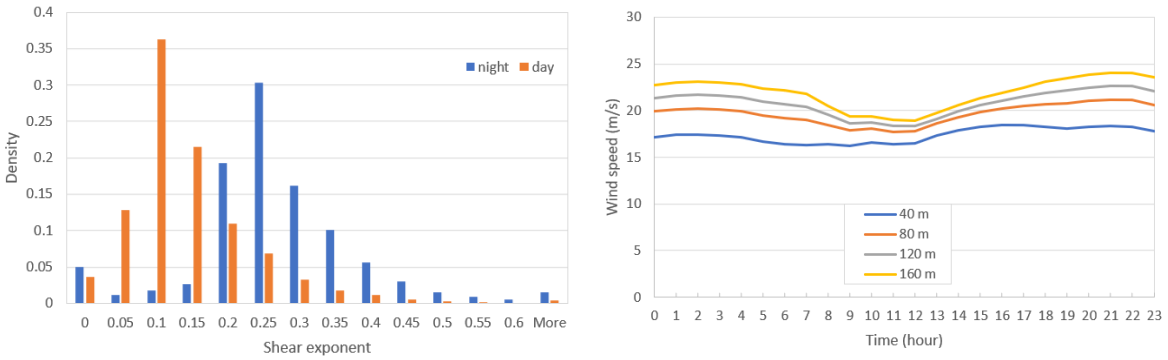

(a) (b)

Figure 3.5: (a) Shear exponent probability density for night and day data. (b) Diurnal variation of wind profile in July 2014.

The seasonal variation also affects the direction from which the wind enters the wind farm. Figure 3.6 presents the wind rose graphs for each season. During winter, winds are mostly flowing from the north and north-northeast. The prevailing wind direction changes during the end of summer to the west-northwest due to the forthcoming monsoon. During the monsoon season, winds are only flowing from the west with significantly higher wind speeds. The post-monsoon season is the transitional phase between the monsoon and winter. Hence, both winds coming from the west and north are identified during this period.

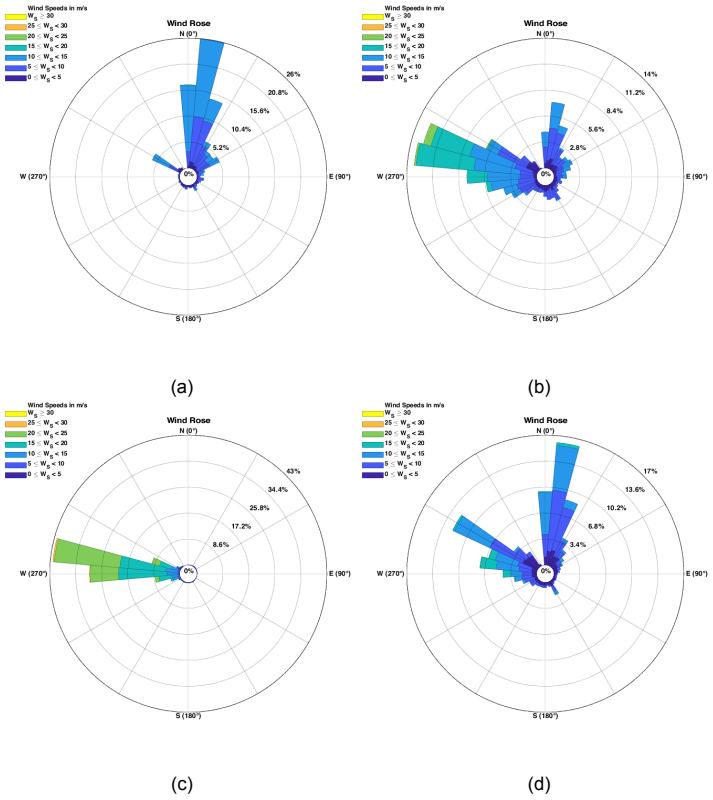

(a) (b)

(c) (d)

Figure 3.6: Wind rose for wind speed at hub height=120m in (a) winter, (b) summer, (c) monsoon and (d) post-monsoon.

It is observed from figure 3.6 that the wind direction in each season coincides with the movement

of the monsoon. The southwesterly monsoon induces the wind that flows from the west as it enters the country and later as it recedes, the monsoon induces the wind from the north. The magnitude of the wind speed is affected by the location of the wind farm. Muppandal wind farm is located to the east of the Aralvaimozhi mountain pass. This pass in the Western Ghats mountain range acts like a funnel that accelerates the wind speed significantly for the winds flowing from the west. While to the north of the wind farm, the flatter topography explains the lower wind speed. This condition can be observed in figure 3.1

3.4.2. Solar irradiance

The monthly average solar irradiance in the Muppandal wind farm is presented in figure 3.7 which indicate its seasonal variation in 2014. The 2015 data is employed in this graphic to understand the seasonal variation better. It is observed that solar irradiance peaks in between winter and summer, followed by a drop for several months during summer and monsoon. A second peak is observed around the end of the monsoon season before it dips to its lowest value during post-monsoon season. As the climate is a complex system, the different progression of the monsoon may have caused the difference between the 2014 and 2015 data. For 2014 data, the peak is in March and the second peak is in September. In July, where the average wind speed is at its highest during the monsoon season, solar irradiance is at its local minimum. The lowest value in 2014 is in the middle of the post-monsoon season, November.

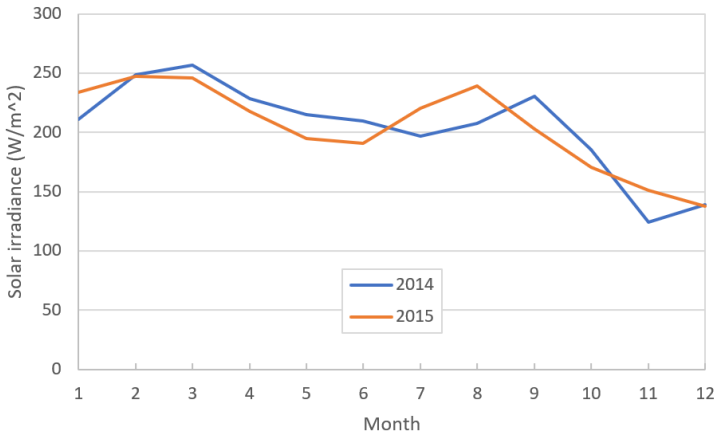

Figure 3.7: Seasonal variation of solar irradiance

In September, the monsoon had moved to the northern part of the country, which explains the lower cloud opacity, which is shown in figure 3.2, and the increase of solar irradiance in the southern part of the country. Diurnal variation of the solar irradiance for local and global maximum and minimum from figure 3.7 are presented in figure 3.8. Similar diurnal variations are observed for different months. The month with the lowest solar irradiance, November, has its maximum average solar irradiance at around 75% of the maximum average in March.

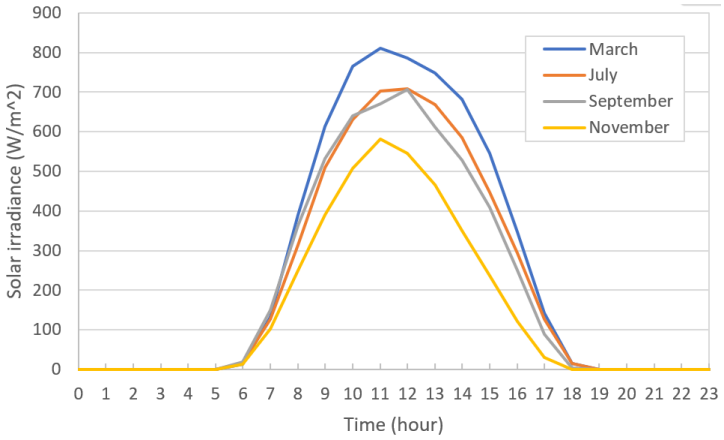

Figure 3.8: Diurnal variation of solar irradiance

3.4.3. Demand profile

To identify the seasonal demand profile variation, hourly averaged demand load data from [43] are employed. Figure 3.9 presents the normalised monthly average demand in 2014. The average demand peaks between winter and summer and begins to drop through summer until the end of the monsoon season. A local maximum is observed in between the monsoon and post-monsoon season, in October. The post-monsoon months have lower average demand in a year, with November demand being the lowest.

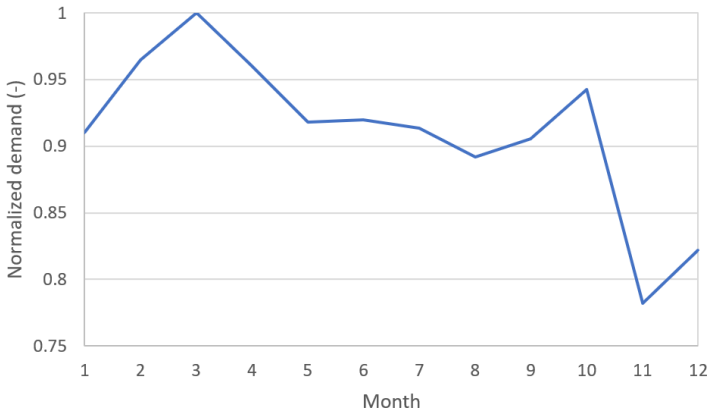

Figure 3.9: Seasonal variation of demand

The diurnal variation of the demand profile is presented in figure 3.10. Typically, the daily demand profile consists of: night lean, morning peak, day lean and evening peak. These features are less evident over the summer period than in winter due to the increase of use in space cooling over the day [43]. Thus the load throughout the day is more constant. In cooler months such as February and November, the uses of space cooling appliances are more concentrated in the evening, thus creating a peak around 7 PM which then recedes at midnight. The increased demand in the evening is retained until past midnight in warmer months such as May and July.

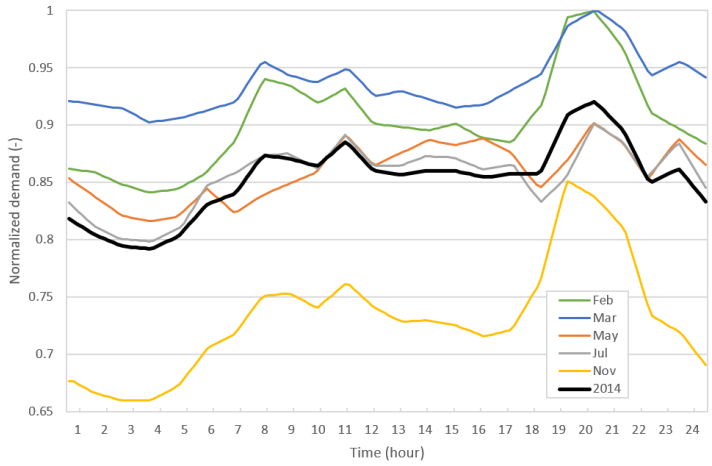

Figure 3.10: Seasonal variation of diurnal demand

3.5. Selected conditions for wind turbine design and hybrid system analysis

To summarise the diurnal and seasonal variation discussion in the previous sections, the interaction between the variations is presented in this section. This section also determines the wind data that is used for the wind turbine design and the solar and demand data for the hybrid power system modelling.

3.5.1. Complementarity analysis

To gain insight into how the variation between the generations and demand relate to each other is important for the hybrid power system design. Figure 3.11 presents the comparison between the variation of the normalised monthly average wind and solar generation sources and the demand. The average solar irradiance is following a seasonal variation similar to that of the demand with the peak in early summer, local minimum in monsoon season which then is followed by local maxima, and reaching their lowest point in the post-monsoon season. It is important to note that despite the confirmed similarity, solar generation only occurs during the day. Thus, let alone following the seasonal demand variation, to meet the daily demand pattern with solar generation alone is impossible.

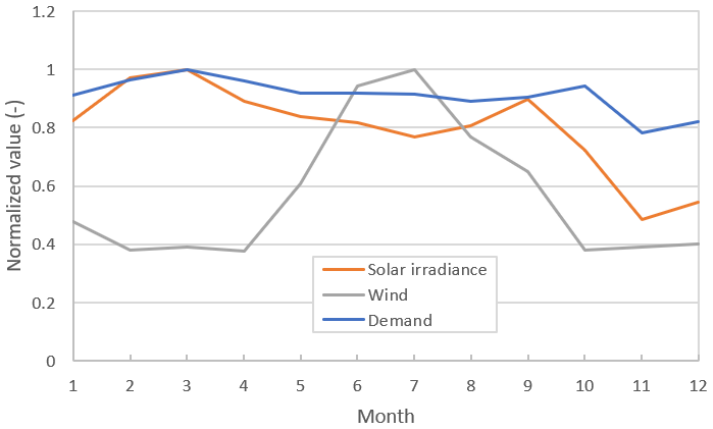

Figure 3.11: Seasonal variation comparison for normalised wind speed, solar irradiance and demand

Wind speed seasonal variation shows a negative correlation with the solar irradiance from the beginning of the year until the end of the monsoon season. Beyond the monsoon season, both the solar

irradiance and wind speed are dropping. As it is also observed that the average demand drops during the post-monsoon season, a hybrid power system that combines the wind and solar generation may be able to match the demand. The power system operation modelling in the later chapters will further analyse this possibility. It is important to note that the wind data employed in figure 3.11 is a preliminary estimation of the wind power and subject to change. Unlike solar irradiance that directly affects the solar PV output, wind turbine power output is in a cubic function of wind speed up to the rated power, where it becomes constant. Moreover, this research studies the impact of different wind turbine specific powers which govern the final wind turbine power output. Thus, at this stage, the actual wind power variation is yet to be found.

3.5.2. Wind speed data for wind turbine design and modelling

As previously mentioned in the methodology, this research analyses three wind turbine design cases: full-year wind turbine that serves as the baseline design, diurnal variation-optimised design, and seasonal variation-optimised design. The baseline design considers the full-year wind data. The diurnal variation-optimised design aims to focus the wind power generation when the solar power generation is at the lowest, which is at night. Thus, this design considers the wind speed data from after the sunset until the sunrise as the input. For the seasonal variation-optimised design, the wind power generation is prioritised on the seasonal period when the solar power generation is at the lowest, which is in the post-monsoon season. As observed from figure 3.11, the low wind speed condition in the post-monsoon season is extended until midsummer. Thus, the wind speed that is taken into account for the seasonal variation-optimised design includes wind speed data from October until April.

The Weibull probability distribution function, which is expressed in:

$$f_X(U;\eta,\beta) = \begin{cases} \frac{\beta}{\eta}\left(\frac{U}{\eta}\right)^{\beta-1} \exp\left(-(U/\eta)^{\beta}\right) & U \geq 0 \\ 0 & U < 0 \end{cases} \tag{3.2}$$

$$\eta = \frac{U_{avg}}{\Gamma(1+\frac{1}{\beta})} \tag{3.3}$$

represents the frequency at which a specific wind speed U is measured. η is the Weibull scale parameter proportional to the mean wind speed and expressed in m/s, calculated in equation 3.3. The scale parameter is a measure of how windy the site is. The Weibull shape parameter, β, tells how peaked is the distribution and defines the shape the distribution. In this research, each dataset is fitted with the Weibull distribution in MATLAB to estimate their shape and scale parameters.

Figure 3.12 and 3.13 presents the histogram and Weibull fit for the night time dataset and the low wind speed seasons dataset, respectively. ”All data” represents the full data that contains 52560 time-steps, and the ”night” and ”season” data are the filtered data for the nighttime only and low wind speed seasons only, respectively. It is observed that the difference between the night and the full data is small, with a slightly higher occurrence of higher wind speed at night. For the low wind speed seasons data, as expected, significant differences are observed. The Weibull shape and scale parameter for each dataset is presented in table 3.1 for the full dataset, 3.2 for the night dataset and 3.3 for the low wind speed seasons dataset. An increase in the hub height results in a higher scale parameter due to the wind shear profile. The parameters in tables 3.1-3.3 will be used as the input for the operational modes of the wind turbine. Together with the solar irradiance and the demand load data, the wind data in these tables are used as the input for the analysis of the grid-connected and or the demand load supplying hybrid power system.

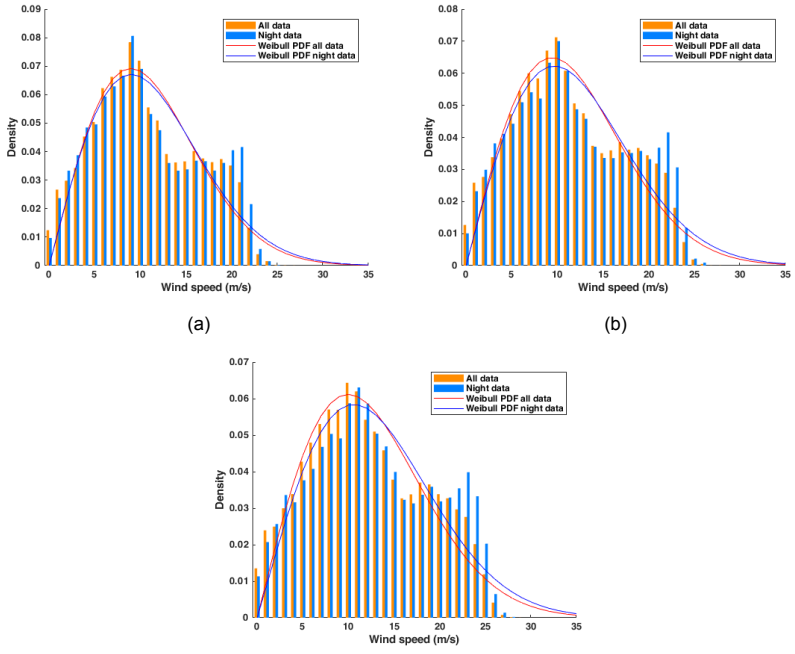

(a) (b)

(c)

Figure 3.12: Histogram and weibull distribution for night-time and full-data wind speed at (a) hub height=80m, (b) hub height=120m, (c) hub height=160m.

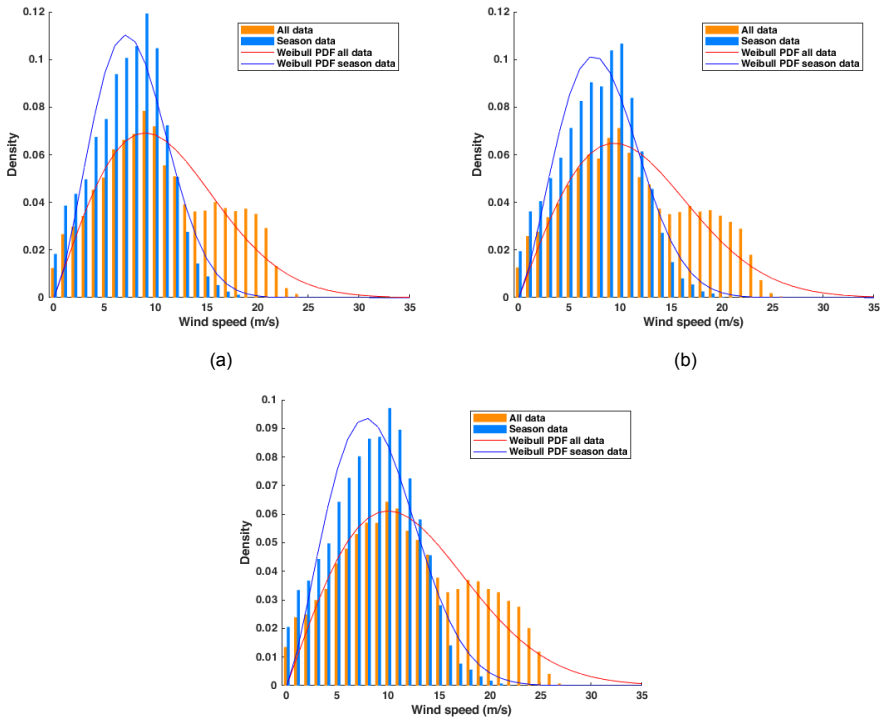

(a) (b)

(c)

Figure 3.13: Histogram and weibull distribution for low wind speed season data and all data wind speed at (a) hub height=80m, (b) hub height=120m, (c) hub height=160m.

Table 3.1: Weibull parameters for Muppandal at various hub heights

Hub height	scale	shape	V_{avg}
160	14.062	2.008	12.46
120	13.25	2	11.74
80	12.501	2.028	11.08

Table 3.2: Weibull parameters for Muppandal night wind data at various hub heights

Hub height	scale	shape	V_{avg}
160	14.81	2.026	13.12
120	13.725	1.989	12.16
80	12.754	1.995	11.3

Table 3.3: Weibull parameters for Muppandal low-wind speed seasons wind data at various hub heights

Hub height	scale	shape	V_{avg}
160	10.04	2.277	8.89
120	9.395	2.32	8.32
80	8.867	2.4	7.86

4

Wind turbine design

This chapter details the design process for the wind turbine that is intended for a hybrid power system. Initially, section 4.1 discusses the general process of wind turbine design and the scope of design applied in this research. Section 4.2 presents the employed cost model to estimate the optimum design of the wind turbine. Section 4.3 explores further how the optimum design is reached.

4.1. General design process and objective

This research aims to explore a new design of a wind turbine that takes the diurnal and seasonal variation into account. In section 2.1, the wind turbine design process employed in this research focus on the conceptual design step, and the detailed design on different components is beyond the scope of the study. Thus, the conceptual design is defined here in the remainder of this section.

As previously mentioned in the site condition analysis, the wind speed distribution and wind shear are parameters that are considered in the design process of this research. These parameters, later, will be used as the input for the conceptual design input. The conceptual design in this analysis focuses on the wind turbine rotor optimisation. The analysis is done by modifying the specific power rating, the ratio of the generator capacity to the rotor size, and aims to identify the optimum rotor diameter that produces the electricity with the minimum cost. Thus, the machine rating is kept constant while the rotor diameter is modified.

Previous studies have used the upscaling method for the conceptual design [26] [18]. Sieros et al. [46] define two approaches of upscaling: theoretical upscaling that utilises similarity rules with linear scaling method and real upscaling that utilises existing data trend. Chaviaropoulos et al. [18] presents geometric linear scaling rules for different components.The linear scaling method is useful in the early stage of the design process as it is necessary to make a rough estimation of wind turbine parameters which will be adjusted later in the detailed analysis. This estimation is performed with direct scaling of an existing reference wind turbine by a certain scaling factor. This method works with some underlying assumptions such as [13]:

1. Same concepts in the number of blades, airfoils type, turbine materials, drive train and support structure

2. Same tip speed ratio

3. Other geometrical parameters linearly correlated to the rotor diameter(with exception of gearbox, generator and power electronics)

This research employs the real upscaling method, with the scaling trend published by the NREL. National Renewable Energy Laboratory (NREL) presents a thorough analysis of the cost and scaling model with scaling trends for each of the components [26]. The model is useful to analyse the impact of scaling and configuration on the cost of electricity and defines the optimum system design with the lowest levelized cost of electricity.

In general, the levelized cost of electricity can be expressed in equation 4.1, where C_t is capital cost , M_t is the operational cost and Q_t is the total output of the project in year t. The term r denotes the discount rate employed with a value of less than one. This term is required to indicate the present value of the costs. In the case where all of the capital cost is incurred upfront in year zero, such as the capital-intensive wind turbine project, then the term C_t factors out of the summation. The capital cost is no longer a function of the project year t and subjected to the discount rate, which then can be expressed as the Total Installed Cost (TIC).

$$LCOE = \frac{\sum_{t=0}^{T} \frac{C_t + M_t}{(1+r)^t}}{\sum_{t=0}^{T} \frac{Q_t}{(1+r)^t}} = \frac{TIC + \sum_{t=0}^{T} \frac{M_t}{(1+r)^t}}{\sum_{t=0}^{T} \frac{Q_t}{(1+r)^t}} \tag{4.1}$$

To simplify the equation, it is assumed that the annual output of the project (Q) and the variable cost per unit (M) is constant each year. With this assumption applied, LCOE can be expressed as the sum of Levelized Fixed Cost (LFC), which calculates the average payment required to pay off the capital costs over the full project lifetime T, and Levelized Variable Cost (LVC), which calculates the average payment to cover the operational costs. LVC equals the total variable cost per the unit of output.

$$LFC = \frac{TIC}{\sum_{t=0}^{T} \frac{Q_t}{(1+r)^t}} \tag{4.2}$$

$$LVC = \frac{\sum_{t=0}^{T} \frac{M_t}{(1+r)^t}}{\sum_{t=0}^{T} \frac{Q_t}{(1+r)^t}} = \frac{M}{Q} \tag{4.3}$$

As the discount rate is less than 1, with using the geometric series method, the denominator in equation 4.2 can be rewritten in a simpler fraction equation, and LFC is expressed as equation 4.4. The terms $\frac{1-(1+r)^{-T}}{r}$ can be expressed as function of the Fixed Charge Rate (FCR). The FCR indicates the fraction of the TIC that is is required over the project life per year to cover the overall capital costs.

$$LFC = \frac{TIC}{\sum_{t=0}^{T} \frac{Q_t}{(1+r)^t}} = \frac{TIC}{\frac{1-(1+r)^{-T} \times Q}{r}} = \frac{TIC \times FCR}{Q} \tag{4.4}$$

$$LCOE = LFC + LVC = \frac{TIC \times FCR + M}{Q} \tag{4.5}$$

The NREL cost model further defines the TIC and identifies the cost for each of the wind turbine project components based on previous conceptual studies and commercial wind turbines. The definition of the cost model employed in this research is presented in the following section.

4.2. Cost model definition

In the NREL cost and scaling model, Fingersh et al. identify the cost and mass of the components as function of the rotor diameter, machine rating, hub height, or a combination of these parameters.

The cost of electricity of the wind turbine is calculated with equation 4.5. The variable cost M includes the Levelized Operation and Maintenance (O&M) Cost, Levelized Replacement Cost and Land Lease Cost. The total initial cost is comprised of the total turbine cost and balance of station cost. This cost parameter includes the following elements [26]:

- Rotor
  - Blades
  - Hub
  - Pitch mechanisms and bearings
  - Spinner/Nose cone
- Drive train, nacelle
  - Low-speed shaft
  - Bearings
  - Gearbox
  - Mechanical brake, high-speed coupling, and associated components
  - Generator
  - Variable-speed electronics
  - Yaw drive and bearing
  - Main frame
- Control, safety system, and condition monitoring
- Tower
- Balance of station
  - Foundation/support structure
  - Transportation
  - Roads, civil work
  - Assembly and installation
  - Electrical interface/connections
  - Engineering permits

The detailed mass and cost function for each of the parameters are presented in the appendix. Figure 4.1 presents the mass of the rotor as function of its radius from several studies. Each study results have different mass functions; Sieros's [46] curve fit exponent of blade mass vs diameter is 2.4974, Jamieson's result yields exponent of 2.0633, NREL baseline yields exponent 2.9158 and WindPACT rotor study yields exponent of 2.6921. The results may differ from one another due to the different compiled datasets considered when generating the curve fit. The windPACT rotor study obtains a significantly lower mass function due to the assumed advancement in technology that makes lighter blades achievable [26]. Despite the differences, all result show agreement of mass the function at rotor radius of 50 meters or lower. This agreement may happen due to the higher wind turbine samples with diameters ranging around 40 to 50 meter than wind turbines with larger radius. Thus, estimation at wider diameters are less homogeneous.

However, such an approach is only useful for scaling up or down between different wind turbine powers. Increasing the diameter means increasing the wind turbine power indirectly. Thus, such models are unsuitable for the optimisation process that aims to get the optimum diameter for a particular machine rating. In other words, the optimisation process in this thesis aims to get the optimum diameter and optimum specific power (machine rating divided by rotor swept area, W/m^2). The need to evaluate the cost of wind turbines with different specific rating motivates the adjustment for the existing mass and cost scaling model. Direct use of the cost model will result in an optimum that is less valid for the optimisation process. The principal difference between the existing model and the one needed for the intended optimisation process results in the need for cost model adjustment. For this thesis, adjustment is made on the blade mass function with the consideration above.

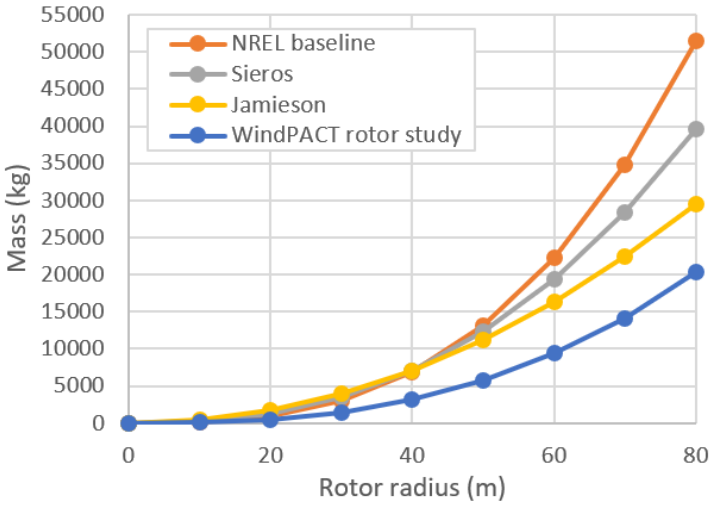

Figure 4.1: Blade mass scaling relationship

In order to initialise the process, commercial wind turbine data are compiled. From the observation of the existing wind turbine data, manufacturers often have several wind turbines with the same machine rating and different diameters (and different specific power). The scaling trend from sets of wind turbines with such configuration is more relevant for the intended optimisation process. The compilation process is prioritised for wind turbines with sufficient mass data, as these data will be used as the base for generating the adjusted mass function. The publicly available data for wind turbine specifications and the nonuniform format of reporting from different sources limits this process. As expected, several pieces of information are missing (year of manufacturing, wind class). The compiled data is then validated with previous studies. The complete dataset is presented in Appendix B.

Figure 4.2 reflects the compiled commercial wind turbine data. Figure 4.2a shows the specific power of the compiled wind turbines is in line with the IEC wind class. Lower specific power wind turbines are intended for low wind speed sites. Lower wind class indicates lower average wind speed and gust and, therefore, lower aerodynamic loadings that affect the structural integrity. Thus, wind turbines that are designed for locations with higher wind class will be exposed to higher loadings relative to wind turbines designed for lower wind class location, and additional structural strength may then be needed to retain its structural integrity. Vice versa, wind turbines designed for lower wind class location may be optimised with a reduction in mass due to the lower structural strength requirement.Figure 4.2b confirms the trend of growing capacity for more recent wind turbines. Figure 4.2c shows the trend of the specific power of wind turbines over the years. The trend line fitted in this figure is equal to the finding in [56] shown in figure 4.3. Thus, it can be concluded that the compiled data are valid, and the mass function adjustment shall use this data. In practice, over the past few years, the market is driving the trend towards the use of lower specific power wind turbines. This phenomenon may have been caused by the favourable increase in capacity factor due to the larger swept area for the same rated turbine capacity. A higher capacity factor also means more stable generation over time, which is beneficial when integrating the wind turbine to the grid. Another cause for the shifting trend of wind turbine specific power is the growth of the average swept area that outpaced the growth of average nameplate capacity. This effect may take place due to the advancement in manufacturing technology, enabling the production of rotors with larger diameter or driven by the demand in the market.

The mass function adjustment process is then followed by estimating the gradient of each set of the wind turbines. The linear curve fits shown in 4.4 identify these sets and are used to determine the gradient per set. The compiled data consists of eight sets of wind turbines with rotor radius between 35-60 meter, and the gradients of these sets are averaged. This averaged gradient represents the gradient for the adjusted mass function. The mass scaling study by Jamieson [6] and Sieros [46] converges with the NREL mass scaling model at rotor radius 40-meter. Such an agreement may happen due to a large sample of commercial wind turbines within this range of diameter, thus higher chance of the use of a

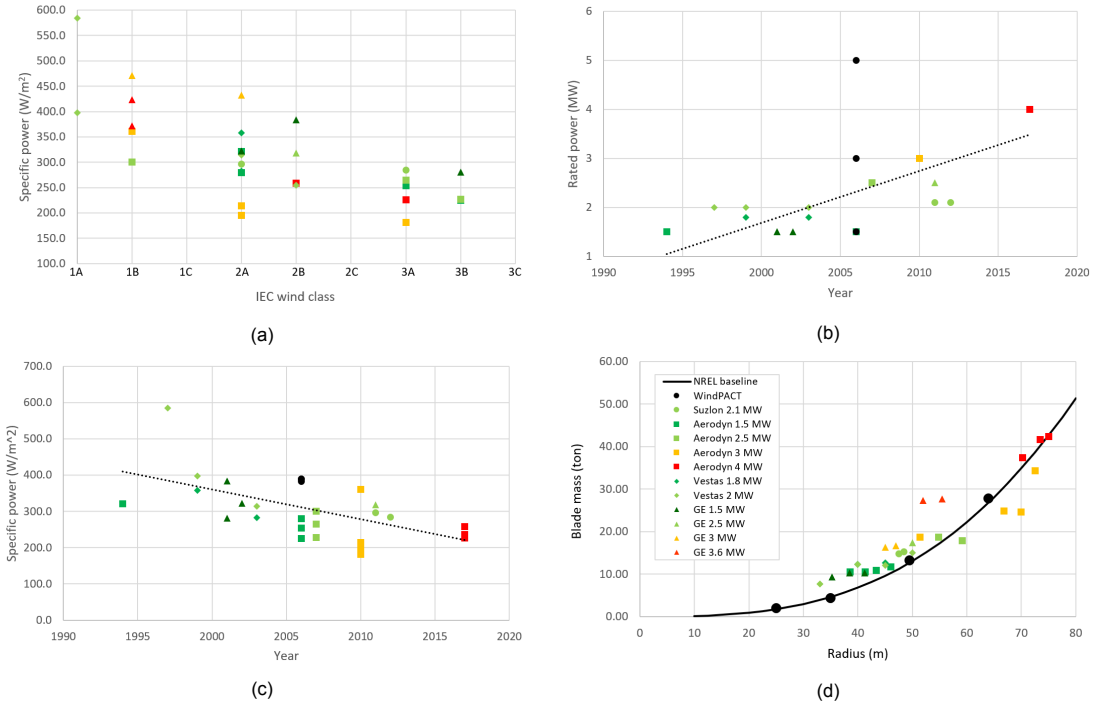

Figure 4.2: (a) presents the wind class of the compiled wind turbines. (b) shows the trend of the increasing WT capacity over years of the compiled data. (c) shows the trend of the decreasing specific power of wind turbine over years of the compiled data. (d) presents blade mass data of compiled wind turbines which shows agreement with NREL model

similar dataset in their respective study. Since a 40-m rotor radius is also reasonably close to the typical size for a 3 MW turbine, as used in this case study, the mass of the 40-meter radius rotor will be used as reference mass to calibrate the new mass function. The new mass function is estimated in the form of $a \times R^b$, with R as the rotor radius. The two unknowns are then determined by using the results from the previous two steps: average gradient and mass.

In Figure 4.4, The new mass function shows lower mass growth with respect to the radius than the NREL baseline function (black). This new function is still higher than the WindPACT final design (blue) for radius below 80m. The WindPACT rotor study final design scaling relationship is a projection function achievable through technology innovation. Thus, it results in lower mass function than what is commercially available today. This correlation between the adjusted mass function and the WindPACT rotor study implies that the new mass function is still within the range of technological capability, thus this result is logical and acceptable. However, this mass function becomes less credible for rotor radius greater than 70 meters, due to the limited number of the reference wind turbine dataset around this radius. Using the mass model at such radius should be done with care as, considering the large deviation of the mass model from the reference. The function may also overestimate the blade mass for radius lower than 30 meters. At rotor radius greater than 80 meter, the validity of this function is questionable due to unproven technological capability. At this range of radii, employing the new mass function results in lower blade mass when compared to the WindPACT rotor study mass function. The NREL mass function and the adjusted mass function are expressed in equation 4.6 and 4.7, respectively.

$$m_{blade,\,NREL} = 0.1452 \times R^{2.9158} \tag{4.6}$$

$$m_{blade,\,adjust} = 17.6245 \times R^{1.1615} \tag{4.7}$$

The lower adjusted mass function is due to the assumption employed, that the machine rating is constant for different rotor radius. In other words, a wider rotor radius implies lower specific power for the adjusted mass function.

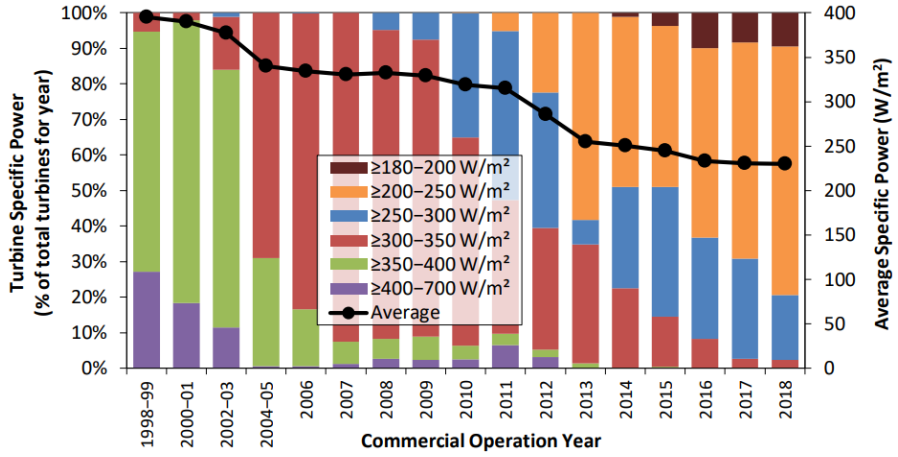

Figure 4.3: Trends in turbine specific power, recreated from [56]

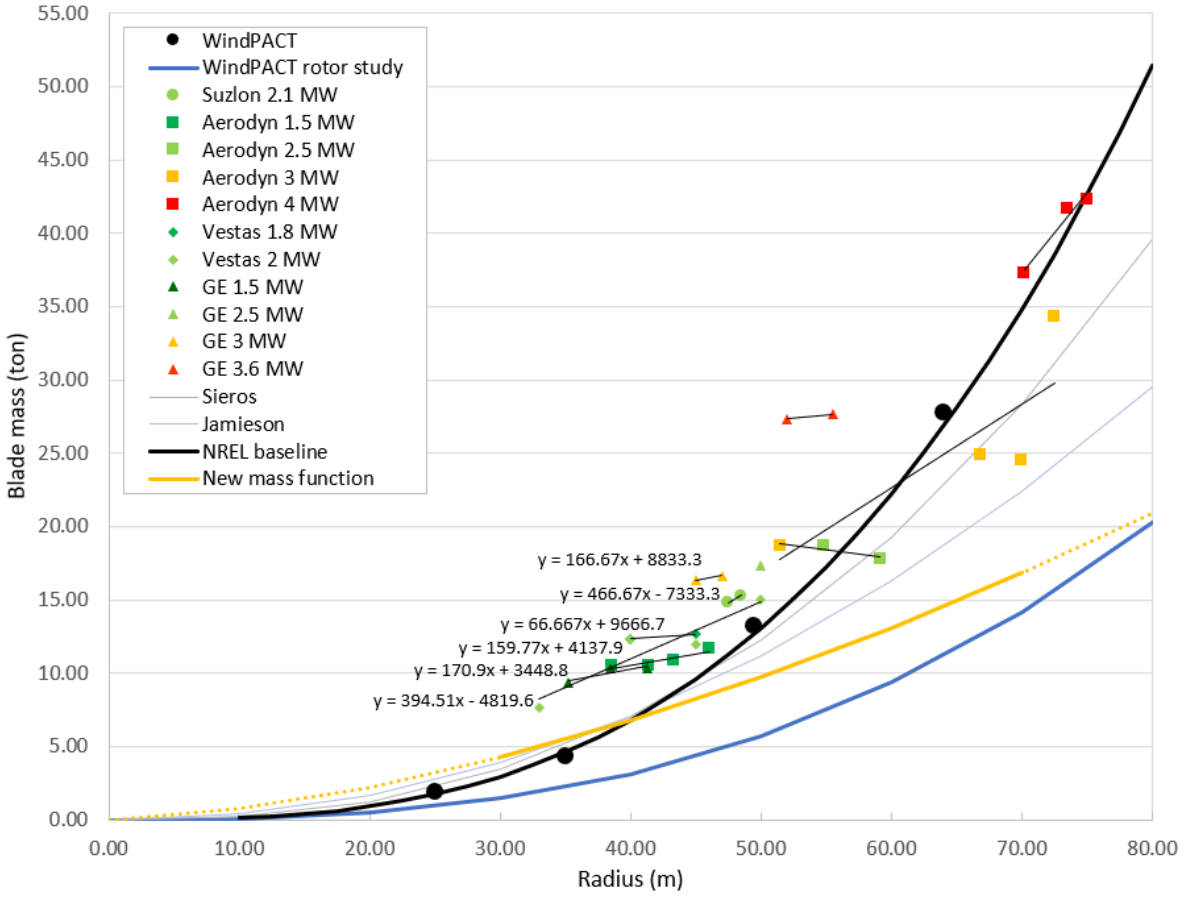

Figure 4.4: Mass model adjustment

4.3. Optimum design

The intended optimisation process in this thesis aims to generate a turbine design with a diameter that produces electricity with the lowest cost. As stated in the previous chapter, the cost of electricity is calculated by dividing the cost to the generated energy, expressed in $ per kWh. In this section, the process in reaching the optimum is investigated by using 4 arbitrary hypothetical sites with different wind speed distributions, which are shown in table 4.2. Subsequently, the optimum designs for these different sites will be analysed. The wind speed frequency distribution determines the wind turbine

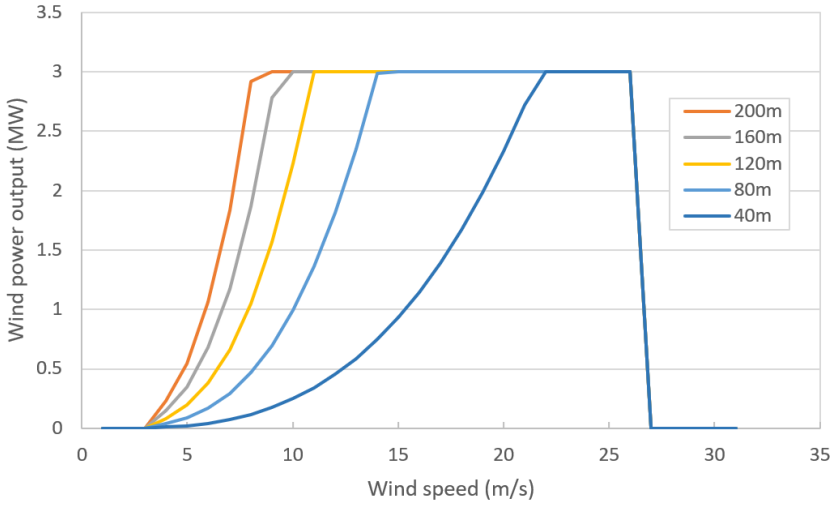

Figure 4.5: 3 MW wind turbine power curve for different rotor diameters

power production and annual energy production by multiplication with the wind turbine power curve. The power curve of the wind turbine gives the relation between power output and the wind speed. A pitch controlled wind turbine power curve is defined by three speeds: cut-in, rated, and cut-off wind speed. Typically, the cut-in and cut-out wind speed of a 3 MW turbine are, respectively, three and between 25-30 m/s [19]. The wind turbine starts generating power when the wind speed is higher than the cut-in wind speed. Between the cut-in and rated wind speed, wind turbine power increased with the wind speed as expressed in the following form:

$$P = \frac{1}{2} C_P A U^3 \tag{4.8}$$

With the power coefficient C_P, as the product of the system efficiencies. A is refers to rotor area and U refers to the wind speed. In this thesis, the power coefficient value is taken from the NREL 5 MW reference wind turbine [32]. As shown in figure 4.5, the rated wind speed is affected by the wind turbine diameter; wind turbines with larger rotor have lower rated wind speed. Between the rated and cut-out wind speed, the wind turbine output is held constant at the rated power level. A cut-out wind speed of 25 m/s is assumed to limit the blade-tip noise and avoid loads due to vibration on the structure. In the following subsections, turbine optimasation uses the power curves in figure 4.5 to generate the annual energy production. The analysis on the optimum design in this section employs assumptions presented in table 4.1. With the calculated AEP and the cost model defined in the previous section, the optimum design with the lowest LCOE can be identified.

Table 4.1: Overview of the used input parameters and variables for the analysis

Parameter	symbol	unit	value	Reference
Cut-in wind speed	U_{cut-in}	m/s	3	[19]
Cut-out wind speed	$U_{cut-out}$	m/s	25	[19]
Coefficient of performance	C_P	-	0.482	[32]
Rated machine rating	P_{rated}	MW	3	
Hub height	z_{hub}	m	120	

In a graph between the cost of electricity (COE) and the rotor diameter, such as in figure 4.9, the optimum lies at a minimum where the gradient or rate of change of COE between different diameters is zero. Thus, the COE is higher for both larger and smaller rotor diameters relative to the diameter where the optimum lies. This condition is presented in equation 4.9, with ΔCOE as the change in the cost of electricity (vertical axis) and ΔD as the change in the diameter (horizontal axis). As ΔD value cannot be zero, the ΔCOE equals to zero in the optimum. The definition of the cost of electricity can be simplified

Table 4.2: Sampe data cases for the analysis on the optimum design

	scale parameter	shape parameter
Case 1	8	2
Case 2	10	2
Case 3	12	2
Case 4	14	2

as the cost component divided by the amounts of energy produced component (AEP). Hence, ΔCOE can be rewritten into equation 4.12. Equation 4.12 identifies that the optimum is reached when the ratio of cost of wind turbines with diameter D_1 and D_2 is equal to the ratio between the AEP of these wind turbines. This equation simply indicates the change in the energy produced for a change in the cost, which will be optimal when both changes are equal. For instance, if the change in cost is lower than the change in AEP, then the COE at rotor diameter D_2 is lower than at diameter D_1. Thus, the optimum lies ahead at a larger rotor diameter than D_2. Vice versa, if the change in cost is greater than the change in AEP, then the optimum lies at a smaller rotor diameter.

$$\frac{\Delta COE}{\Delta D} = 0 \tag{4.9}$$

$$\text{with } \Delta D \neq 0, D_1 < D_2 \tag{4.10}$$

$$\Delta COE = \frac{\Delta cost}{\Delta AEP} = \frac{cost_1}{AEP_1} - \frac{cost_2}{AEP_2} = 0 \tag{4.11}$$

$$\frac{cost_1}{AEP_1} = \frac{cost_2}{AEP_2} \rightarrow \frac{cost_2}{cost_1} = \frac{AEP_2}{AEP_1} \tag{4.12}$$

$$\text{with } cost_1 < cost_2; \ \frac{cost_2}{cost_1} \geq 1 \tag{4.13}$$

In order to visualise the analysis, the four cases with different wind distribution, shown in table 4.2, and 3 MW wind turbines with diameters ranging from 40 to 200 meters are analysed. The result of the normalised AEP for the wind turbines in figure 4.6 shows that a smaller scale parameter leads to a higher difference of AEP between diameters. This conclusion arises due to the lower rated wind speed of the larger diameter wind turbine. A larger diameter wind turbine can utilise the high frequencies of low wind speed (wind data with scale parameter 8) better than a wind turbine with a smaller diameter. This feature is less profound with higher wind speeds (with scale parameter 14) due to the more distributed wind speed. Thus, the AEP growth between different rotor diameters in high wind speed conditions is relatively lower when compared to low wind speed conditions, which is shown in figure 4.6b.

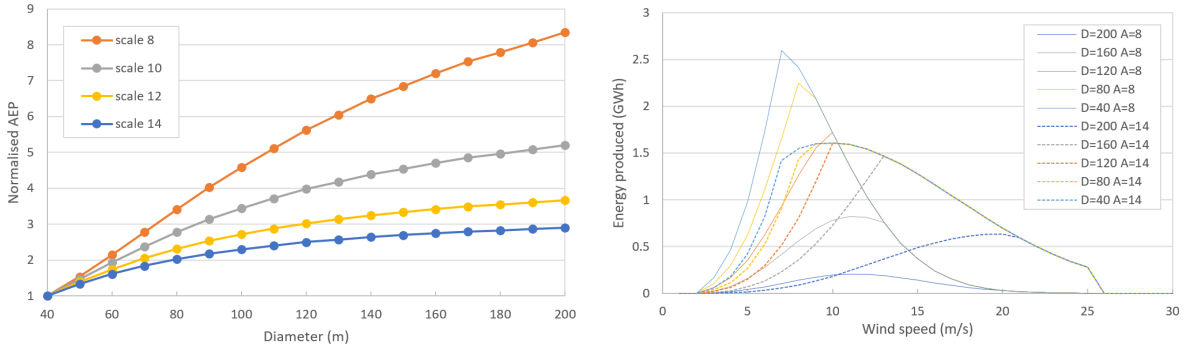

(a) (b)

Figure 4.6: (a) Normalized Annual Energy Production with as function of rotor diameter. (b) Energy production for wind turbine with different rotor diameter, at location with scale parameter 8 (full line) and 14 (dashed line). The Annual Energy Production (AEP) is the area under each lines.

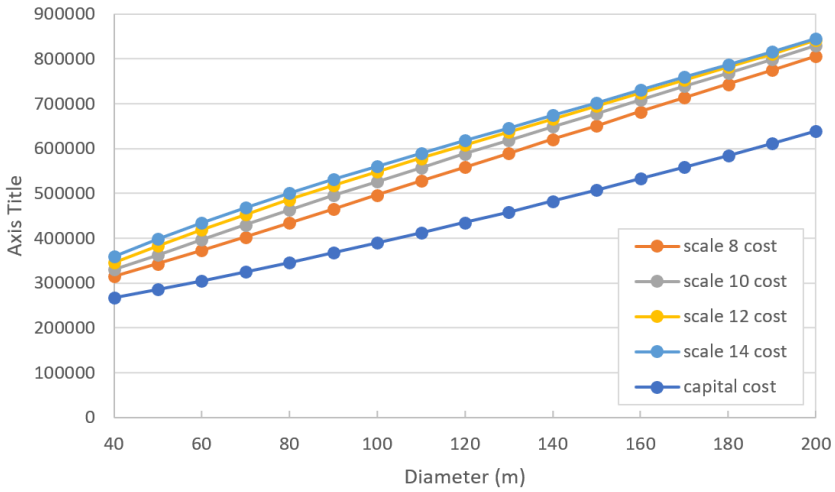

Figure 4.7: Total cost for wind turbines with sample data

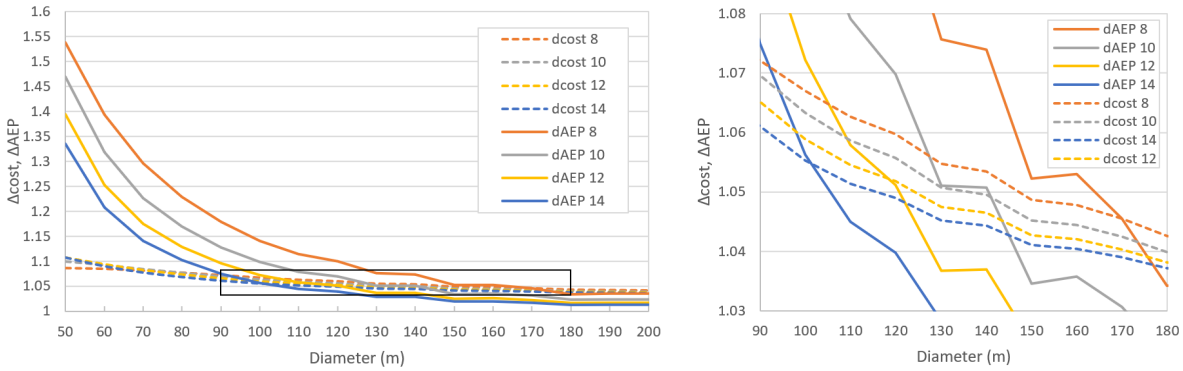

Figure 4.8: (a) The crossings between ΔCOE and Δcost which shows the optimum diameter for different weibull parameter wind data, zoomed in (b)

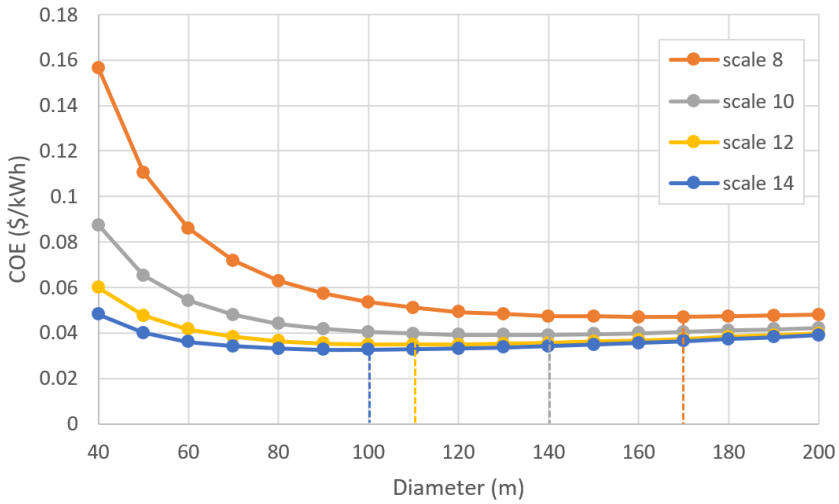

Figure 4.9: Optimum diameter for different weibull parameter wind data

Figure 4.7 shows the total cost for wind turbines within a range of diameters that works in different wind conditions. It is shown here that the capital cost is the same for different wind conditions as none of the wind turbine component costs are functions of the annual energy produced. The total cost

incorporates operating expenses which are a function of the energy produced. Thus the total cost for Weibull scale parameter 14 is higher than those with scale parameter 8. The COE analysis shows that the optimum diameters for wind turbines with wind distribution scale parameter of 8, 10, 12 and 14 are around 170 meter, 140 meter, 110 meter and 100 meter respectively. The optimum is reached when the ΔCOE equals to the Δcost, as shown in figure 4.8 by the crossing between ΔCOE and Δcost. Δcost is observed to be almost horizontal because the total cost curve presented in figure 4.7 is almost linear. Figure 4.8 shows that increasing the diameter at lower wind speed conditions has greater effect on increasing the AEP. This condition is due to the better ability of larger rotor diameters to extract wind energy at lower wind speed conditions.

4.4. Summary

Several key takeaways from this chapter are:

1. The wind turbine design process performed in this research is focused on the conceptual design phase. The result of the conceptual design approach identifies the overall physical and operational parameters of the wind turbine, which is the main interest of this study.
2. The cost model employed in the analysis is adjusted from the NREL cost and scaling model. The adjustment is required due to the different scaling approach pursued in this study, which considers the modification of specific power of the wind turbines. The adjustment results in lower cost and mass scaling when compared to the reference NREL cost and scaling model.
3. The process of reaching the optimum design is analysed and how the optimum shifts as different wind speed distribution are employed is identified. Lower wind speed conditions leads to a higher difference of AEP between different diameters. Thus, the same increase in rotor diameter increases the AEP more at low wind speed conditions than at high wind speed conditions. This condition leads to a larger rotor diameter at the location with lower wind speed conditions and smaller rotor diameter for the location with higher wind speed conditions.

.

5

Hybrid power system and operation modelling

This chapter continues the design process in the previous chapter with the empirical wind dataset gathered. The wind turbine design for the different operational conditions in the hybrid power system and different datasets are presented in this chapter. Section 5.2 presents the optimum design result for zero curtailment scenario. Section 5.3 presents the optimum design result for the grid-connected topology. Section 5.4 presents the optimum design result for the topology where the hybrid power system is supplying a demanded load.

5.1. Outline of the analysis

This section aims to guide the reader regarding the design processes conducted in this chapter that leads to the results presented in the following sections. The wind turbine design in this chapter refers to the three different operational modes stated at the end of chapter 3, namely: the baseline design, the night-time turbine design and low-wind speed period turbine design. The baseline design refers to the full-year wind data. While the night-time and low-wind speed season turbine design refers to a limited wind data, with night-time only and low-wind speed season only wind data. The design process results in the identification of the optimum diameter for each operational modes at different hub heights.

The result is then compared between different operational modes. Due to the different range of operational time between the baseline design and the night-time and low-wind speed period turbine design, the turbine that are optimally designed for the night-time and low-wind speed period are then operated for a full-year period. What to expect here is that these turbines will be operating not at their optimum diameter. Thus, the difference of the performance between the baseline and the night-time and low-wind speed period turbine design can be identified.

This process of analysis is repeated for the three different topology: zero-curtailment mode, grid-constrained and demand load-supplying topology. The zero-curtailment mode refers to the standard design procedure where the AEP is uncurtailed. This infinite evacuation capacity may be interpreted as an infinitely large grid capacity or a significantly higher demand load level than the generation. The grid-constrained topology refers to the situation where the hybrid power system is connected to a grid with a limited capacity, normalized to the nominal capacity of the power generation. The demand load-supplying topology refers to the the situation where the hybrid power system is supplying a demand load with its maximum capacity normalized to the nominal capacity of the power generation.

5.2. Zero-curtailment mode wind turbine design

In this operational topology, the hybrid power system is either connected to a grid with a significantly larger capacity or a demand load that is always larger than the generation capacity. Thus, the generated power from the hybrid power system that includes 3MW of wind turbine and 3MW of solar PV is entirely evacuated without any curtailment. It is important to note that this condition is hypothetical as there is no such a limitless grid capacity or demand load level. This condition is also the case in a standard wind turbine design process where the optimum design considers the AEP without any reduction. The result of this topology serves as the baseline in comparison with the grid-connected and demand load-connected topology. The optimisation analysis result of the complete dataset, which considers both day and night and all season data, is given in table 5.1.

Table 5.1: Optimum diameter for baseline wind turbine

Hub height (m)	Optimum diameter (m)	Cost of Electricity ($/kWh)	AEP (GWh)
160	93	0.03288	17.27
120	100	0.03230	17.40
80	111	0.03190	17.63

The optimum rotor diameter for the lowest cost electricity generation at three different hub heights is presented here. The result shows that at higher hub height, due to the higher occurrence of high wind speed, the optimum diameter moved to a smaller diameter. However, the optimum cost of electricity at higher hub height is higher than at their lower hub height counterpart due to the increased cost of the tower. Thus, the change of the optimum is different from the analysis in the previous chapter, where the hub height is kept at the same level, and only the wind speed distribution difference is considered. Figure 5.1 shows this condition where the dashed line $(80 - 120)$ represents the hypothetical cost of electricity curve of a wind turbine with an 80-meter hub height and wind data at 120-meter hub height. It is shown here, similar to the optimum analysis in the previous chapter, that the optimum diameter shifts to the left to the smaller rotor diameter and lower optimum cost of electricity. The cost of electricity curve shifts upward to a higher cost of electricity when the 120-meter hub height is used.

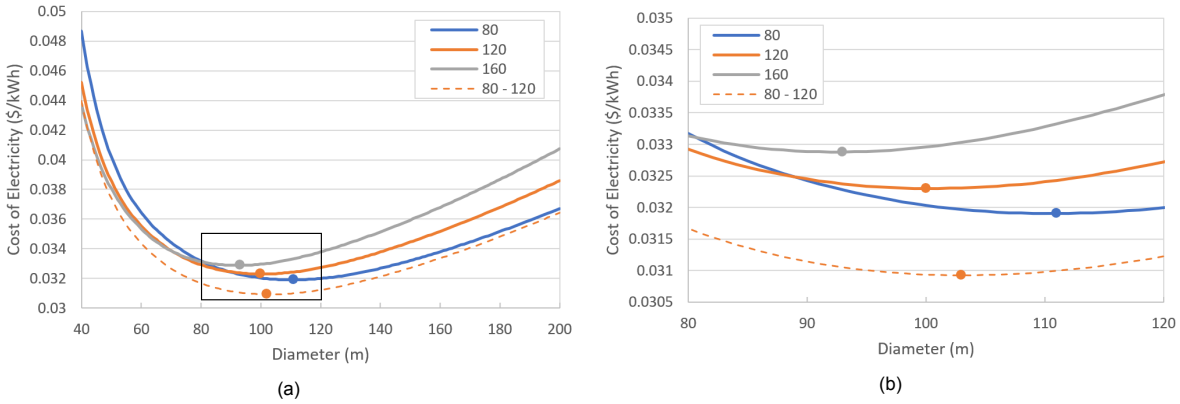

Figure 5.1: (a) The optimum diameter of the baseline design for the zero-curtailment topology at different hub height with a zoomed view in (b).

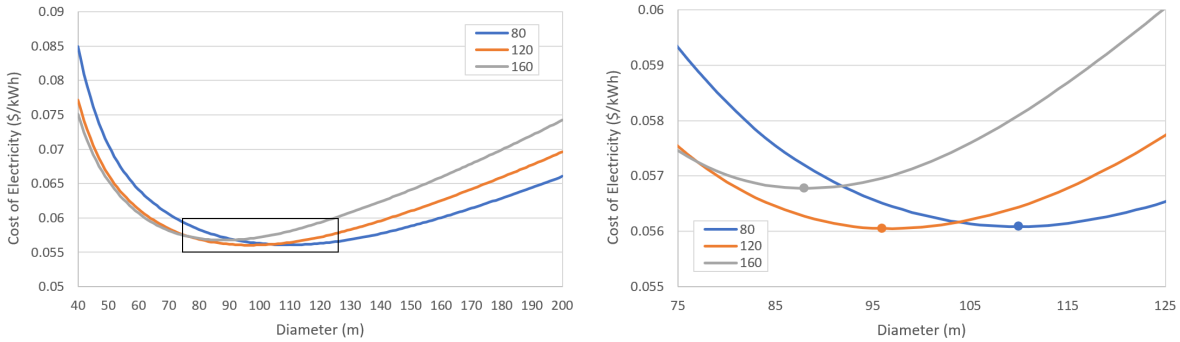

Figure 5.2: (a) The optimum diameter of the night-time turbine design for the zero-curtailment topology at different hub height with a zoomed view in (b).

Figure 5.2 shows the COE curve for the night-time wind turbine which shows the same relationship for the optimum rotor diameter of a turbine designed for only night-time operation. The optimum diameter is slightly smaller than the baseline wind turbine due to the slightly windier condition at night time. However, the COE for the night-time wind turbine is significantly higher, nearly doubling the COE of the baseline wind turbine. This result arises as to the night-time wind turbine AEP is approximately half of the baseline wind turbine AEP. The day and night time are relatively constant throughout the year, and each lasts approximately 12 hours. Thus, the night-time turbine design operated half the time while having a similar wind speed condition to the baseline design, which explains the halved AEP. In general, the COE is consist of capital expenditure (CAPEX) and operating cost (OPEX). The CAPEX is in a function of the turbine physical parameter, and OPEX is a function of the AEP. Thus, the relationship between the COE for the baseline and the night-time wind turbine can be approximated as follows:

$$OPEX = constant \times AEP \tag{5.1}$$

$$LCOE = \frac{CAPEX}{AEP} + \frac{OPEX}{AEP} = \frac{CAPEX}{AEP} + constant \tag{5.2}$$

$$AEP_{night} \approx 0.5 \times AEP \tag{5.3}$$

$$LCOE_{night} = \frac{CAPEX}{AEP_{night}} + constant = \frac{CAPEX}{0.5 \times AEP} + constant = 2 \times \frac{CAPEX}{AEP} + constant \tag{5.4}$$

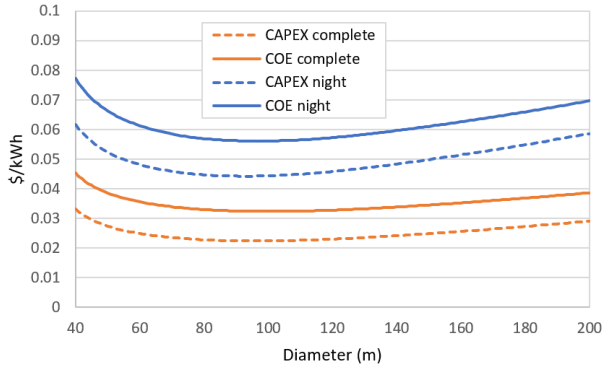

Figure 5.3: Total cost for wind turbines with sample data

Figure 5.3 compares COE of the baseline wind turbine and night-time wind turbine at 120 meter hub height. The figure also shows the separated portion of the CAPEX in the COE. The difference between the COE and the CAPEX refers to the OPEX portion of the COE. Due to the definition of OPEX being a function of the AEP, the OPEX contributes a constant value in the LCOE, regardless the diameter of the rotor. As explained in the chapter on the optimum design analysis, the similar wind speed distribution

leads to the similar optimum rotor diameter. However, the halved AEP doubles the night-time turbine COE, as explained in the equation 5.4.

Table 5.2 presents the optimum diameter for the night-time design. In order to compare reasonably with the baseline design, the night-time design is fully operated during the day and night, even though it is optimised for night-time operation only. The cost of electricity for the full operating night-time design is also presented in table 5.2. This table indicates that the optimum night-time design is similar to the baseline design. For the night-time design to be fully operated will means that the wind turbine is not operating at its optimum design. Given the small difference between the design result, the difference of COE from the baseline design optimum is less than 0.1%.

Table 5.2: Optimum diameter for night-time wind turbine

Hub height (m)	Optimum diameter (m)	COE ($/kWh)	Full operation COE ($/kWh) / COE difference (%)	Full operation AEP (GWh) / AEP difference (%)
160	88	0.05678	0.03291 / 0.09	16.67 / -0.49
120	97	0.05605	0.03232 / 0.04	17.12 / -1.64
80	110	0.05608	0.03190 / 0.00	17.54 / -2.93

The optimum design of the wind turbine for the low wind speed season is given in table 5.3. The dataset for the low wind speed season has a different Weibull distribution, with lower scale parameter. Designing a wind turbine with this wind condition leads the shift of the optimum to a rotor with a larger diameter. The diameter of the rotor is physically constrained by the height of the tower ($D/2 < z_{hub}$). Though, in practice, this limit is unobtainable due to other practical constraints such as the ground clearance. The ground clearance is defined as the distance of the lowest point of the arc created by the rotating blades to the ground. This clearance aids in addressing safety concerns. The required ground clearance height is, however, not present in international design standards as this constraint is hardly activated in the standard wind turbine design. Oteri [40] presents a range of ground clearance heights between 15 to 75 feet (4.6 to 22.8 meter) with the ground clearance of 75 feet / 22.8 meters as the most commonly used height. This range is mainly driven by the different policies and regulations employed at different locations. For a hub with 80-meter height, the maximum rotor size that complies with the constraint is equal to or below 114.4 meters even though by calculation, the optimum rotor diameter is at 143 meters. This constraint is less likely to be activated at higher hub heights; 120 and 160-meter. This condition is presented in figure 5.4 where the dashed line represents the hypothetical COE curve for a wind turbine with 80 meters hub height without any practical constraint.

Due to the operation only in the low wind speed season, the considered AEP is also reduced. Thus, the cost of electricity is increased for the low wind speed season design. In order to reasonably compare with the baseline design, this design is also modelled with the full operation mode. Due to the larger rotor, when the low-wind speed design is fully operated, its AEP is higher than the baseline design. As the design is not operating in its optimum, the additional AEP comes with the cost of an increase in the COE, which is termed as COE difference in table 5.3.

Table 5.3: Optimum diameter for Low-wind speed wind turbine

Hub height (m)	Optimum diameter (m)	COE ($/kWh)	Full operation COE ($/kWh) / COE difference (%)	Full operation AEP (GWh) / AEP difference (%)
160	120	0.05973	0.04073 / 23.88	19.28 / 11.67
120	131	0.05978	0.03859 / 19.47	19.59 / 12.60
80	114	0.06137	0.03283 / 2.89	17.88 / 1.41

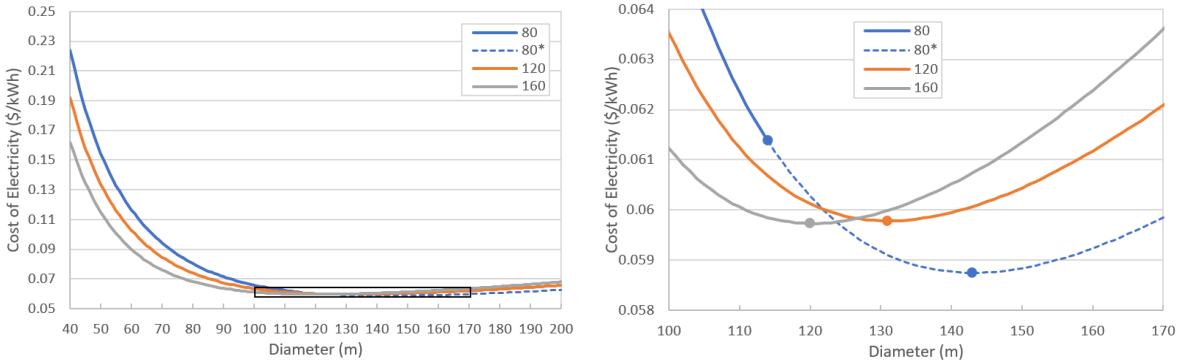

Figure 5.4: (a) The optimum diameter of the low-wind speed season design for the zero-curtailment topology at different hub height with a zoomed view in (b).

5.3. Grid constrained design

In this analysis, the 3 MW wind turbine is coupled with 3 MW solar PV and supplying the grid with a maximum capacity of 3 MW. Solar irradiance reanalysis data of Muppandal, India is obtained from Solcast with a temporal resolution of 10 minutes. A commercial solar panel is used to calculate the solar PV generation curve data. The power generated from the solar PV is prioritized. Thus, in the case of power generation from the hybrid power system being larger than the grid capacity, the wind turbine power shall be curtailed. This will reduce the AEP of the wind turbine. The results for the optimum diameter analysis for three design conditions are given in table 5.4. The result of the full operational night-time optimum design is then compared with the optimum baseline design.

Table 5.4: Optimum diameter for wind turbines with grid constraint

Hub height (m)	Optimum diameter (m)	COE ($/kWh)	Full operational COE ($/kWh)	Full operation grid CF (-)
Full year				
160	86	0.03794	-	0.7282
120	94	0.03740	-	0.7336
80	104	0.03719	-	0.7342
Night-time turbine				
160	88	0.05678	0.03795	0.7342
120	97	0.05605	0.03743	0.7418
80	110	0.05609	0.03724	0.7494
Low-wind-speed-season turbine				
160	110	0.06881	0.03886	0.7852
120	122	0.06974	0.03843	0.7954
80	114	0.06916	0.03731	0.7588

The figure 5.5 shows the comparison of the AEP between the hypothetical-zero curtailment topology and the grid constrained topology. Different operational modes are modeled in both topologies and it is shown here that larger diameter suffers more from curtailment, explained with the reduced AEP. This condition leads the optimum to shift to a lower diameter when compared to the unconstrained design, as occurred to the baseline and low wind speed season design The night-time design is unaffected by the grid constraint because the AEP is calculated for night-time operation only, when there is no solar PV generation. The solar PV generation will not cause a curtailment of the generated wind power by the night-time wind turbine, and therefore, the optimum rotor diameter is the same as the zero-curtailment topology of the previous paragraph. The diameter of the the low-wind speed season turbine at 80 meter hub height is capped with the ground clearance at 114 meter rotor diameter.

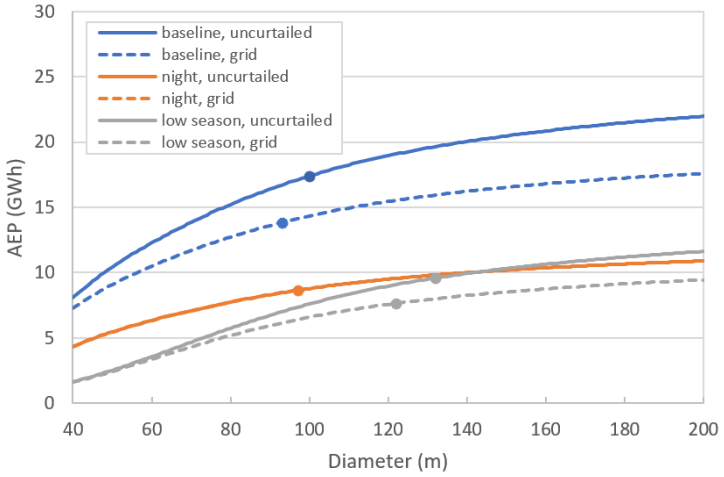

Figure 5.5: AEP of the wind turbines with 120 meter hub height for three operational modes: baseline, night-time, low wind speed season, and two hybrid power system topology: zero curtailment and grid constrained. The night-time design with grid constrained topology overlaps with the night-time design and zero-curtailment topology. The point in each curve refers to the optimum diameter of each operational modes.

5.4. Demand constrained design

In the third operating condition the power that is supplied to the grid is constrained by the demand, which is always equal to or lower than the grid capacity of 3 MW. Also in this case, solar PV generation is prioritised. It is important to note that in this topology, unlike in the grid-connected topology, the solar PV generation can be curtailed when the demand load is low. The result for the demand constraint is in the same direction with the previous wind turbine topology but with a higher amount of curtailment. It is logical as the generation capacity is limited by the demand load, which will reach 3MW only during the peak demand. Thus, the average demand load is lower than the peak, and therefore curtailment occurs more often. The optimum rotor diameter shifts towards lower diameters due to the higher amounts of curtailment. However, the rotor diameter for 80-meter hub height is also capped at 114 meters due to the ground clearance constraint.

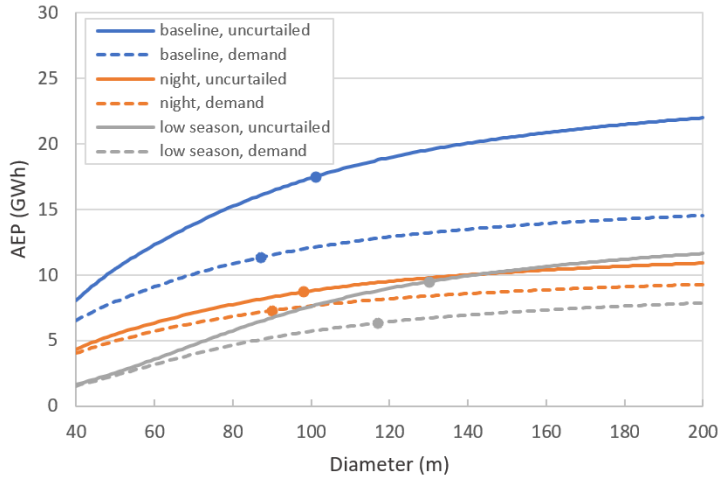

Figure 5.6: AEP of the wind turbines with 120 meter hub height for three operational modes: baseline, night-time, low wind speed season, and two hybrid power system topology: zero curtailment and demand load constrained. The point in each curve refers to the optimum diameter of each operational modes.

Figure 5.6 presents the shift of the optimum rotor diameter and AEP from the hypothetical zero-curtailment topology to the demand constrained topology. The night-time design is observed to have smaller curtailment when compared to the low-wind speed and baseline design. This result arises due

to the limited operation of the night-time design that only considers the period at night when the sun is out. Thus, the curtailment of the design based on this dataset results from the lower demand than the wind generation. This condition is not the case for other datasets as other datasets include the period during the day. Hence, the curtailment for the low-wind speed and the baseline design is not only caused by the lower demand load but also by the solar PV generation.

Table 5.5: Optimum diameter for wind turbines with demand constraint

Hub height (m)	Optimum diameter (m)	COE ($/kWh)	Full operational COE ($/kWh)	Full operation met-demand ratio (-)
Full year				
160	80	0.435568	-	0.7408
120	88	0.04289	-	0.7476
80	98	0.04261	-	0.7497
Night-time turbine				
160	81	0.06414	0.0436	0.7437
120	90	0.06318	0.04290	0.7531
80	102	0.06309	0.04263	0.7598
Low-wind-speed-season turbine				
160	104	0.07983	0.0446	0.7969
120	117	0.08100	0.04423	0.8094
80	114	0.08079	0.04298	0.7862

5.5. Summary

This chapter presents the result of the optimum rotor design for different operational modes and datasets. Several key takeaway from this chapter are:

1. Due to the wind shear, higher hub heights are associated with a higher frequency of high wind speed, which leads to a smaller optimum rotor diameter. However, the additional cost of the tower results in higher COE than wind turbines with lower hub height.

2. The limited operation of the night-time and low-wind speed season results in lower AEP, and therefore, higher optimum COE. These designs are then operated for full-year to be fairly compared with the baseline design, The full-year operation results in the COE of the night-time and low-wind-speed-season turbines being higher than the baseline This result is not surprising as they are not optimal for full operation. The consequence is that designing turbines for better complementary supply or better demand matching comes at a cost.

3. Energy curtailment due to the grid limitation and low demand load leads to a shift of the optimum rotor diameter to a smaller diameter. Larger rotors suffer more from energy curtailment.

4. For a system without storage, curtailment of power generation reduces the technology efficiency, as the curtailed power can not be recovered. Hence, the use of the storage system is essential to utilise curtailed energy, as well as to realise the features of the hybrid power system.

6

Storage system design and implementation

The storage system is integral in any power system that employs renewable energy sources. It is also concluded in the previous analysis that a storage system is necessary to save the curtailed energy, thus reducing the loss from curtailment. Therefore it is interesting to know how this system is configured and at what cost. This chapter presents the analysis of the storage system in the hybrid power system to utilise the curtailment. This chapter is initialised in section 6.1 with the general definition of the storage system employed in this research. The storage requirement for the grid-connected power system and demand load-supplying power system is presented in section 6.2 and 6.3, respectively. Section 6.4 analyses the cost and benefit of the storage system.

6.1. Storage system definition

The need for a storage system is articulated in the previous analysis, and this section defines the system specification. The storage system comprises different technologies with varying characteristics and serves different services. Storage technology selection also depends on the power system project configuration that tailor-made design may require different storage solutions. In this research, the objective of the storage system is to store the curtailed energy due to the limited grid capacity and mismatching demand. This analysis aims to approximate the cost required to utilise the curtailment and improve the hybrid power system performance. Thus, the utility-scale storage system in this research is focused on the Lithium-ion battery to estimate this cost of curtailment utilisation. The lithium-ion battery currently dominates the market for global utility-scale storage [16]. This battery technology also excels in its specifications with high power density, a roundtrip efficiency of 86% and long life cycle with $>$6000 cycles at 80% depth of discharge [2]. The depth of discharge indicates the ratio of the extracted energy during the discharge cycle with respect to the total rated capacity of the battery. Roundtrip efficiency refers to the efficiency of charging and discharging. Thus, it represents the fraction of available electricity after being subtracted by some losses during charging and discharging.The storage system specification employed in the battery model analysis is summarised in table 6.1. The storage model is

Table 6.1: Lithium-ion battery specification for modelling input

Parameter	Value
Roundtrip efficiency	86% [2]
Charge/discharge efficiency	92.75%
Minimum/Maximum state of charge	10%/90%

presented in the methodology chapter, in figure 2.3. This model results in four states of system:

1. Charge. This refers to the situation at a certain time step where there is no evacuation capacity left and therefore, a non-zero curtailment. If the sum of the curtailment and the current SOC is lower than 90% of the maximum capacity of the battery, then the curtailed energy will be charged into the battery bank.
2. Charge and shed energy. This refers to the situation at a certain time step where there is no evacuation capacity left and therefore, a non-zero curtailment. If the sum of the curtailment and the current SOC is higher than 90% of the maximum capacity of the battery, then the curtailed energy will be charged into the battery bank until the SOC of the battery reaches 90% of its maximum capacity. The remainder of the unsaved curtailed energy is termed as the shed energy.
3. Discharge and supply energy. This refers to the situation at a certain time step where there is no curtailment and therefore, a non-zero evacuation capacity. If the current SOC is higher than available evacuation capacity, electricity is discharged and fully occupying the available evacuation capactiy.
4. . FUll discharge and suppy energy. This refers to the situation at a certain time step where there is no curtailment and therefore, a non-zero evacuation capacity. If the current SOC is lower than available evacuation capacity, electricity is discharged and leaving only 10% of SOC int the battery bank.

6.2. Grid-constrained storage system

Figure 6.1 shows the curtailed and evacuated energy of the wind turbine with various diameters and three hub heights. Perfect storage is assumed here; thus, all curtailed energy is stored in the storage or evacuated back to the grid. This assumption is made to determine the maximum state of charge (SOC) of the storage system and the minimum battery capacity to contain this SOC. Some terms used in figure 6.1 is explained here as follows:

- Curtailed energy is the sum of produced energy that is curtailed, which occurs when the grid capacity at a particular time is lower than the wind and solar PV generation. With perfect storage, all this energgy is not lost, but will be used to charge the battery.
- Available grid is the sum of the remaining grid capacity per time step that has not been used to supply generated power from the solar PV and wind turbine to the grid directly. This capacity indicates the possibility to evacuate the stored curtailed energy from the battery to the grid.
- Evacuated energy is the amount of the stored curtailed energy that can be supplied back to the grid. Unless there is any available grid capacity, the curtailed energy remains stored in the battery.
- The Max SOC is the maximum state of charge which governs the required battery capacity, expressed in the unit of kWh.
- Final SOC is the final state of charge of the storage system in the unit of kWh.

The curtailed energy curve crosses the available grid curve at diameter 170, 163 and 158 meters for 80, 120 and 160-meter hub height, respectively. This condition means that for larger rotor diameters, the grid is fully occupied and the curtailed energy remains in the battery as shown by the higher than zero value of the final SOC. However, the optimum grid constrained wind turbine diameter at different hub heights lies between 86 and 122 meters, which is smaller. Therefore, for the optimum turbines the curtailed energy can be fully evacuated when using perfect storage.

From the figure, it is observed that the maximum SOC is high, being around half of the total evacuated energy. This condition arises due to the continuous period of high wind speed and wind power generation at rated power during the monsoon season, presented in figure 6.2. The inadequate grid capacity to evacuate the curtailed energy from the battery forces the battery to keep storing the curtailment and therefore, enlarge the battery capacity requirement. Figure 6.3 shows the SOC of the

battery over the year for different rotor diameters at 160-meter hub height. A larger rotor results in a lower-rated wind speed which implies the higher occurrence of the wind generation at rated power and higher accumulation of stored energy in the battery bank. However, when different hub heights are compared, especially between 160-meter and 120-meter, the result is the opposite. This result is observed in the maximum SOC and evacuated energy in both hub heights. The maximum SOC at 160-meter hub height is lower, and the evacuated energy is higher than at 120-meter hub height due to the higher occurrence of cut-out wind speed at 160-meter hub height. Wind speeds at this level force the wind turbine to stop generating power, which allows the battery to evacuate the stored energy and slows down the accumulation of the stored energy. Due to the roundtrip efficiency of the battery, energy is lost during the charging and discharging process. Thus, only a fraction of the curtailed energy that can be evacuated, shown by the gap between the curtailed energy curve and the evacuated energy curve.

With having the minimum capacity required for the battery identified, an analysis of the different levels of storage capacity is possible. A lower capacity of storage results in energy shedding when the curtailed energy is only partially saved and stored in the battery while the remainder is left unutilised. Figure 6.4 presents the shed energy as a function of the storage capacity for wind turbines at 160-meter hub height. It can be observed here that decreasing the storage capacity from 80% to 60% will double the amount of shed energy. Decreasing it further to 40% capacity will triple the shed energy, and to 20% capacity will quadruple the shed energy. The relationship between storage capacity and shed energy remains linear until 10% storage capacity, where the shed energy starts to rise rapidly with reduction in storage capacity. It is also interesting to note here that around 5% of the perfect storage capacity can save about half of the curtailed energy. Different diameter sizes are reported to have the same relationship, with an exception for the 40-meter rotor diameter wind turbine. This result will become more relevant with a more detailed cost analysis of the storage system, which follows in section 6.4.

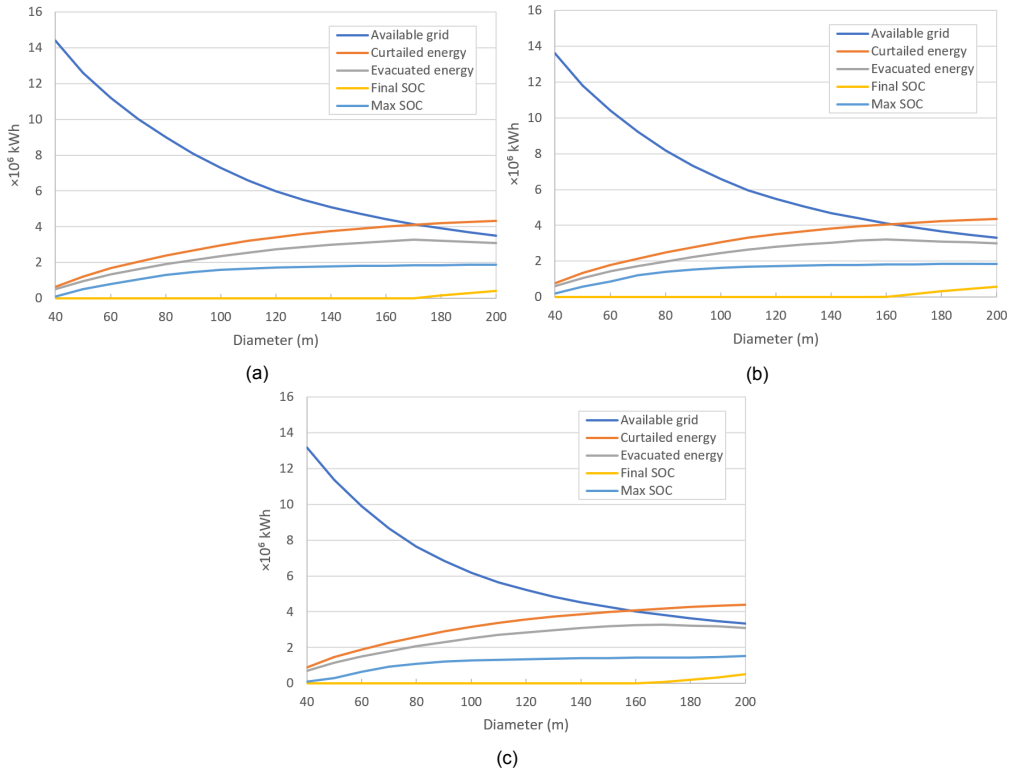

Figure 6.1: Curtailed and evacuated energy with a grid constraint and perfect storage at (a) hub height=80m, (b) hub height=120m, (c) hub height=160m.

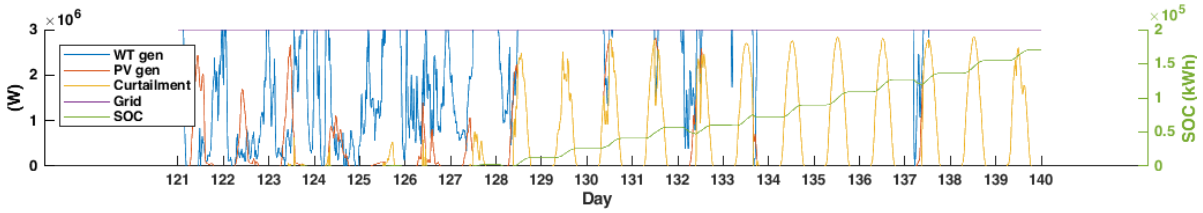

Figure 6.2: Wind power, solar PV generation, grid capacity and battery SOC with 120-meter rotor diameter and 160-meter hub height between day 121 and 140 (May 1-20, 2014). The consecutive rated-power wind generation and high solar PV output from the second week of May 2014 onward gradually increase the SOC until the end of monsoon season

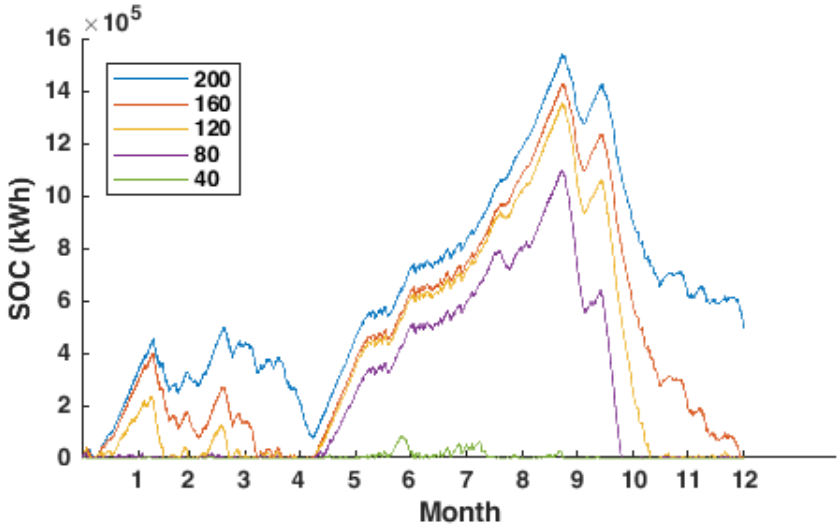

Figure 6.3: SOC of the battery for grid-constrained wind turbine at 160 meter hub height and different rotor diameters. The numbering of the months are located at the end of each months. The SOC curve in figure 6.2 is presented by the yellow curve between month 4 and 5 in horizontal axis

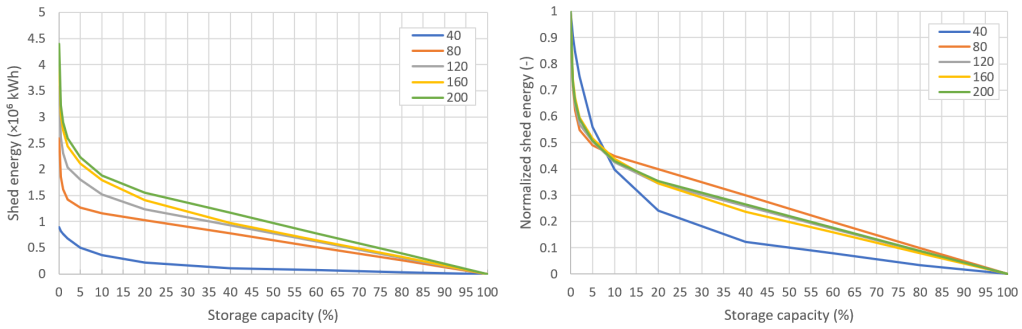

(a) (b)

Figure 6.4: Shed energy for different storage capacity presented in its (a) nominal value and (b) normalised by the shed energy at zero storage capacity value for the grid-constrained topology. The storage capacity is given as a percentage of the perfect storage capacity.

6.3. Demand load-supplying storage system

Figure 6.5 shows the results of the simulation of the system that is constrained by the demand load. Available demand corresponds with the available grid in the previous section, but limited to the demanded load at each time step. These results are similar to those from the grid-constrained topology only with lower available space and higher curtailed energy. This condition happens due to the demand load that is fluctuating with a peak at 3 MW load, unlike the constant grid capacity. The crossing

between the curtailed energy and the available demand curve in figure 6.5 indicates the possibility to supply all of the unmet demand with the curtailed energy, which occurs at the diameter of 105, 96 and 91 meters for 80, 120 and 160-meter hub height, respectively.

However, in practice, the evacuated energy curve is flattening at smaller diameter than the crossing rotor diameters, and the curtailed energy remains stored instead, shown by the increasing final SOC. This situation arises from the assumption employed in this analysis, where the initial SOC is set to be zero. The available space for evacuating the stored energy, which is the unmet demand, occurs before the period with surplus generation in late summer and monsoon season. Thus, unmet demand remains unmet, and energy accumulates in the battery bank at the end of the year. For the rotor diameter beyond the crossing point, the curtailed energy and the required storage capacity increases further due to the assumed perfect storage. This result is shown in the merging value of final SOC and maximum SOC at higher rotor diameters. Additional storage at this point therefore does not improve the capability of meeting the demand, but mostly is used to store overproduction for which there is no demand. Similar to the grid-connected topology, maximum SOC is lower and evacuated energy is higher at 160-meter hub height due to the higher occurrence of cut-out wind speed that allows energy evacuation from the battery. The maximum capacity is, however, significantly different with the demand load-supplying topology requiring twice to three times as much battery capacity.

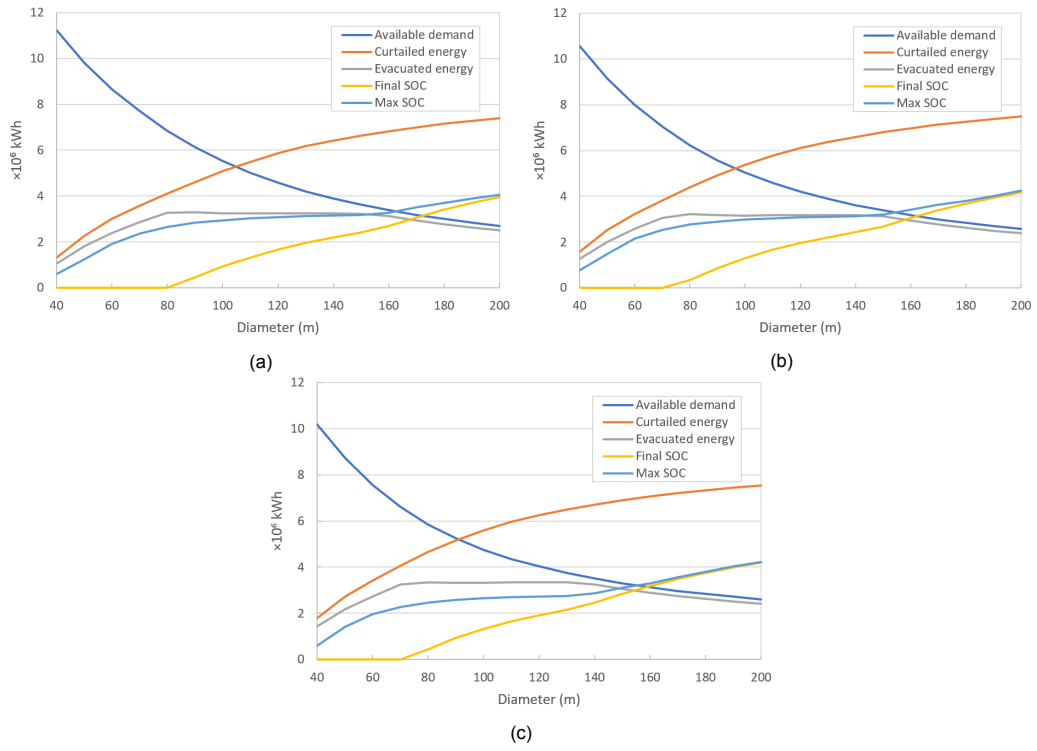

Figure 6.5: Curtailed and evacuated energy with a demand constraint and perfect storage at (a) hub height=80m, (b) hub height=120m, (c) hub height=160m.

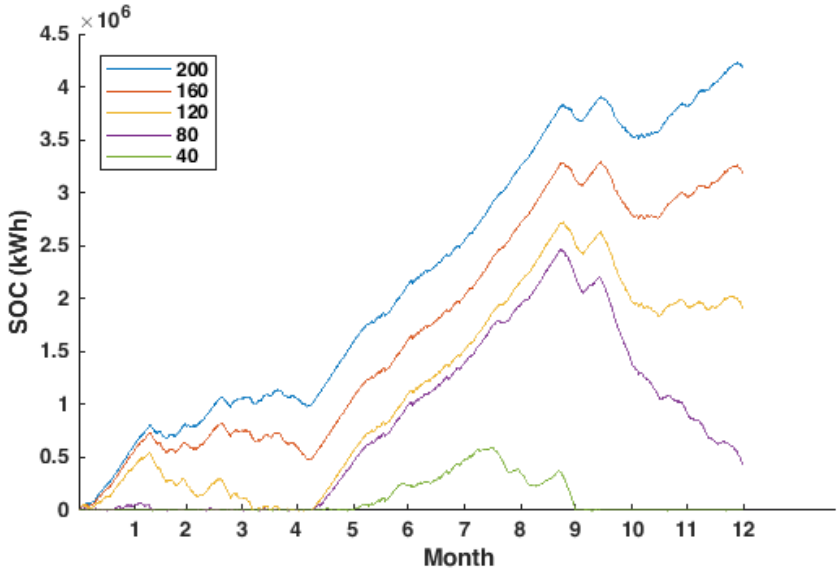

Figure 6.6: SOC of the battery for demand load-supplying wind turbine at 160 meter hub height and different rotor diameters. The numbering of the months are located at the end of each months

Similar seasonal pattern of the SOC is also observed in figure 6.6 for wind turbines with 160-meter hub height and different rotor diameters. The SOC of the battery accumulates from the summer until the end of the monsoon season. In the post monsoon season, the average wind speed and demand load level drops to their lowest, which is shown in figure 3.11. The SOC is dropping due to lower average wind speed and wind power generation in October while the demand load remains the same. This condition is then followed by the decreasing value of the average demand load in November, which results in the higher occurrence of curtailment for wind turbines with larger rotor diameter. Wind turbines with larger rotor diameters have lower rated-wind speed, which allows them to utilise low wind speed condition better than wind turbines with smaller rotor diameters. The lower demand load in this period leads to the inadequate space to evacuate the stored energy, which explains the rising SOC for wind turbines with 160 and 200-meter rotor diameter.

Figure 6.7 presents the shed energy as a function of the storage capacity for wind turbines at 160-meter hub height in the demand load-supplying topology. Similar results as for the grid-connected topology can be observed here. The relationship between the shed energy and storage capacity is linear between 10% and 100% of maximum storage capacity. For lower than 10% storage capacity, the relationship become non linear. At 5% storage capacity, the storage can save around 40 to 45% of the curtailment.

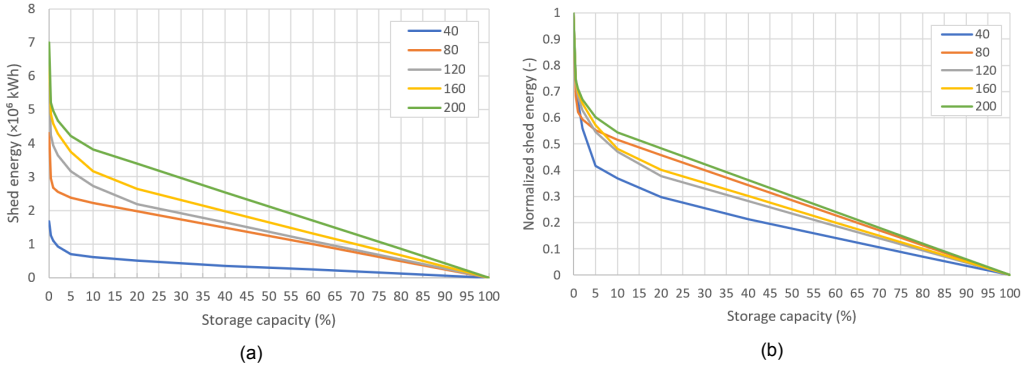

Figure 6.7: Shed energy for different storage capacity presented in its (a) nominal value and (b) normalized value for the demand-constrained topology

6.4. Storage system cost and benefit analysis

The optimum system design result shows the impact of storage system application whose main purpose is to save the curtailed wind energy for later use. Different sizes of the battery determine the level of curtailment that can be saved. The optimum amount of savings is a trade-off between the benefit it brings and the cost it incurred. Cole et al. presented a forecast on the storage system price trend up to the year 2050 for utility scale Lithium ion battery, which will be used to estimate the storage cost in this research. In general, the application of the storage system eases the integration of renewable energy-based power plants in the power system by introducing an additional degree of flexibility. The wind's variability and unpredictability incur difficulties for the system operators in managing the grid and result in an unpriced social cost of wind or integration cost [12]. This cost includes operational cost, transmission cost, curtailment cost, and capacity cost. These costs can be reduced and alleviated by coupling the power system with a storage system. Moreover, the utilisation of stored energy generated from the wind turbine also brings an unpriced pollution reduction benefit. These costs reduction and pollution reduction benefits estimate the benefit of the storage system. The analyses in the following subsections identify the cost of the storage, the saved unpriced social cost that is achieved by employing the storage system and the levelized cost of storage.

6.4.1. Storage capital cost

The capital cost of the lithium-ion battery is estimated from the NREL cost projection study. NREL compiles studies on battery cost projection in [20] from over 25 publications. The low, mid, and highest values from the literature are presented in figure 6.8. For the year 2020, the cost projections for low, mid and high projections are 299.81$/kWh, 332.94$/kWh, and 366.63$/kWh. The mid-value is used in this analysis.

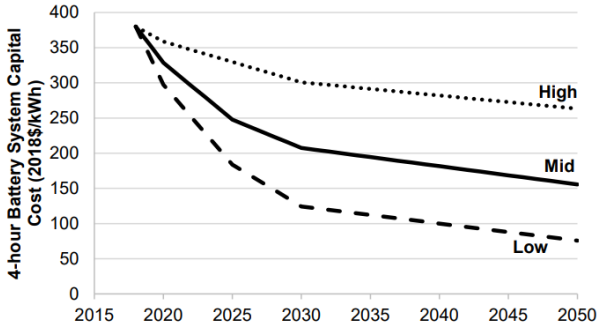

Figure 6.8: Battery cost projections for lithium ion system. [20]

6.4.2. Saved unpriced social costs

Several unpriced social costs and benefits of wind are presented in [2]. The social costs are the products of the variability and partial unpredictability of the wind, which creates difficulties for system operators in managing the grid. As mentioned before, the use of storage may reduce these cost, thus the benefit of having a storage system can be estimated. These costs include:

1. Operational cost
2. Transmission cost
3. Curtailment cost
4. Capacity cost
5. Pollution reduction benefits

To summarise, the parameter of the cost employed in this analysis are presented in table 6.2. These cost are what to be used to estimate the cost reduction or the benefits.

Table 6.2: Unpriced social cost reduction for modelling input

Parameter	symbol	Value	unit
Operation cost	C_{op}	0.004	\$/kWh of the total AEP
Transmission cost	C_{trans}	92.75	\$/kW of wind turbine capacity
Curtailment cost	C_{curt}	curtailment % ×PPA	\$/kWh of the total AEP
Capacity cost	C_{cap}	0.004	\$/kWh of the total AEP
Pollution reduction benefit	C_{pol}	0.099	\$/kWh of the total AEP

1. Operational cost (C_{op})

The operational cost includes the cost of ensuring stable grid operations by continuously balancing total generation with total load despite the variability and unpredictability of renewable energy. The cost ranges from 1.9\$/MWh to 9.7\$/MWh, with an expected value of 4\$/MWh of the total AEP. Operational cost is the cost incurred for ensuring stable grid operations by continuously balancing total generation with total load despite the variability and unpredictability of renewable energy. The ramping of other generators in the system is required to compensate for the variability of the wind. This variability leads to the event of wind energy forecast errors. Reserve capacity, thus, is needed to cover the mismatch in this forecast.
Previous studies estimated different levels of typical errors. [33] presented a prediction model that stated a well-predicted wind farm has a scatter as low as 10% of the installed capacity. Less-accurate prediction wind farms yield a scatter of 20%. The mean absolute error (MAE) of the prediction model is around 15% of the installed capacity. [12] estimated that the day-ahead wind forecast root-mean-squared errors (RMSE) are between 8%-14%. NREL [29] compared day-ahead forecast error distributions from different countries and fitted the data with normal distribution fits. The largest errors are typically around 30%, with the standard deviation ranging around 0.12 to 0.45. A forecast error value of 15% is used to estimate the total generation error in this research. The evacuated energy from storage can supply this forecast mismatch and therefore reduce the error. This discharged energy from the storage is termed as $Q_{discharge}$. The benefit of forecast error reduction ΔC_{op} is calculated in equation 6.1.

$$\Delta C_{op} = \frac{Q_{discharge}}{0.15 \times AEP} \times C_{op} \tag{6.1}$$

2. Transmission cost (C_{trans})

This cost includes the cost of connecting electricity produced by distant and variable renewables to loads. The cost of transmission ranges from 67\$/kW to 570\$/kW of wind capacity. Transmission cost can be translated in \$/MWh by multiplying with $\frac{FCR}{CF \times 8760}$, with FCR as fixed-charged rate and CF as the capacity factor. It is assumed that the cost of transmission is fully compensated by the revenue of transmitting the generated energy. Any extra transmitted energy will be calculated as the benefit or reduction of the overall transmission cost. The use of a storage system can serve this purpose by evacuating the curtailed energy to the grid. The amount of the benefit is calculated by multiplying the sum of the extra transmitted energy (kWh) with the transmission cost in \$/kWh. Thus, a higher capacity factor leads to lower transmission cost. The benefit of the transmission cost reduction is calculated in equation 6.2. TIC_{trans} is the investment on the transmission system. The additional evacuated energy to the grid lowers the final cost of transmission.

$$\Delta C_{trans} = \frac{TIC_{trans}}{AEP} - \frac{TIC_{trans}}{AEP + Q_{discharge}} \tag{6.2}$$

3. Curtailment cost (C_{curt})

This cost occurs during intentional power reduction of wind plants due to grid or market conditions. Curtailment costs are generally socialised through make-whole payment to wind generators for the curtailed energy. This cost can be approximated by the revenues equal to the levelized power purchase agreement (PPA) price ($/MWh) multiplied by the percentage of power curtailed. In the case study location, Tamil Nadu, PPA is estimated around 74$/MWh. In case of 100% storage, all of the curtailed energy is recovered, and the total cost of curtailment is completely alleviated. Thus, the benefit is equal to the total curtailment cost. For partial storage capacity, some of the curtailed energy is shed and unrecovered. The benefit is the reduction of curtailment percentage due to the additional supply of energy from the battery. The curtailment cost reduction is calculated with equation 6.3 where AEP_{full} is the uncurtailed wind generation.

$$\Delta C_{curt} = \frac{Q_{discharge}}{AEP_{full}} \times PPA \tag{6.3}$$

4. Capacity cost (C_{cap})

This cost is indirectly correlated with the operational cost. If the operational cost concerns about the cost for dispatching the backup generation, the capacity cost concerns about the cost of building backup generation (natural gas combustion turbines) to support wind generation to have grid reliability similar to dispatchable generators. The cost ranges between 16$/ to 49$/MW-day with median 106$/MW-day. Multiplying by 24 hours a day, this value equals to 4.42$/MWh. The reduction of the need for back up plan can be estimated from the reduction of the forecast error. Hence, this cost is calculated in 6.4.

$$\Delta C_{cap} = \frac{Q_{discharge}}{0.15 \times AEP} \times C_{cap} \tag{6.4}$$

5. Pollution reduction benefits(C_{pol})

This benefit is estimated with the social cost of each pollutant omitted. The value ranges between 67$/MWh to 187$/MWh with a median of 113$/MWh. Utilising energy generated from the wind that is stored in the battery activates this benefit.

6.4.3. Levelized cost of storage

The Levelized Cost of Storage (LCOS) metric is used to incorporate the present value of the cost and benefit components. Schmidt et al. [2] express this parameter in equation 6.5.

$$LCOS = \frac{TIC_{battery} + \sum_{t=0}^{T} \frac{C_M}{(1+r)^t} + \sum_{t=0}^{T} \frac{C_{charge}}{(1+r)^t} + \sum_{t=0}^{T} \frac{C_{eol}}{(1+r)^t}}{\sum_{t=0}^{T} \frac{Q_{t,discharge}}{(1+r)^t}} \tag{6.5}$$

$TIC_{battery}$ refers to the investment for the total installed cost of the battery, $CAPEX_{battery}$ cost refers to the operation and maintenance, and $Q_{t,discharge}$ refers to the amount of discharged energy from the battery. In order to simplify the equation, several assumptions are employed. Discharged energy is assumed to be constant over different years during the project duration. Charging cost is assumed to be zero due to the fact that the battery is storing the spilt energy from the wind generation curtailment. O&M is also assumed to be constant, and the value is taken from the study. Schmidt et al. suggest zero end-of-life cost, and so does this research. Due to the constant value assumption for the cost components, the equation of LCOS can be simplified with applying the same FCR as the wind turbine

LCOE, which is shown in equation 6.6.

$$LCOS = \frac{TIC_{battery} \times FCR + CAPEX_{battery}}{Q_{discharge}} \tag{6.6}$$

The reductions of the unpriced social costs are then incorporated into the LCOS equation, which results in the equation 6.7. The term Δ refers to the reduction of each of the corresponding costs and $LCOS_{nett}$ refers to the LCOS that incorporates the benefit of the unpriced social cost reduction.

$$LCOS_{nett} = \frac{TIC_{battery} \times FCR + CAPEX_{battery}}{Q_{discharge}} - (\Delta C_{op} + \Delta C_{trans} + \Delta C_{curt} + \Delta C_{cap} + C_{pol}) \tag{6.7}$$

Figure 6.9 presents the result of the cost-reduction benefit for wind turbines with 160-meter hub height and various rotor diameter. It is observed here that the cost-reduction benefit increases at higher rate for lower storage capacity. The rate of benefit addition for an increased battery capacity is flattening at larger rotor diameters. This condition dominates the wind turbine with larger rotor diameter in the demand-load supplying topology, The non-existing space for evacuating the energy from the battery stops the ability for the wind turbine to activate this unpriced social cost-reduction benefit. The benefit of pollution reduction is omitted in this parameter as it is significantly larger than other benefits. Thus, incorporating it in the same figure would make the observation of other parameters harder.

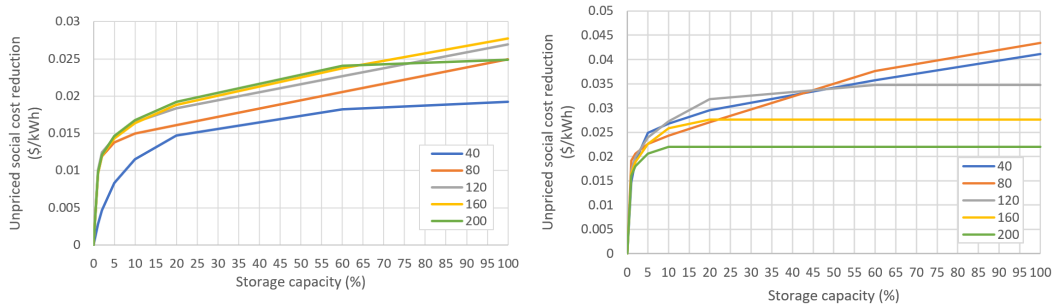

Figure 6.9: Unpriced social cost reduction for wind turbine with 160 meter hub height and various diameter. (a) presents the grid connected topology and (b) presents the demand load supplying topology.

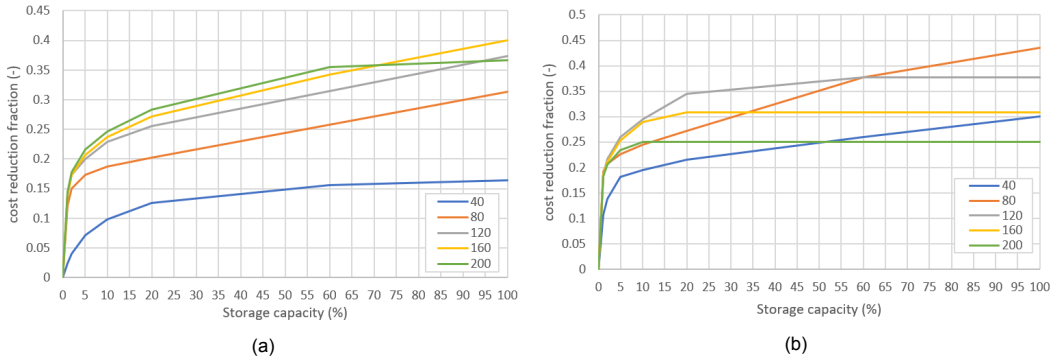

Figure 6.10: Unpriced social cost reduction as a fraction of the total unpriced social cost of the wind generation. (a) presents the grid connected topology and (b) presents the demand load supplying topology.

Figure 6.10 presents the reduction of the unpriced social cost as a fraction of the total unpriced social cost. It is observed here that even at a high capacity of storage, the reduction of the unpriced cost is between 30 and 40%. It is important to note that some of the unpriced social cost, such as the transmission cost, cannot be reduced to zero. The flat lines in figure 6.9 and 6.10 indicates the fully utilised or met-demand. Hence, it is not possible to evacuate and activate the cost reduction. The larger rotor diameter in demand load supplying topology also suffers more from curtailment due to the limited space to evacuate the stored energy. The result of the LCOS is presented in figure 6.12. The cost is

increased linearly with the battery capacity. If one compares the LCOS with the summation of the cost reduction benefits, the LCOS is significantly higher than the calculated benefits. The cost of storage is driven by the required capacity. For the case study location, the consecutive high wind speed during the summer and monsoon accumulates and enlarges the storage capacity. Thus, conclusion from figure 6.9, 6.10 and 6.12a can be termed such as: for instance, an 80-meter rotor diameter and 160 hub height baseline wind turbine operating in a grid-constrained topology requires a storage system with a LCOS of around 3.3 $/kWh which equals to 5% of maximum storage capacity, see figure 6.12a, to be able to reduce the unpriced social cost by around 17%, see figure 6.10a or as much as 0.014 $/kWh, see figure 6.9a.

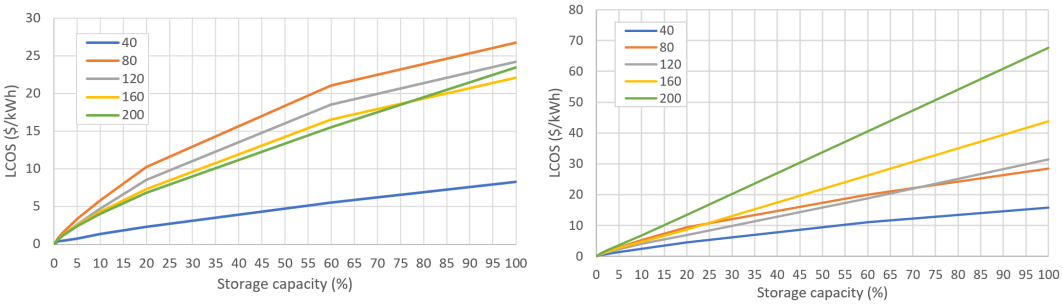

Figure 6.11: LCOS of wind turbine at 160-meter hub height for various rotor diameter in (a) the grid-constrained topology, and (b) the demand-constrained topology.

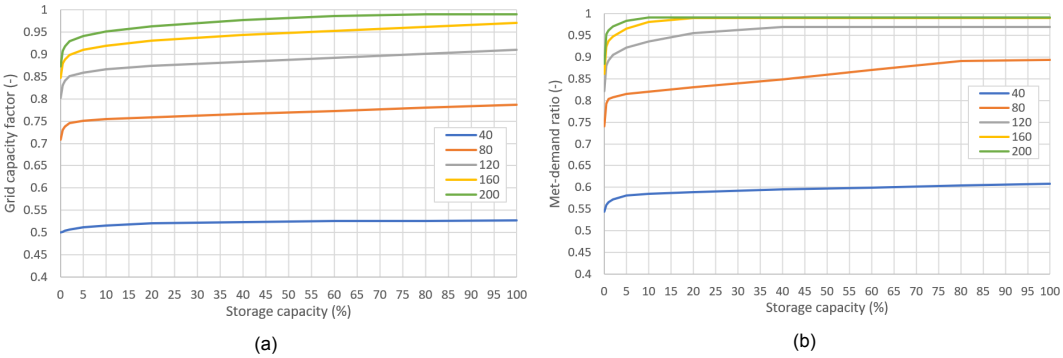

Figure 6.12: (a) The grid capacity factor for wind turbines at 160-meter hub height in a grid-constrained topology. (b) The met-demand ratio for wind turbines at 160-meter hub height in a demand load-supplying topology.

Figure 6.11a presents the grid usage capacity factor for wind turbines with different rotor diameter and at 160-meter hub height in a grid-constrained topology. It can be observed in this figure that the increase of the grid usage frequency, measured in the grid capacity factor. for an additional storage capacity is non-linear for lower storage capacity which become linear at higher storage capacity. Figure 6.11b presents the relationship of the met-demand ratio and different rotor diameters and storage capacity in the demand load-supplying topology. The relationship between the met-demand ratio and different storage capacity is presented in this figure as well, and found to be similar with the grid-constrained topology. Both figures implies the possibility of increasing the grid capacity factor and the met-demand ratio by two methods:

- Employing a higher-capacity storage system. This method allows the hybrid power system to utilize the curtailed wind energy stored in the battery. The cost for increasing these parameters equals to the difference of the LCOS of the initial and final storage capacity employed.
- Increasing the diameter of the rotor increases the grid capacity factor and met-demand ratio. The cost of increasing these parameters with this method equals to the difference of the LCOE of the initial and final rotor diameters.

6.5. Summary

This chapter presents the result of the storage design for different wind turbine operational modes and hybrid power system topology. Several key takeaway from this chapter are:

1. At a certain diameter, the amount of curtailment exceeds the available space to evacuate the stored energy. Thus, increasing the diameter further will increase the requirement of the storage capacity
2. Due to the apparent seasonal variation, storage technology that serves longer periods such as pumped hydro storage and compressed air energy storage are more suitable compared to battery storage. The use of Lithium ion battery in the battery modelling is an approximation on the cost of the required storage.
3. A consecutive days with high wind speed and rated-power wind generation in the summer and monsoon season accumulates the stored energy and enlarges the requirement of storage capacity.
4. The relationship between storage capacity and the amount of curtailment saving is exponential at lower storage capacity (<10% of the maximum storage capacity) and linear at higher storage capacity. Thus the benefit of an additional storage capacity has a diminishing nature. At around 5% storage capacity, the curtailment saving is approximately reach 50%.
5. The benefit of having the reduction of the unpriced social cost does not compensate the cost of storage. This result is driven by the significant seasonal variation of the case study location that increases the requirement of storage capacity. This conclusion may differ for other locations with milder seasonal variation.

7

Discussion

This chapter contains the discussion of the results, initialised with the result interpretation in section 7.1 followed by the implication of the study in section 7.2.In section 7.3, the limitations of the analysis due to the employed assumptions and decisions are presented. This section is followed by sensitivity analysis that regards future uncertainties in section 7.4.

7.1. Result interpretation

This research is stemming from the need for the renewable energy integration into the power system. Previous studies confirm the role of hybrid power system in the effort of the renewable energy integration. Thus, a method of hybrid power system optimisation is proposed in this research by designing the wind turbine that considers the complementary generation nature of the hybrid power system. The proposed design is then evaluated to confirm its technical and economical feasibility. The technical feasibility study evaluates the design alteration, and the economic feasibility study evaluates the costs in generating power of the design.

In general, the research results have identified the optimal design of the wind turbine for the hybrid power system. As the research is broken down in several analyses, each of the results are presented as follows:

1. The literature review in the introduction and chapter 3 that discuss the site condition analysis answers the subquestion 2 and the main question partially. Designing wind turbine that considers the diurnal and seasonal variation requires to consider the change in three site condition parameters: wind speed distribution, wind shear and turbulence intensity. To limit the scope of the analysis in this thesis, only the wind speed distribution is employed in the analysis,

2. The research subquestion 3 that concerns about the design changes of the wind turbine design is answered by the result of Chapter 4 and 5. Chapter 4 presents the wind turbine design process and chapter 5 presents the result for different operational modes. Lower wind speed condition leads to a higher difference of AEP between different diameters. Thus, the same increase in rotor diameter results in the AEP higher gain at low wind speed condition than in high wind speed condition. This condition leads to a wider rotor optimum diameter at the location with lower wind speed condition and, vice versa, smaller rotor diameter for the location with higher wind speed condition. This result details the process of achieve the optimum rotor diameter realisation. This result also confirms the finding in the study of Hirth et al. that wind turbine design with a cost of electricity minimisation objective at high speed location will result in a relatively smaller rotor diameter which they refer as the classical turbine design [28]. In their study of the system friendly

wind turbine design, the system friendliness of the turbine can be increased with the advanced turbine design by employing larger rotor diameter.

Chapter 5 presents the modelling result of different operational modes and answers the research subquestion 1 that regards the optimum design for each operational modes. Different operational modes yield different wind speed distribution, and therefore, different optimum rotor diameters. This analysis is similar with the optimum design analysis in chapter 4 with the only difference in this chapter is that the data from the case study are employed. Hence, a similar conclusion can be taken.

3. Further analysis in chapter 5 answers the research subquestion 4 that questions the performance comparison between the standard operation and the night-time and low-wind speed period operation. The research models the hyrbid power system that consists of wind power and solar PV generation and curtails the wind power in the event of overproduction. This results in higher curtailment for Wider rotor diameter due to the lower rated wind speed and higher AEP. The curtailment is higher for demand load supplying topology when compared to the grid connected topology. The performance of the wind turbines are also measured by the metric of grid capacity factor and met-demand ratio. Subsequently, even with higher curtailment, wind turbines with larger rotor diameter yield higher AEP and, hence, higher grid capacity factor and met-demand ratio.

4. The subquestion 5 regards the storage system benefit and is answered in the chapter 6. The results show that, for referred the case study, the size of the storage capacity to save the curtailment follows a non linear relationship at lower capacity which then become linear at higher capacity . Thus, the first 5-10% of the storage capacity yield the most cost effective saving.
The analysis of the storage system for the case study finds that the consecutive days of high power generation accumulates the stored energy and enlarge the energy storage. When the cost of storage is applied, this condition results in a very high cost of storage system.

7.2. Scientific implication

The imminent renewable integration that is driven by the high necessity to decarbonise the means of generating electricity results in additional challenges to the power system. The need for power system flexibility is imperative to respond the variable and unpredictable fluctuating-renewable generation. This condition motivates the studies in the hybrid power system - a system where multiple generation technologies are employed.

While previous studies on the hybrid power system optimisation focus on the technology selection and capacity sizing of its components, this research take a different approach of optimisation. This research focuses on the analysis of the complementary generation effect on the wind turbine design that is operated in a hybrid power system. The capacity sizing and technology components of the hybrid power system are predetermined, consisting a wind turbine, solar PV and grid connection or demand load with their capacity are normalized into a nominal capacity, In the proposed method, the wind turbine is modeled in the different operational modes and hyrbid power system topologies. This way, the effect of the operational condition on the design of the wind turbine can be isolated and identified. The operational conditions incorporate the standard operation that serves as the baseline condition, night-time operation and low-wind speed period operation. The different operational modes are employed to emphasis the complementary generation between the wind turbine and the solar PV.

The result of only considering a limited time period of wind speed data in the night-time and low-wind speed period to define the diurnal and seasonal wind condition is inline with the study of Weisser et al. [55]. In their study, it is identified that taking the average wind speed distribution leads to under and overestimation of the turbine performance, which is also the case for the low-wind speed season between October and April in the case study location. Thus, wind turbine with a standard design produces lower generation capacity than the wind turbine that is optimally designed for the particular period.

The optimum wind turbine design analysis in chapter 4 contributes a clearer understanding of how the optimum diameter shifts when a different wind speed distribution data is employed. This different wind speed distribution can refer to the description of site at: (1) two different locations, (2) same location but at different heights, (3) same location but at different time or (4) a combination of the conditions. The results indicate that the optimum is reached when the ratio of the final cost to the initial cost incurred for an additional length of diameter, from the initial to the final diameter, is equals to the ratio of the final AEP to the initial AEP.

The result on the operation modelling provides a new insight into the relationship between the wind generation curtailment and rotor diameter. In a topology of hybrid power system with a constrained evacuation method, due to the limited grid capacity and low demand load, wider rotor diameter suffers more from curtailment. Thus, when a cost model is employed, the optimum rotor diameter shifts to lower rotor diameter. In other words, the high level of curtailment makes wind turbine generation with relatively larger rotor diameter becomes less attractive in terms of its cost to generate power.

7.3. Limitations of the research

In the methodology and the modelling, simplifications and assumptions were incorporated, as shown in chapter 2,3,4 and 5. As the simplifications and assumptions impact the outcome of the analysis, these consequences will be assessed in this section.

7.3.1. Optimisation method

The research question aims to explore the wind turbine design that is tailored for the hybrid power system and expresses its technical and economic feasibility. The design process is based on the optimisation of the wind turbine blade and hub height. Thus, the optimisation process of the wind turbine in this research is then decided to search for the minimum cost of electricity. The optimisation result defines the cost of electricity as function of the wind turbine blade length and hub heights. Hence, the minimum cost of electricity can be identified at the optimum rotor and hub height.

However, the finding from the chosen case study in the site condition analysis presented in chapter 3 is that there is a significant seasonal pattern over the year. Thus, an arbitrary day is not the typical representation of the days over the year. For instance, some periods of the year will have higher average electricity spot price than other periods. This effect is neglected in the optimisation method of cost of electricity minimisation. The design for the seasonal wind turbine that refers to the low wind speed period does not identify the added value of the design. An alternative optimisation method that incorporates the variation of electricity spot price electricity is profit maximisation.

Therefore, in order to compensate the lack of analysis depth in the cost minimisation optimisation method, other metric that measure the benefit of the added value for the seasonal design could be employed. As the seasonal design results in relatively larger rotor diameter, the added value is measured as the increased capacity factor and met demand percentage.

7.3.2. Hybrid power components sizing

The sizing of the wind turbine, solar PV and grid or demand capacity are normalized to a single dimension. This sizing decision is however not representative of practice, especially in the case with high seasonal variation. This sizing of the components employed in this research is more of a hypothetical approach that aims to explore the effect of complementary generation to the wind turbine design. Employing the same dimension of capacity allows the identification of overlapping of generation and the complementarity between the wind and solar generation and the demand profile.

7.3.3. Site condition parameters

As discussed in 1.3, the site condition parameters that change when considering the diurnal and seasonal variation, apart from the wind speed, are the turbulence intensity and shear profile. As the optimisation method aims to minimise the cost of electricity, the wind speed distribution plays a significant role in determining the optimum design, as presented in the result of section 4.3. Wind shear affects the vertical wind speed profile and therefore, defines the wind speed at different hub heights.

On the other hand, wind shear and turbulence intensity affect the fatigue life of the wind turbine, and therefore, affect the cost of the wind turbine. This analysis is omitted from the cost analysis of the wind turbine for several reasons mentioned in scope of the analysis in 1.6. The finding in the study of Sathe et al. [42] indicates that wind shear and turbulence intensity have a negative correlation. Thus, when the fatigue induced by the wind shear is relatively higher, the fatigue induced by the turbulence is lower, and vice versa. Therefore, it is important to note that the result in this research neglects this effect. A complete cost of wind turbine analysis that consider different shear and turbulence parameter shall consider this effect.

7.3.4. Mass and cost function

The definition of this parameter is central to this research. The adjustment of blade mass function is based on the compiled dataset of commercial wind turbines. The dataset is confirmed by the previous study, and therefore the mass function is sufficient for this research. However, it is important to note that this result yields uncertainty to some extent due to the limited data of the compiled data. As the compiled data concentrates more on a particular range of diameters (around 80 meter diameter), the validity level of the results is higher in this size range. Therefore, results for rotor diameters outside this range are subject to higher uncertainty. The adjustment of blade mass is then used to adjust of other component's mass and cost scaling.

7.3.5. The effect of different hub heights

Apart from altering the rotor diameter, the hub height is also subjected to the optimisation process. The site condition analysis confirms the shear profile effect on the vertical wind speed distribution that higher hub height has higher average wind speed. The optimum analysis in section 4.3 reveals that the higher hub height shifts the optimum cost of electricity to a higher value. This effect also depends on the mass and cost scaling function employed. Thus, the significance of the hub height in affecting the cost of generation is driven by its mass and cost function of the tower.

7.3.6. Storage system definition

The storage system is an integral part of a hybrid power system, which explains its importance to model it in this research. The storage system employed is a Lithium ion battery. While this storage fits for compensating mismatch in diurnal variation, this technology is however may not be the best option for compensating the long duration of the seasonal variation, especially when there is a significant seasonal variation. The use of lithium ion is an approximation approach to estimate the cost of the storage as it is, based on the reviewed literature, one of the most common technologies for utility scale storage systems. This approximation, however, results in a very high cost of the storage system. Other technology with lower levelized cost such as pumped hydro or compressed air energy storage may fits better for long term storage. However, it is important to note that these storage technologies highly depends on the geographical condition. Pumped hydro requires a reservoir with a certain height difference which may not be available for the case study location as it is located in a location with an arid-savanna climate.

The compensation of the storage cost in this analysis is approximated by identifying the reduction of the unpriced social cost of wind generation such as the cost incurred due to the forecast mismatch and

curtailment. The use of storage enables the use of the stored wind energy at a different timestamp. This stored energy can be utilised to either supply the grid, meet the demand or compensate the forecast error. The results shows that the reduction of this unpriced cost does not pay off the storage cost. The compensation of storage cost can be achieved when one considers the profit for evacuating the stored energy generated from the electricity spot price.

7.4. Sensitivity analysis

The sensitivity analysis considers the case where lower cost of storage is employed. This is due to two possibilities: (1) the scenario in the future where the cost of storage for a Lithium ion battery decreases or (2) the case where different storage technology that is cheaper is employed. Both scenarios lowers the cost of storage to half as much as the initial value. Cole et al. [20] project the capital cost for Lithium ion in 2050 at 150 $/kWh. Mongrid et al. [38] estimate the cost of pumped hydro storage at the value of 165 $/kWh. The value of new storage investment cost of 150$/kWh is used in this sensitivity analysis to represent both the scenario with lowering Lithium ion cost and the lower cost of pumped hydro storage.

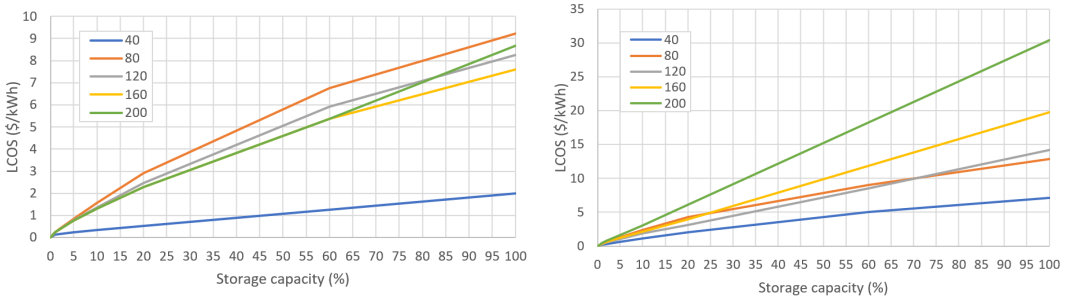

Figure 7.1: The LCOS of wind turbine at 160-meter hub height for various rotor diameter in (a) the grid-constrained topology, and (b) the demand-constrained topology for the future scenario.

A reduction of storage cost to around half of the initial storage capital investment cost reduces the LCOS for both the grid-constrained and demand load-supplying topology. The reduction effect is however higher for the grid constrained topology. The sensitivity analysis results for the grid connected topology in a reduction of the investment cost to around 34.5% of the initial cost and to 40% for the demand load-supplying topology. This cost reduction may increase the attractiveness for the application of the storage system. The other possible ideal scenario is to combine the use of different storage technologies depending on the storage period length. The lithium ion battery can be focused on the shorter period storage, and for the long term storage, other storage technology can be used.

8

Conclusions & Recommendations

At the beginning of this thesis, the need for designing a hybrid power system is identified as a promising solution to answer the imminent renewable energy integration in the future. One way to design the hybrid power system is by designing its technology components. This research focuses on the design of the wind turbine that is operated in a hybrid power system. Typically, a hybrid power system consists of multiple generation technologies. This combination enables the generating technologies to complement each other and, hence, increase the overall performance of the power system. A hybrid power system with wind turbine and solar PV is modeled in the research. The research aims to identify the impact of the complementary generation on the wind turbine design. This motive is exercised by considering the extreme cases where the wind turbine is operated when the solar PV is not generating. The cost of the electricity generation defines the economic feasibility of the result. This chapter serves to conclude the result and the analysis on the aforementioned subject of the wind turbine design, which will be given in section 8.1. Section 8.2 finishes the report with recommendations for further research as well as relevant stakeholders who is concerned about the discussed topic.

8.1. Conclusion

In order to analyse the main research question, several subquestions are generated and analyses have been conducted. The results have led to these conclusions:

Diurnal and seasonal wind turbine design

The design process optimises the wind turbine design for limited periods, that is only at night or only during the low-wind speed season. The result shows that the COE for this wind turbine design is actually higher than the baseline design that considers full-year wind period. When the night-time wind turbine and the seasonal wind turbine are fully operated throughout the year, as expected, they are not operating at their optimum condition. Hoevewer, it is important to note that these wind turbines brings more value during the particular period for which they have been designed by operating at their optimum.

Optimum design analysis

The wind turbine design process that optimises the rotor diameter as conducted in this research results in a better understanding of how the optimum rotor diameter shifts. Lower wind speed conditions shifts the optimum to a larger rotor diameter and vice versa. When the wind turbine is subjected to the

possibility of energy curtailment, due to limited grid capacity or low demand load, larger rotor diameters suffers more from curtailment, and thus the optimum rotor diameter shifts towards a smaller diameter.

Storage system characteristic

A storage system is employed in the hybrid power system to save the loss from curtailment. The saved curtailment is then utilized to reduce the unpriced social cost of the wind generation. Other literature may refer to this cost as the cost of integration of wind energy. It is concluded that for the storage in Lithium-ion batteries, the benefit of having the unpriced social cost reduced does currently not pay off the cost of storage to provide this reduction service. For the case study, it is also found that the relationship between the amount of saving and the maximum required storage capacity is not linear at low storage capacity, which later on becomes linear at higher storage capacity. Thus, this diminishing nature of additional benefit makes the first few percentage addition of the storage capacity the most cost effective.

8.2. Recommendation

Based on the results and the conclusion of this report, several recommendations will be given. The recommendation concerns policy makers, wind farm project developer and researchers in wind energy.

Recommendation for policy makers

- The diurnal and seasonal wind turbine design result indicates the less optimum cost of electricity of the wind turbines. Nevertheless, this design can give some benefits to the system operators and end users by having a more stable generation output. Therefore, a means of policy support such as a subsidy scheme or adjustment in the market regulation and mechanism can make the application of wind turbines with such design more attractive.
- For the case study analysis results, the significant seasonal variance makes the application of a storage system less economic feasible. Thus, grid expansion to export power generation surplus to other states is another way to better utilize the generated energy. Therefore, supporting policies are necessary in the effort of expanding the grid as well as creating an efficient interstate electricity market.

Recommendation for project developers

- The method employed in this study reveals that energy curtailment results in the reduction of profitability of the wind turbine, especially for the wind turbine with larger rotor diameters. Therefore, similar analysis that considers the level of expected curtailment of a particular site/project may be necessary to ensure the deployment of the wind turbine for the project is using the optimum wind turbine.

Recommendation for further research

- In general, the limitation of this research can be the starting point to further explore the topic of diurnal and seasonal wind turbine design. For instance, a different methodology that maximises profit can be employed to further indicate the added value of the design
- Incorporating the diurnal and seasonal variation to the wind turbine design involves with the variation of the wind speed distribution, wind shear and turbulence intensity. The design process in this thesis only considers the wind speed distribution differences and partially, the wind shear profile. Fully incorporating all of the three parameters may give a more comprehensive insight in the feasibility of the diurnal and seasonal wind turbine design. For instance, a research that takes these parameter differences into account can identify the effect of the limited operational modes on the fatigue life of the wind turbine.

- Different location and technology composition of the hybrid power system such as hydro power, offshore wind, or biomass can give insight from different perspective on the generation complementarity of the hybrid power system, considering different energy sources involve different variation in diurnal and seasonal basis.

A

NREL cost and scaling model

This appendix presents the mass and cost model employed in the analysis, which is adjusted from the NREL mass and cost model [26]. The adjustment of the blade mass function is presented in section 4.2. The mass functions, for the NREL version and the adjusted version, are presented as follows:

$$m_{blade,\,NREL} = 0.1452 \times R^{2.9158} \tag{A.1}$$

$$m_{blade,\,Adjust} = 17.6245 \times R^{1.1615} \tag{A.2}$$

In order to incorporate the adjustment to the other component's mass and cost function, especially those that are a function of the diameter, the mass generated from the adjusted function, $m_{blade,\,Adjust}$, is used to estimate the diameter that would have generated the same mass when using the NREL mass function, D_{Adjust}.

$$D_{Adjust} = 2 \times \left(\frac{m_{blade,\,Adjust}}{0.1452}\right)^{\frac{1}{2.9158}} \tag{A.3}$$

As presented in figure 4.4, the adjusted blade mass function results in a lower function than the NREL blade mass function. If the other components are not adjusted, the result will be inconsistent as some components are using the NREL function and some others are not. Thus, the adjusted diameter, D_{Adjust}, should be used to calculate the mass and cost function of components that are function of the diameter, such as hub, nose cone, pitch and bearing system, and many others. The full components mass and cost functions are presented in table A.1, A.2 and A.3

Table A.1: Total Installed Cost (TIC) components of the wind turbine (1)

Component	Parameter	Function
Blade	Mass	$0.1452 \times (R)^{2.9158}$
	Cost	$(0.4019 \times (R)^{3} - 955.24 + 2.7445 R^{2.5025})/(1-0.28)$
Hub	Mass	$0.945 \times (m_{blade}) + 5680.3$
	Cost	$m_{hub} \times 4.25$
Pitch Mechanisms and Bearings	Mass	$(0.1295 \times 3 \times m_{blade}) + 491.31$
	Cost	$2.28 \times (.2106 \times D^{2.6578})$
Pitch system	Mass	(Total Pitch Bearing Mass × 1.328) + 555
Spinner, Nose cone	Mass	18.5 × D - 520.5
	Cost	$m_{nosecone} \times 5.57$
Low-speed shaft	Mass	$0.0142 \times D^{2.888}$
	Cost	$0.01 \times D^{2.887}$
Main Bearing	Mass	$(D \times 8/600 - 0.033) \times 0.0092 \times D^{2.5}$
	Cost	$2 \times m_{bearing} \times 17.6$
Gearbox total	Mass	$70.94 \times P_{rated}^{0.759}$
	Cost	$16.45 \times P_{rated}^{1.249}$
Generator	Mass	$6.47 \times P_{rated}^{0.9223}$
	Cost	$P_{rated} \times 65$
Variable-speed electronics total	Cost	$P_{rated} \times 79$
Yaw drive and Bearing	Mass	$1.6 \times (0.0009 \times D^{3.314})$
	Cost	$2 \times (0.0339 \times D^{2.964})$
Mainframe	Mass	$2.233 \times D^{1.953}$
	Cost	$9.489 \times D^{1.953}$
Platform	Mass	$0.125 \times m_{mainframe}$
	Cost	$1.0875 \times m_{mainframe}$
Electrical connections	Cost	$P_{rated} \times 40$
Hydraulic, cooling system	Mass	$0.08 \times P_{rated}$
	Cost	$P_{rated} \times 12$
Nacelle	Mass	$C_{nacelle}/10$
	Cost	$11.537 \times P_{rated} + 3849.7$
Control & Safety system	Cost	$ 35000
Tower	Mass	$(0.397 \times A \times z_{hub} - 1414) \times 1.5$
	Cost	$m_{tower} \times 1.50$

Table A.2: Total Installed Cost (TIC) components of the wind turbine (2). These components are also in the group of the Balance of Station

Component	Parameter	Function
Foundation	Cost	303.24 × $(z_{hub} \times A)^{0.4037}$
Transportation	Cost	1.581E-5 × ${P_{rated}}^2$ -0.0375 × P_{rated} + 54.7
Roads, Civil work	Cost	2.17E-6 ×${P_{rated}}^2$ -0.0145 × P_{rated} + 69.54
Assembly and Installation	Cost	1.965 × $(z_{hub} \times D)^{1.1736}$
Electrical interface/connections	Cost	3.49E-6 × ${P_{rated}}^2$ -0.0221 × P_{rated} + 109.7×P_{rated}
Engineering, Permits	Cost	P_{rated} × (9.94E-4 × P_{rated} + 20.31)

Table A.3: Annual Operating Expenses

Component	Parameter	Function
Levelized replacement cost	Cost	10.7 × P_{rated}
Operations and maintenance	Cost	0.007 × AEP
Land lease costs	Cost	0.00108 × AEP

B

Compiled wind turbine data

This appendix presents the compiled data of the commercial wind turbines. The consideration of choosing what to compile is the availability of the concerned parameters: rated power, diameter, year of design/introduction, wind class and blade mass. The data are collected from the website of the manufacturers and online database of commercial wind turbine [5]. The compiled data are presented in table B.1.

Table B.1: Compiled commercial wind turbine data

	Power (MW)	D (m)	R (m)	Year	Specific rating (W/m2)	Wind class	Blade mass (ton)
WindPACT	0.75	50	25	2006	382		1.9
	1.5	70	35	2006	389.8		4.3
	3	99	49.5	2006	389.7		13.2
	5	128	64	2006	388.6		27.8
Suzlon	2.1	95	47.5	2011	296.3	2A	14.8
	2.1	97	48.5	2012	284.2	3A	15.3
Aerodyn	1.5	77.1	38.55	1994	321.3	2A	10.5
	1.5	82.7	41.35	2006	279.2	2A	10.5
	1.5	86.7	43.35	2006	254.1	3A	10.9
	1.5	92.1	46.05	2006	225.2	3B	11.7
	2.5	102.9	51.45	2007	300.6	1B/2A	18.7
	2.5	109.7	54.85	2007	264.5	3A	18.7
	2.5	118.3	59.15	2007	227.4	3B	17.8
	3	102.9	51.45	2010	360.7	1B	18.7
	3	133.6	66.8	2010	214	2A	24.9
	3	140	70	2010	194.9	2A	24.6
	3	145	72.5	2010	181.7	3A	34.3
	4	140.4	70.2	2017	258.4	2B/3A	37.3
	4	147	73.5	2017	235.7	S	41.7
	4	150	75	2017	226.4	3A	42.3
Vestas	1.8	80	40	1999	358.1	2A	12.3
	1.8	90	45	2003	282.9	2A	12.7
	2	66	33	1997	584.6	1A	7.7
	2	80	40	1999	397.9	1A	12.3
	2	90	45	2003	314.4	2A/S	12
	2	100	50		254.6	2B	15
GE	1.5	70.5	35.25	2001	384.3	2	9.3
	1.5	77	38.5	2002	322.1	2A/S	10.3
	1.5	82.5	41.25	2001	280.6	3B	10.3
	2.5	100	50	2011	318.3	2B/3A	17.3
	3	90	45		471.6	1B	16.3
	3	94	47		432.3	2A	16.7
	3.6	104	52		423.8	1	27.3
	3.6	111	55.5		372	1	27.7

Bibliography

[1] India wind data download API | NREL: Developer network. URL https://developer.nrel.gov/docs/wind/wind-toolkit/india-wind-download/.

[2]

[3] Contour Map Creator. URL https://contourmapcreator.urgr8.ch/.

[4] Sunrise and sunset times in muppandal. URL https://www.timeanddate.com/sun/@11656467. Library Catalog: www.timeanddate.com.

[5] Wind energy database. URL https://www.thewindpower.net/.

[6] *Upscaling of Wind Turbine Systems*, chapter 4, pages 75–104. John Wiley Sons, Ltd, 2011. ISBN 9781119975441. doi: 10.1002/9781119975441.ch4. URL https://onlinelibrary.wiley.com/doi/abs/10.1002/9781119975441.ch4.

[7] *The Wind Resource*, chapter 2, pages 9–38. John Wiley Sons, Ltd, 2011. ISBN 9781119992714. doi: 10.1002/9781119992714.ch2. URL https://onlinelibrary.wiley.com/doi/abs/10.1002/9781119992714.ch2.

[8] Study Says Renewable Power Still Reliant on Backup from Natural Gas, August 2016. URL https://www.power-eng.com/2016/08/17/study-says-renewable-power-still-reliant-on-backup-from-natural-gas/.

[9] Overcapacity and the challenges of going 100% renewable, July 2017. URL https://www.power-technology.com/features/featureovercapacity-and-the-challenges-of-going-100-renewable-5872868/.

[10] Negative electricity prices: lockdown's demand slump exposes inflexibility of German power, May 2020. URL https://energypost.eu/negative-electricity-prices-lockdowns-demand-slump-exposes-inflexibility-of-german-power/.

[11] U.S. Energy Information Administration. International energy outlook 2019. Technical report, IEA, 2019.

[12] Jay Apt and P. Jaramillo. *Variable renewable energy and the electricity grid*. 01 2014. doi: 10.4324/9781315848709.

[13] T. Ashuri. *Beyond Classical Upscaling: Integrated Aeroservoelastic Design and Optimization of Large Offshore Wind Turbines*. 11 2012. ISBN 978-94-6203-210-1.

[14] Central Electricity Authority. National electricity plan 2016 - volume II transmission. Technical report, Central Electricity Authority.

[15] L. Bird, M. Milligan, and D. Lew. Integrating variable renewable energy: Challenges and solutions. 9 2013. doi: 10.2172/1097911.

[16] Thomas Bowen, Ilya Chernyakhovskiy, and Paul L Denholm. Grid-scale battery storage: Frequently asked questions. doi: 10.2172/1561843.

[17] Deb Chattopadhyay and Mohar Chattopadhyay. Climate-aware generation planning: A case study of the tamil nadu power system in india. 25(6):62 – 78. ISSN 1040-6190. doi: https://doi.org/10.1016/j.tej.2012.06.011. URL http://www.sciencedirect.com/science/article/pii/S1040619012001558.

[18] P. Chaviaropoulos. Similarity rules for w/t up-scaling. Technical report, UpWind, 2007.

[19] Ilhami Colak and Ersan Kabalci. *Control Methods Applied in Renewable Energy Systems*, pages 205–246. Springer International Publishing, Cham, 2014. ISBN 978-3-319-03224-5. doi: 10.1007/978-3-319-03224-5_7. URL https://doi.org/10.1007/978-3-319-03224-5_7.

[20] Wesley J Cole and Allister Frazier. Cost projections for utility-scale battery storage. 6 2019. doi: 10.2172/1529218.

[21] International Electrotechnical Commission. Iec 61400-1:2019. wind energy generation systems - part 1: Design requirements. Technical report, International Electrotechnical Commission, 2019.

[22] International Finance Corporation. Utility-scale solar photovoltaic power plants: A project developer's guide. Technical report, IFC. URL https://www.ifc.org/wps/wcm/connect/Topics_Ext_Content/IFC_External_Corporate_Site/Sustainability-At-IFC/Publications/Publications_Utility-Scale+Solar+Photovoltaic+Power+Plants. Library Catalog: www.ifc.org.

[23] Kaushik Das, Anca Daniela Hansen, Divyanagalakshmi Haribabu Vangari, Matti Juhani Koivisto, Poul Ejnar Sørensen, and Müfit Altin. Enhanced features of wind based hybrid power plants. In *Proceedings of the 4th International Hybrid Power Systems Workshop*, 2019. URL http://hybridpowersystems.org/. 4th International Hybrid Power Systems Workshop ; Conference date: 22-05-2019 Through 23-05-2019.

[24] King J DiOrio N King R Gevorgian V Corbus D Blair N Anderson K Stark G Turchi C Moriarity P Dykes, K. *Opportunities for Research and Development of Hybrid Power Plants*. National Renewable Energy Laboratory Golden, Colo, 2020.

[25] Jr. Eggers, A. J., R. Digumarthi, and K. Chaney. Wind shear and turbulence effects on rotor fatigue and loads control. 125(4):402–409. ISSN 0199-6231. doi: 10.1115/1.1629752. URL https://doi.org/10.1115/1.1629752.

[26] L. Fingersh, M. Hand, A. Laxson, and National Renewable Energy Laboratory (U.S.). *Wind turbine design cost and scaling model*. National Renewable Energy Laboratory Golden, Colo, 2006.

[27] J. F. P. Galvin. The weather and climate of the tropics: Part 6 – monsoons. 63(5):129–137. ISSN 1477-8696. doi: 10.1002/wea.230. URL https://rmets.onlinelibrary.wiley.com/doi/abs/10.1002/wea.230. _eprint: https://rmets.onlinelibrary.wiley.com/doi/pdf/10.1002/wea.230.

[28] Lion Hirth and Simon Müller. System-friendly wind power: How advanced wind turbine design can increase the economic value of electricity generated through wind power. *Energy Economics*, 56: 51 – 63, 2016. ISSN 0140-9883. doi: https://doi.org/10.1016/j.eneco.2016.02.016. URL http://www.sciencedirect.com/science/article/pii/S0140988316300317.

[29] B M Hodge, D Lew, M Milligan, H Holttinen, S Sillanpaa, E Gomez-Lazaro, R Scharff, L Soder, X G Larsen, G Giebel, D Flynn, and J Dobschinski. Wind power forecasting error distributions: An international comparison; preprint.

[30] IGEF. Repowering of old wind turbines in india. Technical report, Indo German Energy Forum.

[31] Muhammad Irfan, Zhen-Yu Zhao, Munir Ahmad, and Marie Claire Mukeshimana. Critical factors influencing wind power industry: A diamond model based study of india. 5:1222–1235. ISSN 2352-4847. doi: 10.1016/j.egyr.2019.08.068. URL http://www.sciencedirect.com/science/article/pii/S2352484719303804.

[32] J Jonkman, S Butterfield, W Musial, and G Scott. Definition of a 5-mw reference wind turbine for offshore system development. doi: 10.2172/947422.

[33] L Landberg. Short-term prediction of local wind conditions. *Journal of Wind Engineering and Industrial Aerodynamics*, 89(3):235 – 245, 2001. ISSN 0167-6105. doi: https://doi.org/10.1016/S0167-6105(00)00079-9. URL http://www.sciencedirect.com/science/article/pii/S0167610500000799. 10th International Conference on Wind Engineering.

[34] R. Luna-Rubio, M. Trejo-Perea, D. Vargas-Vázquez, and G.J. Ríos-Moreno. Optimal sizing of renewable hybrids energy systems: A review of methodologies. *Solar Energy*, 86(4):1077 – 1088, 2012. ISSN 0038-092X. doi: https://doi.org/10.1016/j.solener.2011.10.016. URL http://www.sciencedirect.com/science/article/pii/S0038092X11003835. ISRES 2010.

[35] Helge Madsen, Michael McWilliam, Frederik Zahle, Flemming Rasmussen, Matti Koivisto, and Marie Münster. The lowwind turbine concept for optimal system integration. 07 2019. doi: 10.13140/RG.2.2.15478.65604.

[36] A. Merzic, M. Music, and E. Redzic. A complementary hybrid system for electricity generation based on solar and wind energy taking into account local consumption - case study. In *2013 3rd International Conference on Electric Power and Energy Conversion Systems*, pages 1–6, 2013.

[37] Y.S. Mohammed, M.W. Mustafa, and N. Bashir. Hybrid renewable energy systems for off-grid electric power: Review of substantial issues. *Renewable and Sustainable Energy Reviews*, 35: 527 – 539, 2014. ISSN 1364-0321. doi: https://doi.org/10.1016/j.rser.2014.04.022. URL http://www.sciencedirect.com/science/article/pii/S1364032114002494.

[38] Kendall Mongird, Vilayanur V. Viswanathan, Patrick J. Balducci, Md Jan E. Alam, Vanshika Fotedar, V S. Koritarov, and Boualem Hadjerioua. Energy storage technology and cost characterization report. doi: 10.2172/1573487.

[39] Ministry of New {and} Renewable Energy. Annual report 2018-19. Technical report, MNRE. URL https://mnre.gov.in/img/documents/uploads/0ce0bba7b9f24b32aed4d89265d6b067.pdf.

[40] F Oteri. Overview of existing wind energy ordinances. Technical report.

[41] Acacia Pepler, David Jones, and Karl Braganza. Explainer: what is 'precipitable water', and why does it matter? URL http://theconversation.com/explainer-what-is-precipitable-water-and-why-does-it-matter-73358. Library Catalog: theconversation.com.

[42] A. Sathe, J. Mann, T. Barlas, W.A.A.M. Bierbooms, and G.J.W. van Bussel. Influence of atmospheric stability on wind turbine loads. *Wind Energy*, 16(7):1013–1032, 2013. doi: 10.1002/we.1528. URL https://onlinelibrary.wiley.com/doi/abs/10.1002/we.1528.

[43] Saurabh Gupta, Ramit Malhotra, P R Krithika, Tanushree Bhattacharya, and K Ramanathan. *DSM Action Plan for Tamil Nadu*. TERI. URL http://bookstore.teri.res.in/books/705.

[44] Shubham Sharma and Sunanda Sinha. Indian wind energy & its development-policies-barriers: An overview. 1-2:100003. ISSN 2665-9727. doi: https://doi.org/10.1016/j.indic.2019.100003. URL http://www.sciencedirect.com/science/article/pii/S2665972719300030.

[45] Bose Shuvendu and Gupta Sudhanshu. Analysis of existing framework for renewables and RE policy in india. Technical report, German Agency for International Cooperation. URL http://www.indiaenvironmentportal.org.in/files/file/Analysis-of-Existing-Framework-for-Renewable-and-RE-policy-in-India.pdf.

[46] G. Sieros, P. Chaviaropoulos, J. D. Sørensen, B. H. Bulder, and P. Jamieson. Upscaling wind turbines: theoretical and practical aspects and their impact on the cost of energy. *Wind Energy*, 15(1):3–17. doi: 10.1002/we.527. URL https://onlinelibrary.wiley.com/doi/abs/10.1002/we.527.

[47] W. De Soto, S. A. Klein, and W. A. Beckman. Improvement and validation of a model for photovoltaic array performance. 80(1):78 – 88. ISSN 0038-092X. doi: https://doi.org/10.1016/j.solener.2005.06.010. URL http://www.sciencedirect.com/science/article/pii/S0038092X05002410.

[48] Roland Stull. *Practical Meteorology: An Algebra-based Survey of Atmospheric Science*. Univ. of British Columbia, 1.02b edition. ISBN 978-0-88865-283-6. URL https://www.eoas.ubc.ca/books/Practical_Meteorology/.

[49] Roland B. Stull. Practical meteorology: An algebra-based survey of atmospheric science. 2016.

[50] W. Tong. *Wind Power Generation and Wind Turbine Design*. WIT Press, 2010. ISBN 9781845642051. URL https://books.google.nl/books?id=wU9bgvrl4rQC.

[51] UNFCCC. Nationally Determined Contributions (NDCs) | UNFCCC, July 2020. URL https://unfccc.int/process-and-meetings/the-paris-agreement/the-paris-agreement/nationally-determined-contributions-ndcs#eq-1.

[52] Wilfried G.J.H.M. Van Sark, Henrik C. Van der Velde, Jan P. Coelingh, and Wim A.A.M. Bierbooms. Do we really need rotor equivalent wind speed? *Wind Energy*, 22(6):745–763, 2019. doi: 10.1002/we.2319. URL https://onlinelibrary.wiley.com/doi/abs/10.1002/we.2319.

[53] Rozenn Wagner, Michael Courtney, Torben Larsen, and Uwe Paulsen. Simulation of shear and turbulence impact on wind turbine performance. 01 2010.

[54] National Wind Watch. National Wind Watch | Output From Industrial Wind Power, July 2020. URL https://www.wind-watch.org/faq-output.php.

[55] D. Weisser and T.J. Foxon. Implications of seasonal and diurnal variations of wind velocity for power output estimation of a turbine: a case study of grenada. *International Journal of Energy Research*, 27(13):1165–1179, 2003. doi: 10.1002/er.938. URL https://onlinelibrary.wiley.com/doi/abs/10.1002/er.938.

[56] Ryan H Wiser and Mark Bolinger. 2018 wind technologies market report. Technical report.